THE ROLE OF BETA-GLUCURONIDASE IN ENTEROHEPATIC RECYCLING AND PROSTATE CANCER PROGRESSION

by

Brandon Robert Haefling

B.Sc., University of Victoria, 2018

A THESIS SUBMITTED IN PARTIAL FULFILLMENT OF

THE REQUIREMENTS FOR THE DEGREE OF

MASTER OF SCIENCE

in

THE FACULTY OF GRADUATE AND POSTDOCTORAL STUDIES

(Pharmaceutical Sciences)

THE UNIVERSITY OF BRITISH COLUMBIA

(Vancouver)

October 2021

The following individuals certify that they have read, and recommend to the Faculty of Graduate and Postdoctoral Studies for acceptance, a thesis entitled:

THE ROLE OF BETA-GLUCURONIDASE IN ENTEROHEPATIC RECYCLING AND PROSTATE CANCER PROGRESSION

submitted by Brandon Robert Haefling in partial fulfillment of the requirements for

the degree of Master of Science

in Pharmaceutical Sciences

Examining Committee:

Abby Collier, Professor, Faculty of Pharmaceutical Sciences, UBC
Supervisor

Michael Coughtrie, Professor and Dean, Faculty of Pharmaceutical Sciences, UBC
Supervisory Committee Member

Karla Williams, Assistant Professor, Faculty of Pharmaceutical Sciences, UBC
Supervisory Committee Member

Mads Daugaard, Associate Professor, Faculty of Medicine, UBC
Additional Examiner

Additional Supervisory Committee Members:

Michael Cox, Associate Professor, Department of Urological Sciences, UBC
Supervisory Committee Member

Mohsen Sadatsafavi, Associate Professor, Faculty of Pharmaceutical Sciences, UBC
Supervisory Committee Member

Abstract

Phase II metabolism regulates endo- and xenobiotic levels through compound inactivation and elimination. The major phase II drug metabolizing enzyme family, UDP-glucuronosyltransferases (UGTs), conjugate a broad variety of substrates through glucuronidation. Historically, drug metabolism research focused extensively on UGT activity and compound elimination, with minimal comparative data investigating beta-glucuronidase (βG) catalyzing the reverse recycling reaction. Despite this, available research shows βG activity is upregulated in a variety of clinically relevant conditions including human immunodeficiency virus (HIV) and cancer. The purpose of this thesis is to characterize βG expression and activity in health and disease, providing novel insights into the role of recycling in chemical homeostasis in the body. In Chapter 2, the first comprehensive profile showing differential βG expression and activity across 14 distinct human tissues was developed. Greatest enzyme activity was observed in prostate, caecum, liver and adrenal, with intestinal tissues showing closest UGT:βG activity at pH 7.4 suggesting further investigation into the recycling role in the gut. Measuring *E. coli* and human βG at each respective optimal pH revealed that bacterial strains showed enzyme activity comparable or greater to that in human. However, human βG activity increased 13-fold from pH 7.4 to pH 5.4 (native lysosomal pH), suggesting that more acidic environments favour the human enzyme. These findings demonstrate that enterohepatic recycling is likely due to a combination of both bacterial and human βG. In Chapter 3, the role of βG in prostate cancer was assessed. Upregulated βG activity was related to disease progression, with greatest activity reported in PC3 cells and adenocarcinoma tissue. In androgen-sensitive models, elevated enzyme activity suggests a role for βG in locally recycling androgens whereas the recycling of other endobiotics may stimulate cancer growth in androgen-insensitive models. Total UGT activity was greatest in

PNT1A cells and adenocarcinoma tissue, with UGT2B17 more commonly expressed in prostate cell lines and UGT2B15 in prostate tissues. Overall, βG is upregulated in androgen-sensitive and androgen-insensitive models and may represent a novel prostate cancer biomarker and/or therapeutic target.

Lay Summary

The balance between compound elimination and recycling within the body plays a fundamental role in metabolism. If the metabolic balance becomes dysregulated, either locally or systemically, disease may occur. The recycling enzyme, beta-glucuronidase, contributes to drug toxicity in drug metabolism and prostate cancer progression. This thesis provides the first comprehensive body map characterizing enzyme activity and expression across 14 distinct tissue types, with novel findings in intestinal tissues relating to drug metabolism. My data demonstrates that beta-glucuronidase is differentially active and expressed in certain intestinal regions, showing how both human and bacterial enzymes respond optimally in unique pH environments. Human beta-glucuronidase activity was elevated with decrease in pH suggesting the enzyme is more likely to recycle compounds in acidic intestinal environments compared to some bacteria. In prostate cancer, beta-glucuronidase activity and expression increase with disease progression suggesting a role for locally recycling androgens, providing fuel for cancer growth.

Preface

All work presented in this thesis was carried out by Brandon Haefling under the supervision of Dr. Abby Collier in the Faculty of Pharmaceutical Sciences at The University of British Columbia. Dr. Abby Collier and Brandon Haefling were responsible for experimental designs. This thesis was written by Brandon Haefling, with revisions provided by Dr. Abby Collier. All experimental work was completed by Brandon Haefling except for the cases listed below.

Chapter 1: Data analysis of published genomic and transcriptomic databases was performed by Dr. Alexander Smith. This analysis provided initial interest for investigating βG expression and activity at the protein level in the context of prostate cancer development. The experimental results are reported in Chapter 3 of this thesis.

Chapter 2: Dr. Alexander Smith conducted activity assays to determine βG activity in prostate and adrenal tissue lysates at pH 7.4. Dr. Smith performed these experiments in July 2020 as Brandon Haefling was physically unable to do so due to a broken hand.

Chapter 3: Western blot experiments were conducted by Blair MacDonald to determine protein expression of UGT1A1, 1A3, 1A4, 1A6 and 2B7 in prostate cell lines. Resulting data was analyzed by Blair.

All experiments using human tissues in Dr. Collier's laboratory were approved by The University of British Columbia Research Ethics Board as follows:

1. Human Ethics Approval: H14-00092
2. Biosafety Approval: B18-0009

Table of Contents

List of Tables

List of Figures

List of Abbreviations

βG	Beta-glucuronidase
°C	Degrees Celsius
$t_{1/2}$	Half-life
λ_{em}	Emission wavelength
λ_{exc}	Excitation wavelength
4MU	4-methylumbelliferone
4MUG	4-methylumbelliferyl-β-D-glucuronide
ACTH	Adrenocorticotropic hormone
ADT	Androgen deprivation therapy
AIDS	Acquired immune deficiency syndrome
Akt	Protein kinase B
ANOVA	Analysis of variance
AR	Androgen receptor
ARE	Androgen response element
AS	Active surveillance
BM	Basement membrane
BPH	Benign prostatic hyperplasia
CRPC	Castration-resistant prostate cancer
CV	Coefficient of variation
CYP	Cytochrome P450
DBD	DNA-binding domain
DHEA	Dehydroepiandrosterone
DHT	Dihydrotestosterone
DME	Drug metabolizing enzymes
EBRT	External beam radiation therapy
ECM	Extracellular matrix
EGF	Epidermal growth factor
EGFR	Epidermal growth factor receptor
EndoH	Endoglycosidase-H
ER	Endoplasmic reticulum
ERK	Extracellular signal-regulated kinase
ETS	E26 transformation-specific
FDA	Food and Drug Administration
FGF	Fibroblast growth factor
FGFR	Fibroblast growth factor receptor
GAG	Glycosaminoglycan
GI	Gastrointestinal tract
GlcA	Glucuronic acid
GlcNAc	N-acetylglucosamine
GST	Glutathione-S-transferase
FU	Fluorescence units
HIV	Human immunodeficiency virus
HIV-1	Human immunodeficiency virus type 1
HIV-2	Human immunodeficiency virus type 2

HMP	Human Microbiome Project
HRP	Horseradish peroxidase
HS	Heparan sulfate
IGF-1	Insulin-like growth factor-1
IHC	Immunohistochemistry
IL-6	Interleukin-6
kDa	Kilodalton
KGF	Keratinocyte growth factor
L1	Loop 1
L2	Loop 2
LBD	Ligand-binding domain
LC-MS	Liquid chromatography-mass spectrometry
LH	Luteinizing hormone
LHRH	Luteinizing hormone-releasing hormone
MAPK	Mitogen-activated protein kinase
mCRPC	Metastatic castration-resistant prostate cancer
mL1	Mini Loop 1
mL2	Mini Loop 2
mL1,2	Mini Loop 1,2
mRNA	Messenger RNA
NAT	N-acetyltransferase
NCOA1	Nuclear receptor coactivator 1
NCOA2	Nuclear receptor coactivator 2
NDS	Normal donkey serum
NEPC	Neuroendocrine prostate cancer
NL	No Loop
NSAID	Non-steroidal anti-inflammatory drug
NTD	N-terminal domain
OS	Overall survival
PAP	Prostatic acid phosphatase
PCa	Prostate cancer
PFS	Progression-free survival
PNGase F	Peptide:N-glycosidase F
PSA	Prostate-specific antigen
PTEN	Phosphatase and tensin homologue
PVDF	Polyvinylidene difluoride
RB	Retinoblastoma
RNA	Ribonucleic acid
RP	Radical prostatectomy
RPM	Revolutions per minute
RPT	Radiopharmaceutical therapy
SCNC	Small cell neuroendocrine carcinoma
SDS-PAGE	Sodium dodecyl sulfate-polyacrylamide gel electrophoresis
STAT3	Signal transducer and activator of transcription 3
STS	Steroid sulfatase
SULT	Sulfotransferase

T	Testosterone
TBS-T	Tris buffered saline with 0.5% tween-20
TF	Transcription factor
Tip60	Tat-interactive protein
TME	Tumour microenvironment
TMPRSS2	Transmembrane protease serine 2
UGS	Urogenital sinus
UGT	UDP-glucuronosyltransferase
UDP	Uridine diphosphate
UDPGA	Uridine diphosphate-glucuronic acid

Acknowledgements

A thesis is the writings of one individual describing the collective effort and ideas that bring a research project to life. Completing this thesis required the support and guidance from many individuals, all of whom I am greatly indebted. Firstly, I would like to thank my supervisor Dr. Abby Collier for her invaluable technical expertise, practical advice, and mentorship I had the fortune of receiving during my graduate studies. I am grateful to Abby for providing me the opportunity to explore my intellectual curiosities here at The University of British Columbia and be introduced to the world of pharmaceutical sciences. While my degree required developing technical knowledge, the best teaching moments were non-technical. Dr. Collier taught me to be courageous, collaborative, accepting of new ideas and value the importance of making personal connections with others. Scientists are humans after all.

I would like to thank all members of my MSc committee, Dr. Michael Coughtrie, Dr. Karla Williams, and Dr. Michael Cox, as well as my MSc committee chair, Dr. Mohsen Sadatsafavi. The collective expertise allowed my research project to grow in new directions, while providing me with an invaluable learning opportunity at each committee meeting. Each member was generous with their time, provided useful advice, and offered continuous support throughout my MSc program, for which I am deeply appreciative.

To my fellow laboratory members, Dr. Alexander Smith, Dr. Yuejian Liu, Dickson Lai, Rayda Sheikh, Hayley Price, and Michael Doerksen, thank you for the great memories and in providing a supportive, friendly work environment. I wish you all the best with your future careers.

I would like to thank all members of the Kumar lab for allowing me to use equipment that allowed my research to progress. Everyone was very accommodating and friendly, making it easy to schedule time for equipment use.

To my fellow graduate students, thank you for the many experiences and journeys over the last two years. Universities foster international friendships. I am grateful for the many interesting people I have had the pleasure of knowing in this faculty, many of whom have families outside of North America. In an international environment, learning about different cultures and customs has only increased my desire to travel to those parts of the world. One day, I will.

I would like to thank the Faculty of Pharmaceutical Sciences for providing modern facilities and equipment in which to carry out my research, in addition to financial support.

To my family and friends, I am grateful for the love and support over the last two years. The encouragement has helped me push through setbacks to advance with my research. Each achievement in my life is through a collective effort, never alone. In which case, we did it.

Lastly, I would like to acknowledge Dr. Frank Abbott. Your cheerful nature and passion about science sparked my curiosity. It is because of you that I enrolled in graduate studies here at the Faculty of Pharmaceutical Sciences. For your support in pursuing this experience, I thank you.

Dedication

This work is dedicated to those that inspire and support me through the journeys in life. To my mother Mary, thank you for teaching me the value of patience and humility. The pursuit of something meaningful takes time and effort. The willingness to make mistakes is just a prerequisite for future success. To my father Robert, you taught me the value of responsibility, becoming resilient and learning the compound effects of showing up every day. To my sister Lauren, you embody how to move through life with a smile. I appreciate your positivity and ability to make work feel like play.

Secondly, I would like to thank my friends that push me to become the best version of myself, while learning to be grateful for each opportunity along the way. The meaningful relationships developed with friends, both in and outside of graduate school, have provided fulfillment in my life. I am indebted to those that continue to have my best interest at heart and help me identify personal areas for growth and improvement.

I am very grateful for the role of mentorship in my life and dedicate my thesis to my many mentors, past and present, for which their guidance and advice has remained invaluable and immensely practical in my life. Moreover, to mentors whom I have never met, your teachings and practical wisdom in books and podcasts have had a profound impact on my life during graduate school and positively changed my outlook on the world.

Lastly, I dedicate this work to my late Aunt Patty. Your bravery and optimism in fighting cancer will not be forgotten. Although you are not physically with us anymore, you will always remain alive in our stories, memories, and of course, our hearts. I now have an emotional attachment to my research, which allows me to see the forest through the trees and realize that each experiment counts in trying to move the needle towards improving cancer survivorship.

Chapter 1: Introduction

1.1 Metabolizing enzymes – a biochemical pharmacology perspective

1.1.1 Overview

A series of enzymes (also called "metabolic pathways") function to remove endo- and xenobiotics from the body. The drug metabolizing enzymes (DMEs) catalyzing these reactions are divided pharmacologically into two phases: phase I and phase II. Phase I metabolism, which includes the cytochrome P450 (CYP) superfamily, catalyze reduction and oxidation reactions that may provide suitable function groups for subsequent conjugation reactions in phase II (Iyanagi, 2007). Phase II conjugation reactions are catalyzed by a series of different enzyme superfamilies including the Glutathione-S-transferases (GSTs), N-acetyltransferases (NATs), Sulfotransferases (SULTs), and UDP-glucuronosyltransferases (UGTs). Each superfamily encodes multiple unique isoforms with broad substrate specificity (Xu *et al*., 2005). Phase II metabolism plays a key role in detoxification, where many of these enzymes function as transferases, covalently linking chemical moieties and peptides to lipophilic substrates to facilitate the excretion of biologically inactive products (Jančová *et al*., 2010). Many conjugation reactions proceed by a S_N2 mechanism where a nucleophilic functional group from the substrate attacks an electrophilic position on the chemical group to be transferred. While conjugation reactions define phase II metabolism, not all reactions generate more water-soluble products. The formation of certain N-acetylated and methylated products shows decreased water-solubility suggesting that not all phase II metabolic processes improve the uptake of compounds into the bile or urine for elimination (Josephy *et al*., 2005). However, glucuronidation and sulfation, catalyzed by UGTs and SULTs respectively, are the dominant phase II reactions producing water-soluble products. Of all conjugation reactions, glucuronidation is the most important

metabolic pathway for the detoxification and elimination of clinical drugs, environmental carcinogens and dietary chemicals among vertebrates (Jančová & Šiller, 2012). Additionally, UGTs are highly kinetically favoured for the elimination of androgens, particularly testosterone and dihydrotestosterone (DHT), whereas SULTs often metabolize dehydroepiandrosterone (DHEA) (McNamara *et al*., 2013). Therefore, the main conjugating enzymes studied in this thesis are the UGTs, where protein expression and activity were determined across distinct human tissues. The obligate partner to UGTs, and central focus of this thesis, is beta-glucuronidase (βG) which catalyzes a recycling reaction that reverses phase II metabolism and compound glucuronidation.

My preliminary research characterizing βG expression and activity across distinct human tissues (Chapter 2) led to two major findings: (1) intestinal enzyme activity decreased along the small intestine before an activity spike in the caecum and (2) enzyme activity was high in prostate and adrenal samples. These findings prompted investigation into the role of βG in enterohepatic recycling (Chapter 2) and prostate cancer development/progression/malignancy (Chapter 3) respectively. The following section provides an overview on the UGT enzyme superfamily: identified human isoforms and enzyme subfamily classifications.

1.1.2 UGT nomenclature

There are currently 117 members composing the mammalian *UGT* gene superfamily (Mackenzie *et al*., 2005). Each member is categorized into one of four gene families: *UGT1*, *UGT2*, *UGT3*, or *UGT8*. The *UGT1* family includes genes built from a first, unique exon 1 joined with shared exons 2-5 (Meech & Mackenzie, 1997); The resulting protein products display variable amino termini and conserved carboxyl termini. Moreover, shared exons are also

observed in the *UGT2* family, particularly *UGT2A1* and *UGT2A2* genes, where a distinct exon 1 connects to shared exons 2-6 (Mackenzie *et al*., 2005). Exon sharing is not seen in the *UGT2A3* gene, *UGT2B* subfamily, and *UGT3* and *UGT8* families (Mackenzie *et al*., 2005). Collectively, these gene families encode 22 human proteins: UGT1A1, 1A3, 1A4, 1A6, 1A7, 1A8, 1A10, 2A1, 2A2, 2A3, 2B4, 2B7, 2B10, 2B11, 2B15, 2B17, 2B28, 3A1, 3A2 and 8A1 (Meech *et al*., 2019). The structure and function of human UGT isoforms will be discussed below.

1.1.3 UGT structure

The UGT enzymes (EC 2.4.1.17) are type I transmembrane proteins located in the endoplasmic reticulum (ER) and nuclear membrane within the cell (Meech & Mackenzie, 1997; Radominska-Pandya *et al*., 2002). Mature enzymes are around 530 amino acids in length and contain key functional domains (Tukey & Strassburg, 2000; Miley *et al*., 2007). The amino-terminal domain is in the ER lumen and provides the substrate binding site whereas the carboxyl-terminal domain sticks out into the cytoplasm and serves as the co-substrate docking site (Meech & Mackenzie, 1997). A 17-residue transmembrane region provides a link between the functional domains and anchors the protein to the ER membrane (Meech & Mackenzie, 1998). Additionally, UGT isoforms are localized to the ER by an amino-terminal signal peptide sequence that is removed once the protein becomes embedded in the membrane (Ouzzine *et al*., 1999). A dilysine motif near the carboxyl-terminus serves as an ER retention signal, enabling the protein to remain intact in the ER to catalyze glucuronidation reactions (Meech & Mackenzie, 1998). Importantly, UGT isoforms are shown to exist either as individual protein subunits or in protein complexes as dimers and tetramers where the amino-terminus plays a role in oligomerization (Peters *et al*., 1984; Meech & Mackenzie, 1997). While UGT enzymes are

extensively studied in phase II metabolism, the complete crystal structure of any isoform is yet to be fully elucidated due to the challenges of obtaining structural information for membrane-bound proteins (Fujiwara *et al*., 2016). To date, mammalian UGT2B7 and UGT2B15 are the only partially characterized isoforms with available crystal structures for the uridine diphosphate-glucuronic acid (UDPGA) binding domain at the carboxyl-terminal (Miley *et al*., 2007; Zhang *et al*., 2020). Compared to protein structure, the functions of multiple human UGT isoforms are well characterized in the literature.

1.1.4 UGT function

Glucuronidation is the most important conjugation reaction catalyzed by UGT enzymes commonly expressed in the liver, gastrointestinal (GI) tract, kidney and lung. The transfer of sugar from uridine diphosphate (UDP)-sugar donors to lipophilic substrates produce bulky, more water-soluble glucuronides that are more readily eliminated from the body through bile or urine (Meech *et al*., 2019). A diverse range of endo- and xenobiotic compounds are metabolized by UGT isoforms with differing substrate specificity. In general, distinct isoforms expressed in different bodily tissues metabolize a unique set of substrates.

Although UGT enzymes catalyze the transfer of a glycosyl donor to a substrate to improve hydrophilicity, certain UGT gene families encode proteins that utilize different co-substrates. Only the UGT1 and UGT2 enzymes, which make up 19 of the 22 human isoforms, catalyze the transfer of glucuronic acid (GlcA) to a substrate. UGT3A1 transfers N-acetylglucosamine whereas UGT3A2 can transfer either UDP-glucose or UDP-xylose. Lastly, UGT8A1 utilizes galactose as the glycosyl donor to covalently attach to certain substrates (Meech *et al*., 2015). Glucuronidation reactions that attach unique sugar groups to substrates

involve a variety of functional groups that produce either O-linked, N-linked or S-linked glucuronides (Tukey & Strassburg, 2000). This thesis focuses on O-linked glucuronides where certain UGT isoforms including 1A1, 1A6, 2B7, 2B15, and 2B17 are responsible for metabolizing bilirubin, serotonin, morphine, androstane-3α-17β-diol and dihydrotestosterone respectively (Miners *et al*., 2006; Turgeon *et al*., 2001).

Lack of UGT expression may lead to diseases/syndromes as levels of endo- or xenobiotic substances accumulate in the body. For example, Crigler-Najjar syndrome affects UGT1A1 expression such that hyperbilirubinemia occurs due to the absence of glucuronidation and subsequent clearance (Burchell *et al*., 1995). Moreover, the conjugation reactions performed by UGT enzymes result in the inverted configuration at the anomeric carbon on GlcA thereby producing β-D-glucuronides (Tukey & Strassburg, 2000). The stereochemical change improves substrate specificity for a certain glycosyl hydrolase, βG, which operates as the obligate partner to UGT enzymes and catalyzes the removal of GlcA to recycle active compounds.

1.2 Glycosyl hydrolases

1.2.1 The lysosome

Eukaryotic cells contain organelles which allow for the compartmentalization of different functions. The lysosome is a key organelle which plays a role in cellular digestion, housing acid hydrolases for the degradation of biological macromolecules (Cooper, 2000). The discovery of the lysosome has been known since the 1950s (Duve *et al*., 1953). Compared to the surrounding cytosol at pH 7.2, the lysosome maintains an acidic environment around pH 5 (Cooper, 2000). Proton pumps, specifically vacuolar H^+-ATPase, actively transport protons from the cytosol to the lysosome to achieve constant pH (Cooper, 2000; Johnson *et al*., 2016). The internal

environment within the lysosomal lumen provides the optimal pH for many acid hydrolases, which varies between pH 4.5 and 5.5 (Mellman *et al*., 1986). Importantly, the acidic optimal pH helps protect against unwanted cellular degradation if the lysosome ruptures and hydrolases are exposed to the alkaline pH environment of the cytosol as enzyme activity will be significantly reduced in these conditions (Cooper, 2000). This thesis centers around βG, an acid hydrolase initially suggested to reside within the lysosome since the mid 1950s (Gianetto & Duve, 1955).

1.2.2 Beta-glucuronidase structure

The acid hydrolase βG is found within the lysosomes of many different cell types and exists freely in multiple human body fluids (Sperker *et al*., 1997). The *GUSB* gene on chromosome 7 is 21-kilobases and contains 12 exons, ranging from 85-376 base pairs in length, for encoding the protein (Paigen, 1989; Sperker *et al*., 1997; Miller *et al*., 1990). The βG monomer is synthesized as a 80 kilodalton (kDa) precursor before cleavage of a 18-amino acid residue signal peptide from the carboxyl-terminus generates the mature 78 kDa form (Jain *et al*., 1996; Islam *et al*., 1999). Each monomer is composed of three domains: a jelly roll barrel domain, an immunoglobulin constant domain and an α/β barrel domain, at which the active site resides (Jain *et al*., 1996; Islam *et al*., 1999). Individual monomers aggregate together to form active βG tetramers through disulfide bond formation (Shipley *et al*., 1993). Each protein complex houses four catalytic sites and shows thermostability up to 70°C (Sperker *et al*., 1997; Awolade *et al*., 2020). Importantly, glycosylation plays a role in directing a newly synthesized protein to the lysosome. Mannose 6-phosphate residues on oligosaccharide chains produced through N-glycosylation at four asparagine residues (Asn-173, Asn-272, Asn-420, Asn-631) serve as a recognition signal for targeting the βG protein to the lysosome. Mannose 6-phosphate

receptors in the *trans*-Golgi network recognize mannose 6-phosphate on oligosaccharide chains and the resulting ligand-receptor complex is packaged into a vesicle for transport to the lysosome (Dahms *et al.*, 1989; Shipley *et al*., 1993). Understanding βG protein structure and its co-ordinated migration to the lysosome provides necessary background information before discussing enzyme function.

1.2.3 Beta-glucuronidase function

Beta-glucuronidase (EC 3.2.1.31) is an acid hydrolase that functions as an exoglycosidase, catalyzing a hydrolysis reaction that cleaves a terminal glucuronic acid residue (Sperker *et al*., 1997). This enzyme belongs to the glycosyl hydrolase family 2, along with β-galactosidase and β-mannosidase (Henrissat, 1991). Specifically, βG operates on substrates with O-glycosyl linkages where glucuronic acid is covalently attached to a hydroxyl group on the substrate (Henrissat, 1991; Tukey & Strassburg, 2000). This recycling enzyme is capable of cleaving glycosidic linkages from a broad range of endo- and xenobiotic substrates including glycosaminoglycans (GAGs), bilirubin and androgens (Nakamura *et al*., 1990; Naz *et al*., 2013; Whiting *et al*., 1993; Hadd & Blickenstaff, 1964). Importantly, βG is capable of metabolizing every glucuronide, albeit with differing substrate affinity. Enzymatic catalysis occurs in the α/β barrel domain, where Glu^{540} and Glu^{451} function as a catalytic dyad (Islam *et al*., 1999; Jain *et al*., 1996; Wong *et al*., 1998). The catalytic mechanism proceeds with a concerted general acid-nucleophile approach where Glu^{451} functions as the proton donor and Glu^{540} as the nucleophile (Hassan *et al*., 2013). The reaction catalyzed by βG results in the retention of the anomeric carbon at the hydrolysis site such that both substrate and product have the same stereochemistry (McCarter & Withers, 1994; Wang & Touster, 1972). Retaining mechanisms require the key

catalytic residues, Glu^{451} and Glu^{540}, to be located on opposite sides of the glycosidic bond to be hydrolyzed (Henrissat *et al*., 1995). The ability of βG to cleave a diverse array of glucuronides provides a systemic recycling function that regenerates mostly active compounds and counteracts detoxification of substances through UGT enzymatic activity. While βG is integral to maintaining endo- and xenobiotic compound homeostasis within the body, elevated or reduced activity may lead to diseases.

1.2.4 The role of beta-glucuronidase in disease

1.2.4.1 Hyperbilirubinemia

Bilirubin is primarily produced from the breakdown of heme and the degradation of red blood cells. The accumulation of unconjugated bilirubin, which is poorly water-soluble, is known to contribute to development of kernicterus and jaundice (Watchko & Tiribelli, 2013; Porter & Dennis, 2002). These disorders are commonly seen in newborns (Memon *et al*., 2016). To reduce circulating bilirubin levels, water solubility is improved through phase II metabolism and conjugation reactions. Specifically, UGT1A1 plays a key role in the conjugation of bilirubin, producing either mono- or diglucuronide compounds that can be excreted into the bile and eliminated from the body (Memon *et al*., 2016). However, the emergence of hyperbilirubinemia is not only dependent on the presence of UGT activity and conjugation. The activity of βG converts bilirubin glucuronides into active bilirubin, thus increasing levels in the body. Elevated βG levels present at the intestinal brush border, and in breast milk, may contribute to enterohepatic recycling of bilirubin and lead to the development of neonatal jaundice (Sirota *et al*., 1992; Gourley & Arend, 1986). The role of βG in disease is due not only to enzyme overexpression and increased activity, but also arises from a lack of expression and activity.

1.2.4.2 Sly syndrome

Mucopolysaccharidosis type VII, or Sly syndrome, is an autosomal recessive lysosomal storage disease that results in the absence of βG expression and activity (Sly *et al*., 1973). This genetic disease affects *GUSB* on chromosome 7, which prevents the proper production of the beta-glucuronidase enzyme (Allanson *et al*., 1988). Currently, 49 disease-causing mutations have been identified, with the majority being missense mutations followed by nonsense mutations and deletions (Montaño *et al*., 2016; Tomatsu *et al*., 2009). Deficiency of βG results in the accumulation of partially degraded GAGs including heparan, dermatan and chondroitin sulfate in the lysosome which contributes to cellular and organ dysfunction (Montaño *et al*., 2016). Affected patients are characterized by cognitive impariment, short stature, bone dysplasia, and hydrops fetalis especially in newborns (Sly *et al.*, 1973; Tomatsu *et al.*, 2009; Montaño *et al*., 2016). Although patients with Sly syndrome show similar clinical features, the magnitude of the phenotype may vary from mild to severe. Importantly, this genetic disease is one of the earliest disorders to peak clinical interest in βG and its role in human disease.

1.2.4.3 Beta-glucuronidase in Human Immunodeficiency Virus/Acquired Immune Deficiency Syndrome (HIV/AIDS)

Human immunodeficiency virus (HIV) impairs the host immune system by attacking cells that play a role in fighting infections. Decreased immune function leaves the body vulnerable to further infection and disease. Left untreated, HIV virus type 1 (HIV-1) and HIV virus type 2 (HIV-2) can decimate immune cell populations, particularly CD4+ T lymphocytes, and lead to acquired immune deficiency syndrome (AIDS), a chronic illness (Sharp & Hahn, 2011). This disease, characterized as a sexually transmitted disease, was first clinically identified

in 1981 (CDC, 1981). Importantly, HIV/AIDS led to clinical interest in βG a decade later as specific enzyme activity in serum was 16-fold greater in patients with late stage disease compared to HIV-negative control patients (Saha *et al*., 1991). Disease stage progression was associated with increased enzyme activity. Within the same study population, HIV-positive patients with CD4+ lympocyte counts < 200/mm^3 showed over 3-fold increase in serum βG activity compared to positive patients with lympocyte counts > 200/ mm^3 (Saha *et al*., 1991). These results suggest a relationship between βG activity and immune deficiency where serum enzyme activity increases with decreasing CD4+ lymphocyte count. While it is not fully understood why βG presence and activity in serum is elevated with HIV progression, one explanation involves enzyme release from cells in response to toxins (Saha *et al*., 1991). The initial interest in βG and its potential role in HIV/AIDS was transient, reflected by the lack of available literature papers in recent years further exploring the enzyme and its involvement in immune cells. Moreover, as βG becomes implicated in more diseases it becomes imperative to determine the mechanism(s) of βG involvement in disease etiology, and as well; whether the eukaryotic or prokaryotic version of the enzyme should be the therapeutic focus.

1.3 Beta-glucuronidase in the intestines

1.3.1 The gut microbiome

1.3.1.1 Diversity in bacterial beta-glucuronidase

The human intestines provide a dynamic interface between host and microbes. The gut microbiota is the collection of microorganisms that provide a broad range of functions encoded through genes of the microbiome (Valdes *et al*., 2018). The number of microbial genes detected from Human Microbiome Project (HMP) samples roughly outnumber human genes by 30-fold (Shreiner *et al*., 2015). Interestingly, the gut microbiota is sometimes referred to as an additional "organ" given the versatile biological functions it plays in producing metabolites not accessible by the host and influencing the immune system (Valdes *et al*., 2018; Sekirov *et al*., 2010).

The intestines provide unique chemical and physical environments to bacteria from over 50 different phyla. Microbes from Bacteroidetes and Firmicutes are dominantly expressed followed to a lesser extent by Proteobacteria, Verrucomicrobia and Actinobacteria (Eckburg *et al*., 2005; Sekirov *et al*., 2010). Microbial composition is highly variable, changing based on age, diet, smoking and genetic factors (Hopkins *et al*., 2001; Valdes *et al*., 2018). Moreover, gut microbes in a healthy individual become more densely populated moving distally through the intestines from a relatively sparse population in the stomach and duodenum (10^1-10^3 bacterial cells/gram of intestinal content) to a dense population in the colon (10^{11}-10^{12} bacterial cells/gram of intestinal content) (O'Hara & Shanahan, 2006; Sekirov *et al*., 2010). Variability in gut microbes is also observed within each intestinal section, where location plays a role in distinguishing bacteria that reside in the intestinal lumen compared to those embedded in the intestinal mucosa or found adjacent to the intestinal epithelium (Sekirov *et al.*, 2010). Additionally, availability of certain carbon sources influences the presence of certain bacteria in

specific intestinal regions where the caecum provides the major site for the metabolism of non-digestible carbohydrates (Louis *et al*., 2007). A visual overview of the GI tract and the diversity of microorganisms found within the body is summarized below (Figure 1.1).

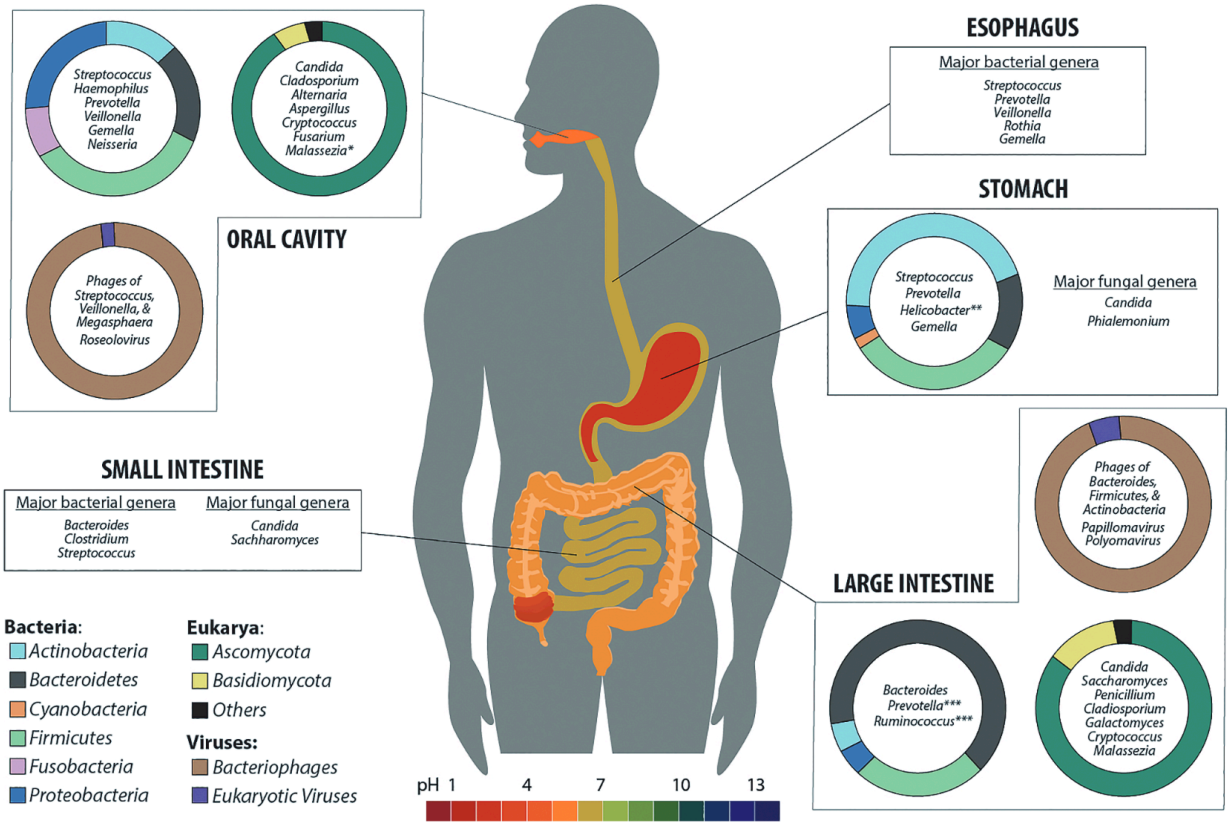

Figure 1.1: Microbes occupy distinct environments along the GI tract
The unique physical and chemical environments within the GI tract allow certain microbes to thrive. Among bacteria, occupancy along the intestines is dictated by pH, nutrient availability, and ability to metabolize local substrates. Actinobacteria is the dominant phyla in the stomach whereas Bacteroidetes is dominant moving distally through the large intestine. Proteobacteria, which includes *E. coli*, is minorly represented in both the small and large intestines. Figure derived in original format with no modifications (Hillman *et al*., 2017). Reproduced with permission under CC-BY https://creativecommons.org/licenses/by/4.0/.

Some bacterial phyla express βG in the gut. From the HMP GI database, 279 unique version of bacterial βG have been identified (Pollet *et al*., 2017). The enzyme are categorized based on structural differences and the presence of certain loop structures commonly found among different phyla. Specifically, enzymes are classified into the following six structural

groups based on loop structure near the active site: Loop 1 (L1), Mini Loop 1 (mL1), Loop 2 (L2), Mini Loop 2 (mL2), Mini Loop 1,2 (mL1,2) and No Loop (NL). Enzymes with larger loops are more efficient at processing smaller glucuronides compared to those that display mini or no loop structures (Pollet *et al*., 2017; Biernat *et al*., 2019). Along with variable substrate affinity, optimal pH for bacterial βG ranges from pH 4.5-7.4 (Biernat *et al*., 2019). Of the dominant phyla, Bacteroidetes βG exists in mL1, L2, mL2, mL1,2 and NL forms whereas Firmicutes show enzymes with L1, mL1, L2, and NL structures (Pollet *et al.*, 2017). Moreover, the minor phylum Proteobacteria only contain L1 βG. As *E. coli* βG is studied in this thesis, the following sections will provided details on enzyme structure and function.

1.3.1.2 *E. coli* beta-glucuronidase structure

The identification of bacterial βG was initially determined in *E. coli* and related members of the Enterobacteriaceae family (Michikawa *et al*., 2012). X-ray crystallography shows that the prokaryotic enzyme exists as a 597 amino acid monomer and becomes functional in a tetrameric form. Similar to the structure of other glycosyl hydrolase family 2 enzymes, *E. coli* βG contains a sugar binding domain at the amino-terminal and an α/β barrel domain at the carboxyl-terminal which contains the active site. An immunoglobulin constant domain connects the two domains from the amino- and carboxyl-termini. Additionally, this bacterial enzyme displays a 17-amino acid L1 architecture near the active site from residues 360-376 (Wallace *et al*., 2010). The larger loop reduces available space at the active site restricting the catalysis of larger glucuronides. The next section provides an overview on *E. coli* βG function and how steric constraints allow for the metabolizing of smaller glucuronides with high affinity.

1.3.1.3 *E. coli* beta-glucuronidase function

The reaction mechanism for *E. coli* βG proceeds through a catalytic dyad. The key glutamate residues, Glu^{413} and Glu^{504}, are located at the active site and catalyze the hydrolytic cleavage of glycosidic linkages (Wallace *et al*., 2010). The mechanism is characterized by a two-step process where Glu^{413} functions as a general acid and donates a proton before Glu^{504} acts as nucleophile (Lin *et al*., 2021). Although bacterial βG metabolizes glucuronides, active site loop structures modify substrate affinity.

Enzymes classified by smaller or no loop architectures target larger glucuronides with greater affinity. Bacteroidetes, a dominant bacterial phylum, are commonly expressed in the large intestine and efficiently metabolize glucuronides from complex carbohydrates due to smaller loop structures providing less steric constraint at the active site (Little *et al*., 2018). While *E. coli* βG is ineffective at metabolizing larger carbohydrates and cannot extract the necessary carbon sources from the large intestine, it is optimized to metabolize smaller substrates in the proximal intestinal regions due to its specific operon.

Possessing a βG operon sensitive to smaller glucuronides, which is present across microbes in the Enterobacteriacea family, provides an efficient and advantageous way to obtain carbon sources in the competitive gut environment. The operon encodes three genes (gusA, gusB, gusC) where the respective products are βG, an inner-membrane GlcA specific transporter and nonspecific outer-membrane channel (Little *et al*., 2018). If glucuronides are detected locally, the glucuronide repressor, which regulates transcription of the operon, will dissociate and enable synthesis of βG and key membrane proteins to facilitate uptake of glucuronides into the bacterial cytosol for hydrolysis and liberation of free GlcA to serve as an energy source (Little *et al.*, 2018). The existence of both prokaryotic and eukaryotic βG suggests that the

enzyme is evolutionary conserved and the importance of hydrolyzing glucuronic acid from substrates serves an important biological function.

1.3.1.4 Prokaryotic and eukaryotic beta-glucuronidase

The evolutionary history of βG is reflected by a 45% sequence identity between the human and *E. coli* versions of the enzyme (Paigen *et al*., 1989; Hassan *et al*., 2013). Human and *E. coli* βG both function by a similar reaction mechanism that requires a catalytic dyad of glutamate residues to function as either a general acid or nucleophile. Both active sites are found in the α/β barrel domain near the carboxyl-terminus where the main difference is the position of each catalytic residue: Glu^{413} and Glu^{504} in *E. coli* and Glu^{451} and Glu^{541} in human (Wallace *et al*., 2010; Islam *et al*., 1999). Although the domains are similar between prokaryotic and eukaryotic versions, key structural differences are observed. Human βG contains a lysosomal targeting motif in domain 1 whereas *E. coli* βG possesses a bacterial loop with L1 architecture near the active site on domain 3 (Jain *et al*., 1996; Hassan *et al*., 2013; Wallace *et al*., 2010). As a result, spatial considerations and substrate specificities differ between the two enzymes. The human βG active site is more open whereas the *E. coli* active site is more confined. Therefore, the human enzyme can accommodate bulkier substrates and is more efficient at metabolizing larger polysaccharides such as GAGs. In comparison, *E. coli* βG has evolved to optimize improved binding with smaller substrates that fit the more narrow space. Moreover, both enzymes show different optimal pH values that reflect the pH of the surrounding environment. The absence of organelles in prokaryotes means βG resides freely in the *E. coli* cytoplasm and has an optimal pH of 7.4 (Biernat *et al*., 2019). In eukaryotes, βG is found within acidic lysosomes and operates optimally around pH 5.4 or lower (Weyel *et al*., 2000; Sperker *et al*.,

1997; Islam *et al*., 1999). These physical and chemical differences in structure and optimal environment do not discount the ability of both bacterial and human enzymes to catalyze reactions that contribute to enterohepatic recycling, but do highlight the importance of correct pH conditions when studying these phenomena *in vitro*, a consideration that will be highlighted later in the experimental findings of this thesis.

1.3.2 Enterohepatic recycling

Enterohepatic recycling is a biological phenomenon that is of interest for normal human biology as it is necessary for recycling biochemically expensive endobiotics and reducing the energy burden on the body (Roberts *et al*., 2002). In clinical medicine, pharmacology and toxicology the pathway increases compound half-life, alters pharmacokinetic/toxicokinetic profiles and interferes with correct drug dosing. The process involves hepatic conjugation followed by intestinal deconjugation, converting compounds from hydrophilic to lipophilic, thus improving retention in the body through absorption across the intestinal epithelium and transport through the portal circulation to the liver (Figure 1.2) (Roberts *et al*., 2002). In this thesis, phase II metabolism in the liver and subsequent enterohepatic recycling will center around the most common conjugation reaction, glucuronidation and deconjugation by βG.

Biotransformation of glucuronides in the liver can lead to either removal of water-soluble glucuronides by kidney filtration, or biliary excretion directly into the intestine. The ability of compounds to enter the biliary system depends on key biological factors: molecular weight, polarity, chemical structure modifications, species and sex (Parker *et al*., 1980). The covalent linkage of GlcA to a substrate forms a bulky, more water-soluble product with improved polarity that is more soluble in bile and transported into the proximal part of the small intestine. It is here

in the intestine where βG activity alters the chemical properties of glucuronides, thereby reversing phase II metabolism and promoting compound recycling by reabsorption into the systemic circulation.

A broad range of endo- and xenobiotic substances are subject to enterohepatic recycling. Bile acid, bilirubin and steroid glucuronides are recycled in the gut following the removal of glucuronic acid (Dobrinska, 1989; Roberts *et al*., 2002; Adlercreutz *et al*., 1979). Additionally, commonly prescribed drugs such as morphine, non-steroidal anti-inflammatory drugs (NSAIDs) indomethacin and diclofenac, and anti-cancer drug Irinotecan are shown to undergo enterohepatic recycling (Parker *et al*., 1980; Duggan *et al*., 1975; Reuter *et al*., 1997; Catimel *et al*., 1995).

The physiological role of enterohepatic recycling in the body may be either beneficial or harmful. Firstly, bile acid recycling may be beneficial as it allows for the reuse of compounds that are physiologically expensive to continually synthesize (Roberts *et al*., 2002). As a result, this endobiotic is recycled several times per day in the body (Dobrinska, 1989). Conversely, the recycling of certain xenobiotic substances may contribute to physiological damage, especially within the intestines. Intestinal ulcers, diarrhea and dose-limiting toxicity remain clinical concerns for patients taking NSAIDs and Irinotecan where drug dosing regimens must be appropriately modified to avoid toxicity and provide the therapeutic dose (Duggan *et al*., 1975; Pellock & Redinbo, 2017; Bhatt *et al*., 2020; Wallace *et al*., 2010). Interestingly, the enterohepatic recycling of endobiotics such as bilirubin is more associated with human βG whereas microbial βG is believed to contribute to drug recirculation within the body. Despite that these assertions are routinely made, this has not been rigorously tested until now. Original work in this thesis demonstrates that both bacterial and human intestinal βG can contribute to

enterohepatic recirculation of xenobiotics, using the coumarin derivative 4-methylumbelliferone (4MU) as an experimental substrate for proof-of-principal. Additionally, original work in this thesis demonstrates that human βG activity is optimal at pH 5.4 (the pH of the lysosome), and also higher at pH 6.8, which is close to the pH of the mid-GI tract (as may be found in the context of a tissue lysate). Since previous 4-methylumbelliferyl-β-D-glucuronide (4MUG) assays were validated at pH 7.4, the resulting activity data does not reflect human enzyme activity at optimal pH, likely contributing to lower reported values (Trubetskoy & Shaw, 1999). Human βG activity is orders of magnitude higher at its native pH; this means that many prior studies ascribing enterohepatic recycling solely to bacteria in the gut, and tissue specific recycling as "irrelevant" compared to glucuronidation are likely confounded. Therefore, a novel contribution of this thesis is the re-evaluation of human βG, at optimal pH, in the context of enterohepatic and local tissue recycling. The design and development of therapeutic enzyme inhibitors could target the diverse array of βG encoded by human and/or gut microbiome, where the latter includes 279 unique bacterial enzymes identified in the HMP database (Pollet *et al*., 2017). Initial efforts focused on *E. coli* βG where a well-characterized crystal structure aided drug design in blocking the enzyme and preventing the metabolism of smaller glucuronides in the gut (Bhatt *et al*., 2020; Wallace *et al*., 2010).

In the following section, the role of βG contributing to disease will extend beyond enterohepatic recycling to focus on cancer. Specifically, the relationship between βG and prostate cancer (PCa) progression will be further discussed. This research direction came from findings in the original profile of human tissue βG expression and activity (Chapter 2). Highest enzyme levels were observed in liver, kidney and intestine (as expected), but equally high levels of βG expression and activity were found in the adrenal and prostate as the liver (highly

unexpected). In exploring the role of βG in the prostate, an association with prostate cancer progression/severity was revealed (Chapter 3).

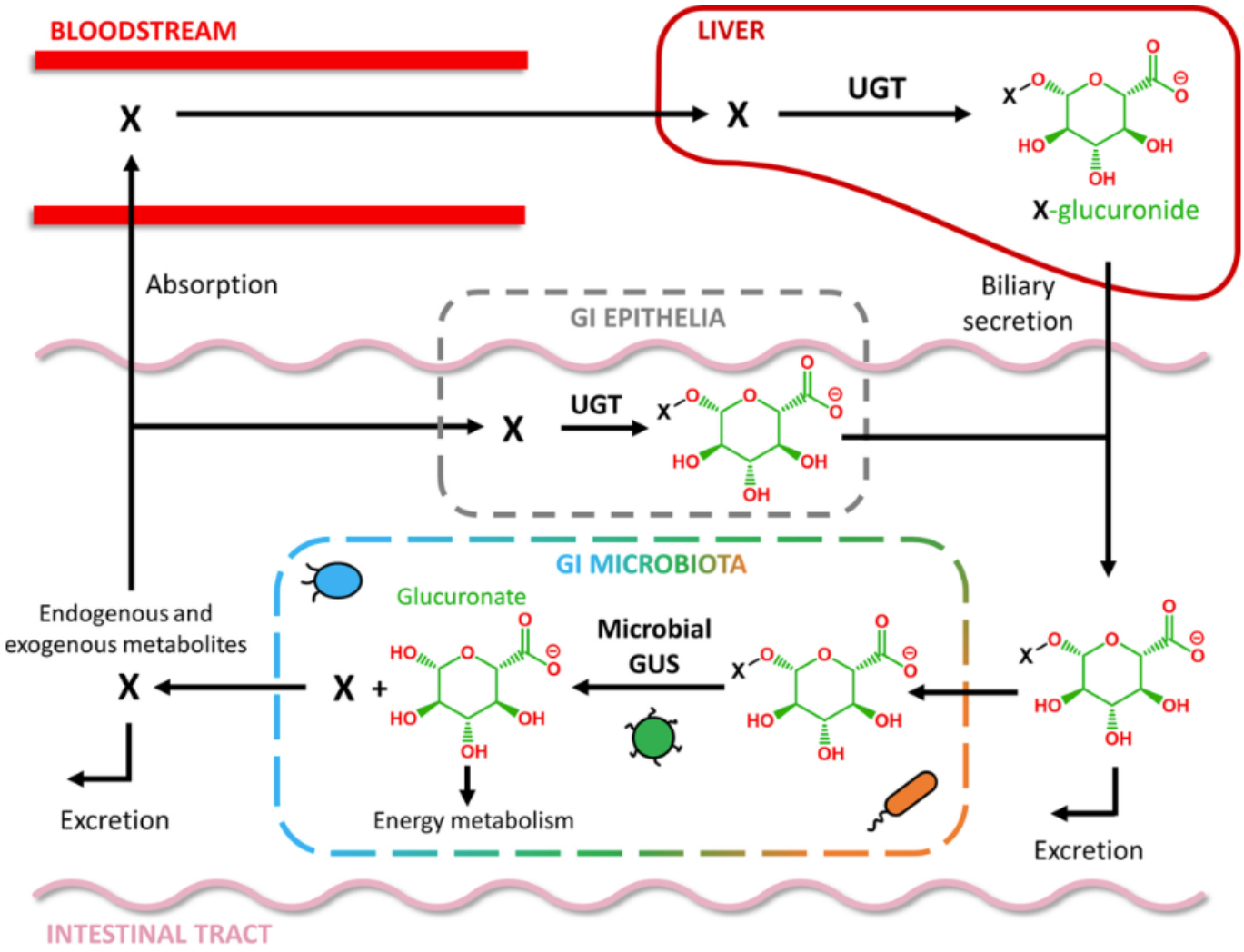

Figure 1.2: Enterohepatic recycling reverses phase II conjugation in the intestine
Hepatic conjugation produces glucuronides that enter the intestine through the biliary system. Human and bacterial βG cleave GlcA from a variety of substrates and transform hydrophilic substrates into lipophilic products. Clinical interest in intestinal βG focuses on xenobiotic recycling and the development of intestinal ulcers and severe diarrhea in patients. Therapeutics are commonly chemical inhibitors designed to target the diverse microbial βG that occupy the gut. A major question concerning enterohepatic recycling is not whether βG activity contributes to compound recycling but rather if the enzyme involved is prokaryotic or eukaryotic in nature. Figure derived in original format with no modifications and published by The American Society for Biochemistry and Molecular Biology, Inc. (Pellock & Redinbo, 2017).

1.4 The prostate and prostate cancer

1.4.1 βG in the prostate

The prostate gland develops from the embryonic urogenital sinus (UGS) (Cunha *et al*., 2018). As an exocrine gland, a major function of the prostate is the secretion of alkaline seminal fluid, which constitutes 30% of semen and nourishes the sperm (Zhang *et al*., 2018). Proper development and differentiation of the prostate depends on androgens and the ability to initiate downstream signalling events and transcription of target genes. These signalling molecules are involved in both health and disease, where a connection between androgens and PCa development was identified in the early 1940s (Heinlein & Chang, 2004; Huggins & Hodges, 1941). One mechanism for retaining androgens in the body is through recycling, often catalyzed by βG. In 1947, researchers first identified that βG is upregulated in a variety of cancers and may play a role in steroid recycling (Fishman & Anylan, 1947). Although this paper focused on estrogen metabolism, the presence of androgens may also stimulate βG upregulation in the body (Fishman & Farmelant, 1953). Investigation into prostatic βG shows that enzyme activity is elevated almost 4-fold in prostatic carcinoma compared to benign prostatic hyperplasia samples (Pearson *et al*., 1989). The upregulation of this recycling enzyme at the gene, messenger RNA (mRNA) and protein levels, in addition to elevated activity levels with cancer progression, suggests that it may play a role in recirculating local androgens, providing adequate fuel for growth of an androgen-dependent gland. As can be observed from literature cited above (1947, 1953, 1989), although initial findings were promising, consideration of βG has never been intensively explored in the context of PCa, and was last a focus of interest more than 30 years ago. This thesis builds on initial interest in βG and the potential role compound recycling may play in prostate cancer.

1.4.2 Prostate cancer epidemiology

Prostate cancer is the most diagnosed non-cutaneous cancer and the third leading cause of death among Canadian men (Canadian Cancer Society, 2021). In 2020, an estimated 23,300 men were diagnosed with PCa accounting for 20% of all cancer diagnoses. Roughly 1 in 9 Canadian males will develop the disease over their lifetime, and 1 in 29 will die from it (Canadian Cancer Society, 2021). Prostate cancer in Canada is not a rare cancer.

This cancer is a disease of the aging. Disease occurrence increases from roughly 1 in 350 for men below 50 years old to 1 in 52 for men between the ages of 50-59. The greater the age, the higher the incidence and mortality rate. In men over 65 years old, ~60% will develop PCa (Rawla, 2019). Additionally, worldwide estimates from 2018 indicate that PCa occurrence is greater in developed countries. However, these numbers may be inflated due to the increased access to novel diagnostic tools and screening procedures (Ferlay *et al*., 2019). The five- and ten-year survival rates for men in the United States diagnosed with localized PCa are both 98% respectively. However, if metastasis occurs, a steep drop in 5-year survival to 30% is observed (SEER Cancer Statistics, 2018). Globally, PCa incidence and mortality rates are either declining or stabilizing in many countries (Culp *et al*., 2020). While this trend is promising, estimates of PCa mortality are expected to double by 2040 due to the growth of an aging population worldwide (Ferlay *et al*., 2019).

Age is not the only risk factor that contributes to PCa development. Genetic, environmental and dietary factors play a role in disease progression (Rawla, 2019). Family history is a PCa risk factor where cancer incidence in an immediate family member increases the risk of development 2-3-fold (Whittemore *et al*., 1995). Cancer incidence also varies by race and ethnicity where data from the United States shows African American men are most likely to

develop PCa followed by Caucasian men with lowest occurrence in Hispanic and Asian men (Crawford, 2009). Moreover, tobacco and cigarette smoke and alcohol consumption are associated with PCa risk (Perdana *et al*., 2016). High consumption of saturated animal fat and red meat are linked to cancer risk as the elevated fat intake increases testosterone levels and meat cooking may promote the formation of mutagenic heterocyclic amines. However, while some dietary studies identify foods that may increase PCa risk, others indicate that some products may play a role in cancer prevention. It is suggested that catechins in green tea, isoflavones in soybeans and lycopene from tomatoes may have anti-carcinogenic properties that help decrease cancer risk (Perdana *et al*. 2016; Rawla, 2019).

1.4.3 Androgen receptor signalling and role in prostate cancer

The androgen receptor (AR) belongs to the steroid hormone nuclear receptor family. Other members of this family include the estrogen receptor, progesterone receptor, glucocorticoid receptor and mineralocorticoid receptor. The AR is a ligand-dependent transcription factor (TF) that promotes the downstream transcription of AR-regulated genes promoting growth and survival (Tan *et al*., 2015; Davey & Grossmann, 2016). The gene encoding the AR is located on the X chromosome and consists of 8 exons producing a functional 110-kDa protein receptor 919 amino acids in length. The receptor contains three functional domains: the N-terminal domain (NTD), DNA-binding domain (DBD) and the ligand-binding domain (LBD) (Tan *et al*., 2015). The NTD is the most variable domain whereas the DBD is the most conserved (Davey & Grossmann, 2016). Additionally, a hinge region connects the DBD and LBD of the AR (Tan *et al*., 2015). In its unbound form, the AR resides in the cytoplasm in a chaperone complex bound to heat-shock proteins. Androgen binding at the LBD induces a

conformational change resulting in the dissociation of the heat-shock proteins, the binding of importin-α and the translocation of ligand-receptor dimer to the nucleus (Dehm & Tindall, 2007; Tan *et al*., 2015). The DBD contains two zinc fingers which recognize specific target DNA sequences known as androgen response elements (ARE) found within promoter and enhancer regions of AR-regulated genes (Tan *et al*., 2015; Davey & Grossmann, 2016). Going from unbound cytosolic receptor to the downstream transcription of genes promoting cell growth and proliferation requires key signalling molecules known as androgens.

1.4.4 Androgens as signalling molecules

Androgens are steroid hormones critical to normal male sexual development and differentiation. These sex steroids are synthesized from cholesterol, primarily in the adrenal gland and the gonads, through a series of concerted enzymatic reactions (Hu *et al*., 2010). Dehydroepiandrosterone and testosterone are the main androgens synthesized at each site respectively. Specifically, major production of DHEA occurs within the zona reticularis of the adrenal cortex whereas testosterone is generated in the Leydig cells within the testes (Miller & Auchus, 2011). Hormone production is driven by adrenocorticotropic hormone (ACTH) in the adrenal cortex and luteinizing hormone (LH) in the testes (Hu *et al*., 2010). Compared to other steroids, androgens are a class of compounds composed of 19 carbons (Payne & Hales, 2004).

The prostate gland requires androgens to stimulate proper growth and development. Testosterone travelling to the prostate is carried through the circulation by binding to either sex hormone-binding globulin or albumin with differing affinity (Rosner *et al*., 1991; Baker, 2002). Within the prostate, 5α-reductase converts testosterone into the more potent androgen DHT (Bennett *et al*., 2010). The DHT molecular structure differs from that of testosterone due to the

removal of a single double bond lost through reduction (Tan *et al*., 2015). This chemical modification produces a ligand shown to have 2-fold greater binding affinity and 5-fold reduction in dissociation rate from the AR relative to testosterone (Grino *et al*., 1990). Additionally, DHT was 2.4 times more potent than testosterone at maintaining prostate weight and stimulating prostate epithelial cell function in rats (Wright *et al*., 1996). Therefore, DHT is the superior androgen and primary ligand for the AR in the prostate.

The balance of testosterone and dihydrotestosterone levels within the prostate is maintained by phase II metabolism. Glucuronidation of both androgens occur at the 17-hydroxy position to produce O-linked glucuronides. The transformation from lipophilic steroid to bulky, water-soluble glucuronide helps facilitate elimination from the body and provides a useful mechanism for regulating intraprostatic androgen levels. Of the UGT isoforms, UGT2B15 in the prostatic luminal cells and UGT2B17 in the basal cells metabolize and inactivate androgens for subsequent elimination (Bélanger *et al*., 2003; Meech *et al*., 2019).

1.4.5 Prostate cancer development

Cancer development is characterized by a set of distinctive features. The transformation of normal to malignant cells may arise from the following series of hallmarks: self-sustaining growth signals, inhibitory growth signal insensitivity, apoptosis evasion, limitless replicative potential, angiogenesis and ability to invade surrounding tissues (Hanahan & Weinberg, 2000). Subsequent hallmarks have been added to the list, namely the evasion of immune system recognition and reprogrammed energy metabolism (Hanahan & Weinberg, 2011). Importantly, cancer arises gradually, not suddenly. Genomic instability leads to the accumulation of mutations

that may promote the emergence of cancer hallmarks as described above. As cancer is a genetic disease, the development of PCa can be characterized by mutations to certain genes.

Malignant prostate formation is the result of a multi-step process involving a series of genetic mutations. While PCa is associated with a low mutational burden, the genetic alterations are substantial enough to contribute to disease (Grasso *et al*., 2012). Cancer development occurs through both non-AR and AR driven mutations. Firstly, the most common PCa genetic alteration involves E26 transformation-specific (ETS) members *ERG* and *ETV1* joined with transmembrane protease serine 2 (*TMPRSS2)* to produce *TMPRSS2-ERG* and *TMPRSS2-ETV1* gene fusions. The linkage of these genes removes the first four exons encoding the N-terminus of ETS transcription factors making transcription of the remaining exons under the control of the ARE for *TMPRSS2* (Sizemore *et al*., 2017). Moreover, gain of function mutations are observed in the proto-oncogene *MYC* and loss of function mutations in phosphatase and tensin homolog *(PTEN*) and retinoblastoma susceptibility (*RB1*) genes preventing the production of functional tumour suppressor proteins (Koh *et al*., 2010). Additionally, increased risk of PCa is associated with mutations in DNA repair genes (*BRCA1*, *ATM*, *CHEK2*, *BRCA2*) (Pritchard *et al*., 2016). Lastly, genetic alterations affecting the androgen signalling pathway include *AR* gene amplifications, gain of function mutations in AR coactivator *NCOA1/2*, loss of function mutations in AR corepressor *NCOR1/2* and *FOXA1* mutations (Wang *et al*., 2018). These genetic changes promote tumour growth and cancer progression. Overall, AR expression and signalling is crucial for primary PCa development and progression (Heinlein & Chang, 2004).

1.4.6 Localized prostate cancer treatment

Treatment options for PCa differ depending on whether the disease is localized to the prostate or has metastasized to surrounding tissues. Appropriate therapeutic decisions are made by considering the patient's initial prostate-specific antigen (PSA) levels, clinical disease stage, Gleason score, existing comorbidities and age (Keyes *et al*., 2013). Early stage localized PCa can be effectively managed through active surveillance (AS), radical prostatectomy (RP) and external beam radiation therapy (EBRT) depending on disease severity. The first approach, AS, focuses on continuous monitoring and benefits patients with low-risk disease. Importantly, classifying PCa cases as "low-risk" will vary depending on what criteria is used and the observed disease characteristics (Dall'Era *et al*., 2012). Most clinicians consider AS a suitable option for patients with low PSA levels (≤10 ng/mL), low Gleason score (≤ 6) and low clinical stage (≤ T2a) based on prostate biopsy sample (Dall'Era *et al*., 2012; Keyes *et al*., 2013). New biopsies are recommended every 6-12 months to determine whether disease is progressing and may require further treatment in the form of surgery or radiation. Radical prostatectomy is a common surgical approach to treating localized PCa and involves removing the entire prostate gland and surrounding tissues to clear the area of cancerous cells. Recent retrospective data shows men with localized PCa benefit more from RP than AS with a reduction in PCa mortality and mean 2.9-year life extension (Bill-Axelson *et al*., 2018). Moreover, EBRT is another approach to treat localized PCa that administers high dose radiation specifically to malignant cells while sparing surrounding healthy tissue. Ultimately, the therapeutic options for patients with localized disease are quite promising as RP and EBRT show 10-year overall survival (OS) of 88.9 and 82.6% respectively (Kibel *et al*., 2012). However, failure to remove or kill all metastatic cells may lead

to disease recurrence and the emergence of a more aggressive form of PCa. At this stage, alternative therapeutic options for PCa treatment must be considered.

1.4.7 Androgen deprivation therapy

Androgen deprivation therapy (ADT) is the gold standard systemic approach for treating metastatic and advanced local PCa. The main objective is the systemic reduction of androgens, which decreases available ligand to stimulate AR signalling and promote transcription of AR target genes. As PCa is a hormone-dependent cancer, and the prostate is dependent on androgens, ADT aims to eliminate the fuel source that drives cancer growth (Shafi *et al*., 2013). Both surgical and chemical approaches are used to achieve castration levels of serum testosterone defined as <50 ng/dL (Sharifi *et al*., 2005; Harris *et al*., 2009). The original ADT approach was bilateral orchiectomy, or the surgical removal of the testes. Serum testosterone levels after surgery were around 15 ng/dL (Crawford *et al*., 2019). However, more recent ADT options involve medical castration rather than surgical castration.

Drugs targeting the inhibition of the hypothalamic-pituitary-gonadal axis, androgen biosynthesis enzymes and the AR are now first-line treatment options (Figure 1.3). Luteinizing hormone-releasing hormone (LHRH) agonists, such as leuprolide and goserelin, play a role in feedback inhibition at the anterior pituitary gland to prevent the secretion of LH and the downstream production of testosterone in the Leydig cells of the testes (Crawford *et al*., 2019). Certain drugs function as CYP inhibitors, blocking testosterone synthesis from cholesterol. Abiraterone acetate is a commonly used selective CYP17 inhibitor, which does not suffer from the same toxicity effects associated with use of the anti-fungal ketoconazole as a non-specific CYP17A1 inhibitor (Teo *et al*., 2019; Rice *et al*., 2019). Anti-androgens are another branch of

ADT which function in the prostate as AR antagonists and do not impact circulating testosterone levels. First-generation antagonists include flutamide, bicalutamide, and nilutamide, which have been succeeded in recent years by second-generation compounds enzalutamide and apalutamide as improved AR antagonists (Harris *et al*., 2009; Rice *et al*., 2019). Lastly, finasteride acts as a 5α-reductase inhibitor, blocking the conversion of testosterone into dihydrotestosterone within the prostate.

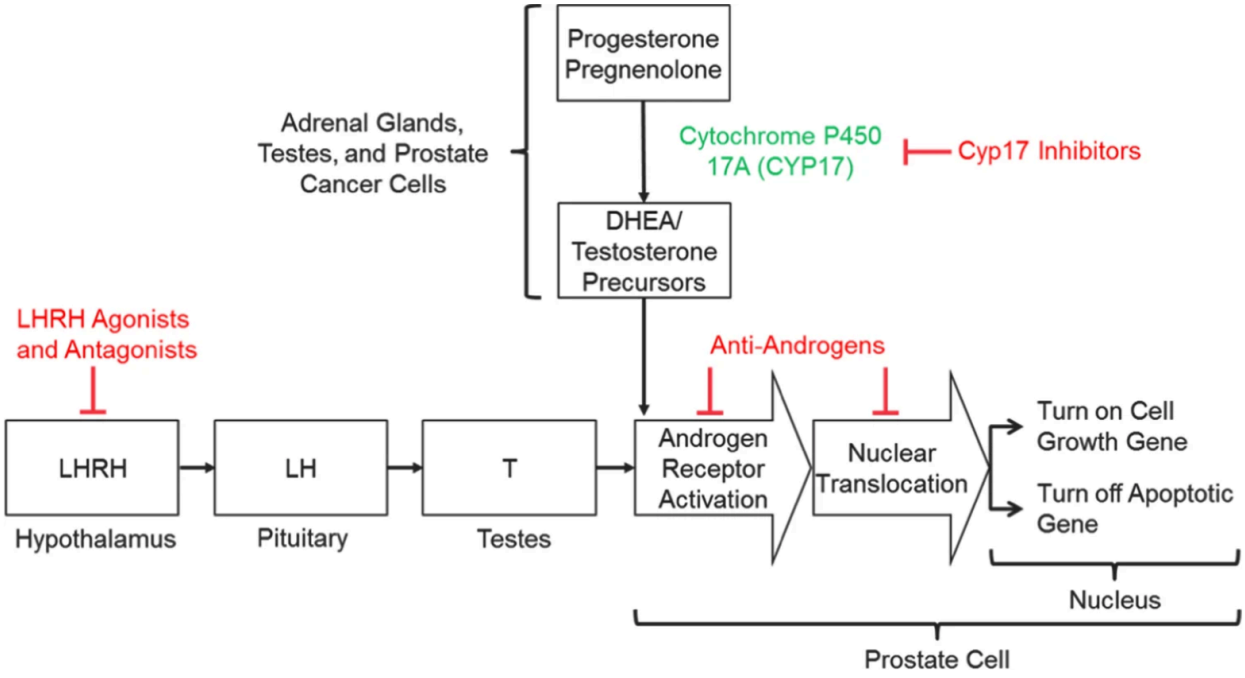

Figure 1.3: ADT inhibits distinct drug targets to reduce circulating testosterone level
Prostate cancer is an androgen-dependent disease and ADT aims to reduce testosterone and dihydrotestosterone levels to eliminate the main fuel source for cancer growth. Drugs target the hypothalamic-pituitary-gonadal axis, CYP enzymes and the AR receptor to prevent testosterone production and AR signalling events. Certain drug classes are designed to inhibit separate targets in different parts of the body, where the main objective is to suppress the transcription of AR target genes. Figure derived in original format with no modifications (Crawford *et al*., 2019). Reproduced with permission by CC-BY https://creativecommons.org/licenses/by/4.0/.

Many PCa patients benefit from ADT as shown by extended OS and improved quality-of-life. Treatment often provides patients with locally advanced or metastatic PCa relief from bone pain, reduction in spinal cord compression and ureteral obstruction, and decline in PSA

levels observed in 80-90% of metastatic cancer cases (Sharifi *et al*., 2005; Harris *et al*., 2009). However, these benefits are only transient and ADT, while initially effective at generating a therapeutic response, is not curative. Disease progression is commonly observed in patients after a median 2-3 years following ADT initiation (Harris *et al*., 2009). The time to disease relapse is more pronounced in patients with metastatic PCa, where ADT remains effective for 14-20 months before tumours become treatment-resistant (Sharifi *et al*., 2005; Shafi *et al*., 2013). The start of disease progression often marks an expected survival timeline of 16-18 months in PCa patients. However, 5-10% of ADT patients remain alive 10 years after starting ADT suggesting that the therapeutic effect and delayed onset of disease relapse will vary among individuals (Harris *et al*., 2009). The growing ineffectiveness of ADT, where PSA levels rise despite serum testosterone at castration levels, signals the emergence of castration-resistant prostate cancer (CRPC) (Crawford *et al*., 2019).

1.4.8 Castration-resistant prostate cancer

Disease progression coupled with ADT failure leads to CRPC. Prostate cancer may become androgen-independent, yet AR signalling remains active promoting further growth and proliferation through ligand-dependent and ligand-independent mechanisms (Figure 1.4) (Harris *et al*., 2009). The cross-talk between signalling pathways leading to AR activation poses a therapeutic challenge as the amount of potential drug targets expands in CRPC.

Ligand-independent activation of AR signalling is enhanced in CRPC compared to primary PCa. Non-androgenic pathways play a key role in stimulating AR signalling. Certain growth factors including insulin-like growth factor-1 (IGF-1), keratinocyte growth factor (KGF) and epidermal growth factor (EGF) function as ligands for receptor tyrosine kinases and initiate

signalling cascades through either the protein kinase B (Akt) or mitogen-activated protein kinase (MAPK)/extracellular signal-regulated kinase (ERK) pathways that result in the phosphorylation of the AR and its translocation to the nucleus (Culig *et al*., 1994; Arcaro, 2013). Additionally, cytokines like interleukin-6 (IL-6) also stimulate the non-androgenic activation of the AR, especially the NTD, through downstream activation of MAPK and signal transducer and activator of transcription 3 (STAT3) pathways (Ueda *et al*., 2002). Moreover, CRPC may survive by downregulating expression of retinoblastoma (RB) and phosphatase and tensin homologue (PTEN) tumour suppressors reducing cell cycle regulation and apoptotic signals (Sharma *et al*., 2010; Pienta & Bradley, 2006). Additionally, elevated AR expression was observed with increased expression of nuclear receptor coactivator 1 (NCOA1) and nuclear receptor coactivator 2 (NCOA2) leading to more frequent AR translocation to the nucleus (Gregory *et al*., 2001). The upregulation of AR coactivator Tat-interactive protein (Tip60) is androgen-sensitive and accumulates in the nucleus with decreased androgen levels (Halkidou *et al*., 2003). Lastly, certain AR splice variants with gain-of-function mutations are produced in a truncated form that lack the LBD and remain active, driving transcription of target genes in the absence of any available ligand. The most studied variant, AR-V7, shows elevated expression in CRPC (Watson *et al*., 2010). Other AR genetic alterations create ligand-dependent mechanisms leading to prolonged growth and proliferation signals.

Upregulated AR expression increases sensitivity to androgens, despite castration levels, making more receptor sites available for binding. This first ligand-dependent CRPC mechanism is referred to as the hypersensitive pathway and involves *AR* gene amplification, which is commonly observed in 25-30% of CRPC cases compared to only 1-2% in primary PCa (Pienta & Bradley, 2006; Taplin, 2007). Certain AR mutations also broaden ligand specificity, allowing

receptor activation through the binding of progesterone, estradiol, and use of anti-androgens nilutamide and hydroxyflutamide (Taplin, 2007). Two common AR mutations in the LBD involve the amino acid substitution of threonine for alanine at residue 877 and tyrosine for histidine at residue 874 (McDonald *et al*., 2000). Beyond AR modifications, alternative ligand-dependent mechanisms include elevated activity of 5α-reductase and the upregulation of steroidogenic enzymes involved in testosterone synthesis from cholesterol. The role of 5α-reductase is to increase available DHT reserves in the prostate, the more potent ligand for the AR. Following ADT, serum testosterone levels may decline by 95%, but DHT levels in the prostate remain relatively high and only drop by up to 60% (Pienta & Bradley, 2006).

The ligand-dependent pathways utilizing androgens to stimulate AR signalling mainly involve the ability to locally generate testosterone, which can be readily converted to DHT in the prostate. However, CYPs and 5α-reductase are not the only mechanisms that may be upregulated in CRPC. Androgen recycling is often overlooked as a ligand-dependent mechanism to activate the AR. Specifically, βG removes GlcA from testosterone and dihydrotestosterone glucuronides allowing active ligands to be recycled rather than eliminated. In a castration environment, where systemic androgen levels are low, the ability of tumours to reuse resources that act as a major fuel source for growth is advantageous. Therefore, this thesis focuses on the role androgen recycling may play in promoting PCa development and understanding how βG expression and activity change from normal prostate to primary PCa and CRPC.

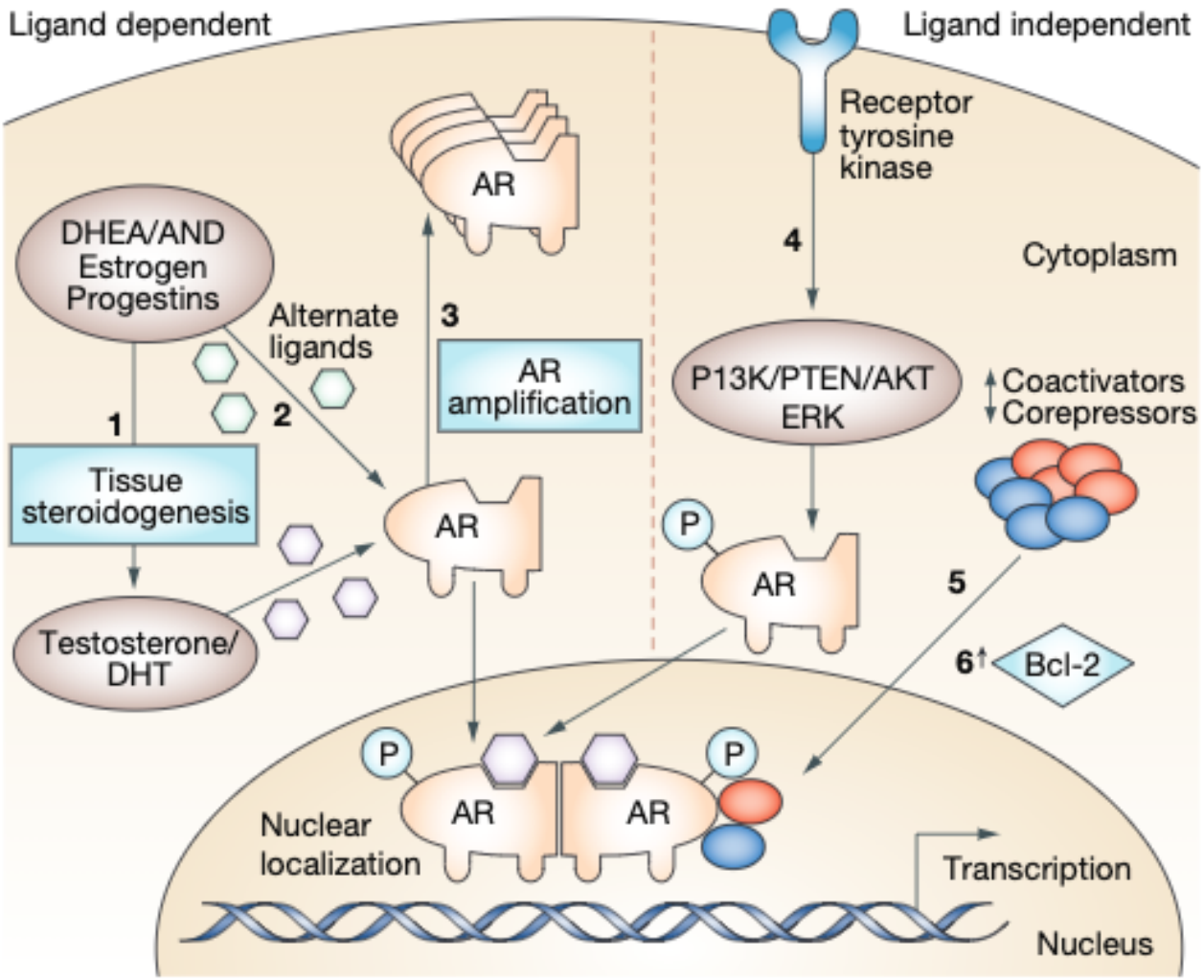

Figure 1.4: Ligand-dependent and ligand-independent mechanisms drive growth in CRPC Disease progression on ADT leads to CRPC where multiple mechanisms directly or indirectly activate AR signalling in the prostate cell. Cancer that becomes castration-resistant offers a therapeutic challenge as inhibition of one signalling pathway may allow an alternative pathway to stimulate the AR. Genetic alterations to the AR, broader ligand specificity, upregulation of AR co-activators and steroidogenic enzymes, and growth factor and cytokine signalling cascades all characterize the main mechanisms for cancer growth in CRPC. Figure derived in original format with no modifications and published by Macmillan Publishers Limited (Harris *et al*., 2009).

1.4.9 Chemotherapeutic approaches to castration-resistant prostate cancer treatment

Chemotherapeutic approaches are often provided to patients where hormonal therapies failed. Over the past four decades, a series of anti-cancer drugs have been administered to patients with metastatic castration-resistant prostate cancer (mCRPC). Estramustine, an estradiol that provides anti-androgen and anti-microtubule effects, was the first treatment option approved for mCRPC patients in 1981 (Nader *et al*., 2018; D'Amico, 2014). Mitoxantrone, a type II topoisomerase inhibitor, became the second approved therapy for treating mCRPC and the standard of care in 1996 after receiving approval based on palliative benefits, not survival benefits (Nader *et al*., 2018; Quinn *et al*., 2017). A combination therapy approach of mitoxantrone with prednisone provided pain relief, where an additional benefit of prednisone use was the reduction of adrenal DHEA production by inhibiting the release of ACTH from the pituitary through negative feedback inhibition (Tannock *et al*., 1989).

The first approved anti-cancer drug that showed OS improvement for mCRPC patients was docetaxel in 2004, where survivorship improved 1.9-2.4 months for patients receiving either docetaxel plus prednisone or docetaxel alone compared to mitoxantrone (Teo *et al*., 2019). While docetaxel remains the standard of care, a second-generation taxane approved in 2010, cabazitaxel, is commonly used in mCRPC cases that are unresponsive towards docetaxel treatment (Quinn *et al*., 2017). Many chemotherapeutic approaches to treating mCRPC are administered as combination therapies.

Docetaxel and cabazitaxel use in mCRPC treatment are often administered with other therapeutics. Previous phase III trials showing improved median survival in mCRPC patients used many different combinations including docetaxel with estramustine (SWOG 99-16), docetaxel with prednisone (TAX327), docetaxel with ADT (CHAARTED) and cabazitaxel with

prednisone (TROPIC) (Petrylak *et al*., 2004; Teo *et al*., 2019; Quinn *et al*., 2017). New combination chemotherapy approaches currently in phase II or phase III clinical trials include docetaxel with abiraterone (ABIDO), docetaxel with enzalutamide (CHEIRON), cabazitaxel with abiraterone (ABI-CABAZI) and cabazitaxel with enzalutamide (NCT02522715) (Quinn *et al*., 2017). These therapeutic options pair an anti-cancer drug with either a specific CYP17 inhibitor or AR antagonist. Despite the OS benefits observed in mCRPC patients receiving chemotherapy, treatment is not curative. Future therapies are needed to extend both OS and progression free-survival (PFS) and improve quality of life in patients suffering with mCRPC.

1.4.10 Radiopharmaceutical and immunotherapeutic approaches to systemic treatment of castration-resistant prostate cancer

Radiopharmaceutical therapy (RPT) is a targeted approach used to treat CRPC patients by delivering radioactive atoms to specific sites within the body (Sgouros *et al*., 2020). Compared to radiotherapy, this novel technique administers radiation internally at the target site. In 80% of CRPC patients, bone is the primary metastatic site where cancer spread disrupts the structural integrity of bone leading to increased pain (Body *et al*., 2015). Patients experiencing prolonged pain show a decrease in quality-of-life (Goyal & Antonarakis, 2012). First generation RPT in prostate cancer, strontium-89 and samarium-153, are bone-seeking β-emitters designed to irradiate bone metastases (Sgouros *et al*., 2020; Goyal & Antonarakis, 2012). While effective in palliative care, these intial therapies did not show any improvements to overall survival in CRPC patients (Teo *et al*., 2019; Goyal & Antonarakis, 2012). Additionally, β particles showed undesirable maximum tissue penetration which increased the risk of marrow toxicity (Goyal & Antonarakis, 2012).

The failure of strontium-89 and samarium-153 to increase survival shifted RPT from β- to α-emission. Radium-223 represented the next generation RPT as the first radiopharmaceutical to show improved survival in CRPC patients with symptomatic bone metastases (Goyal & Antonarakis, 2012). In the ALSYMPCA phase III trial, patients receiving radium-223 showed a significant improvement in median overall survival of 14.0 months versus 11.2 months in the placebo group (Parker *et al*., 2013). Besides targeted radiation, immunotherapy remains an effective systemic approach to treating mCRPC.

Clinically approved immunotherapies strengthen the immune system to recognize and destroy prostate cancer cells. Sipuleucel-T was the first cancer vaccine approved in 2010 by the United States Food and Drug Administration (FDA) for treatment of patients with asymptomatic or minimally symptomatic CRPC (Cheever & Higano, 2011). Historically, significant responses to immunotherapies are less common in prostate cancer compared to metastatic lung cancer, melanoma and renal cell carcinoma (Fay & Graff, 2020). The lack of therapeutic success is not fully understood but may be partly attributed to prostate cancer being a "cold" tumour with an immunosuppressive microenvironment (Fay & Graff, 2020).

Sipuleucel-T aims to modify immune cells to become more responsive to unique immunogenic antigens displayed by prostate cancer cells. More specifically, the vaccine contains a fusion protein, PA2024, that combines recombinant prostatic acid phosphatase (PAP) and granulocyte-macrophage colony-stimulating factor (Cheever & Higano, 2011; Fay & Graff, 2020). Incubation with PA2024 stimulates the production of PAP-specific T cells capable of identifying and killing prostate cancer cells that display PAP, a commonly expressed enzyme (Cheever & Higano, 2011). Phase III clinical trial APC8015 initially showed sipuleucel-T significantly improved median survival as patients in the treatment arm lived 25.9 months versus

21.4 months in the placebo arm (Small *et al*., 2006). Subsequently, IMPACT, a larger phase III trial reported a 4.1-month median survival extension where patients receiving sipuleucel-T lived 25.8 months compared to 21.7 months in the placebo group, accounting for a 22% reduction in mortality (Kantoff *et al*., 2010). Improvements to overall survival, not progression-free survival, led to approval of sipuleucel-T by the FDA. While the therapeutic arsenal for treating mCRPC remains limited, both RPT and immunotherapy approaches provide promise for improved efficacy with future treatment options.

1.4.11 Role of beta-glucuronidase in prostate cancer progression

The βG enzyme was first identified as elevated in cancer in 1947, but little to no follow-on work has been performed in PCa, reflecting βG's status as a somewhat "orphan" enzyme (Fishman & Anylan, 1947). Investigating the role of βG in PCa development aims to further the understanding of androgen, or other endobiotic, recycling pathways as important mechanisms for PCa progression and metastasis. By hydrolyzing O-linked glycosidic bonds, hydrophilic testosterone and dihydrotestosterone glucuronides are transformed into active, hydrophobic products available locally for subsequent binding to the AR. Importantly, androgen recycling leveraged by tumours to maintain a circulating reservoir of testosterone and dihydrotesterone suggests that βG inhibition may be of therapeutic interest to prevent tumours from reusing this fuel source to grow.

The initial laboratory interest for βG in androgen recycling, and its contribution to PCa, arose from genomic and transcriptomic data. Based on data analysis of large published databases by colleague Dr. Alexander Smith (*data not shown)*, βG copy number amplification is observed in 45% of CRPC cases, which is more than double the percentage found in PCa (Barbieri *et al*.,

2012). Additionally, *GUSB* expression is amplified in 0.5% of PCa cases and 2.5% of CRPC cases (Liu *et al*., 2018; Kumar *et al*., 2016; Abeshouse *et al*., 2015). These data showing increased βG copy number and gene expression led to investigating the expression and activity of this recycling enzyme at the protein level.

Chapter 3 of this thesis aims to understand changes in enzyme expression and activity across a range of cell lines and tissue lysates. Elevated βG expression and activity in samples ranging from normal, PCa and CRPC supports the role for androgen recycling in cancer etiology, progression and metastasis. The mechanism for this is not revealed in this thesis, but the underlying association is strongly confirmed at the protein expression and activity level for the first time. Additionally, the effects of lower pH in the lysosome and tumor microenvironment elevating βG activity were confirmed. These pH effects have not previously been accounted for, and may have resulted in underestimating the magnitude of βG recycling. Finally, differentials in the available model cell lines when studying UGT and βG have been identified, potentially guiding future *in vitro* model selection. Herein, it is intended to show that βG may in time present a therapeutic target to prevent or mitigate PCa progression and/or metastasis. Further investigation of the βG mechanism may also reveal other interactions of the enzyme with PCa pathways, some of which may function as androgen-independent. This thesis aims to provide support for the role of βG in PCa development, including its potential prognostic or diagnostic value as a biomarker.

Chapter 2: Beta-glucuronidase expression and activity in human body: implications for enterohepatic recycling

2.1 Introduction

Homeostasis of endo- and xenobiotics is maintained through elimination and recycling processes in the body. Endo- and xenobiotic levels are regulated through conjugation and deconjugation reactions catalyzed by UGT and βG and SULT and steroid sulfatase (STS) enzymes, respectively. The UGT/βG metabolic pathway involves the addition or removal of GlcA from a substrate, thereby modifying chemical hydrophilicity and elimination from the body. While βG is known to hydrolyze GlcA from a broad range of endo- and xenobiotic substrates, its expression and activity levels throughout the human body are poorly characterized. A contributing factor to lack of available data is that historically, inhibiting βG activity using saccharolactone has been standard protocol when assessing the rate of glucuronidation since the 1950s (Levvy, 1952). Minimal comparative data on enzyme expression and activity reduces the ability to make accurate comparisons between tissues in the human body (Sperker *et al.*, 1997). In this thesis, the first Aim was to determine βG expression and activity in a broad range of normal healthy tissues to establish a comprehensive enzyme profile in the human body. Identifying differences in UGT and βG activity across tissues led to the development of detoxification:recycling ratios for different organs describing the metabolic equilibrium and potential local and systemic toxicity concerns. Of particular interest were the UGT:βG results at pH 7.4 in intestinal tissue lysates, which prompted further exploration of enzyme activity in the gut.

The GI tract is home to a variety of pH environments ranging from more acidic in the proximal sections to more alkaline in the distal sections of the small and large intestines (Evans

et al., 1999; Fallingborg, 1999; Koziolek *et al.*, 2015). βG activity in intestinal tissue lysates was studied at 3 pH values: pH 7.4, pH 6.8 and pH 5.4. The latter pH value corresponds to the optimal pH for βG within the lysosome (Weyel *et al.*, 2000). However, optimal pH reported in the literature also extends to more acidic values between pH 4-5 (Awolade *et al.*, 2020; Islam *et al.*, 1999). The pH value 7.4 represents physiological pH of the cytosol and most other organelles, whereas pH 6.8 represents the slightly acidic pH environment in the small intestine and may be indicative of intestinal lysates where all organelles are lysed together (Evans *et al.*, 1999). In this chapter, human and bacterial βG activity is compared at pH 7.4, 6.8 and 5.4 to better understand the ability gut microbes have in cleaving glucuronides and determine whether contributions to enterohepatic recycling arise from both prokaryotic and eukaryotic βG.

The activity of βG was assessed in five non-pathogenic *E. coli* cell lysates at unique pH levels. Of microbial species composing the dynamic gut microbiota, *E. coli* βG is thoroughly studied where both structure and function are known (Biernat *et al.*, 2019; Little *et al.*, 2018). Importantly, optimal pH for *E. coli* βG is pH 7.4, which differs from that of the human version of the enzyme (Awolade *et al.*, 2020). This difference arises due to the presence of organelles and compartmentalization of function in eukaryotic cells. Although bacterial and animal βG are structurally different, the importance of cleaving glucuronic acid from substrates is reflected by the conserved nature of the enzyme across the animal kingdom (Figure 2.1A). Human βG resides within the lysosome and is distinguished by a lysosomal targeting motif whereas *E. coli* βG displays a unique loop structure near its active site and is found in the cytosol (Figure 2.1B,C) (Hassan *et al*., 2013; Wallace *et al*., 2010). Both enzymes are subject to different pH environments.

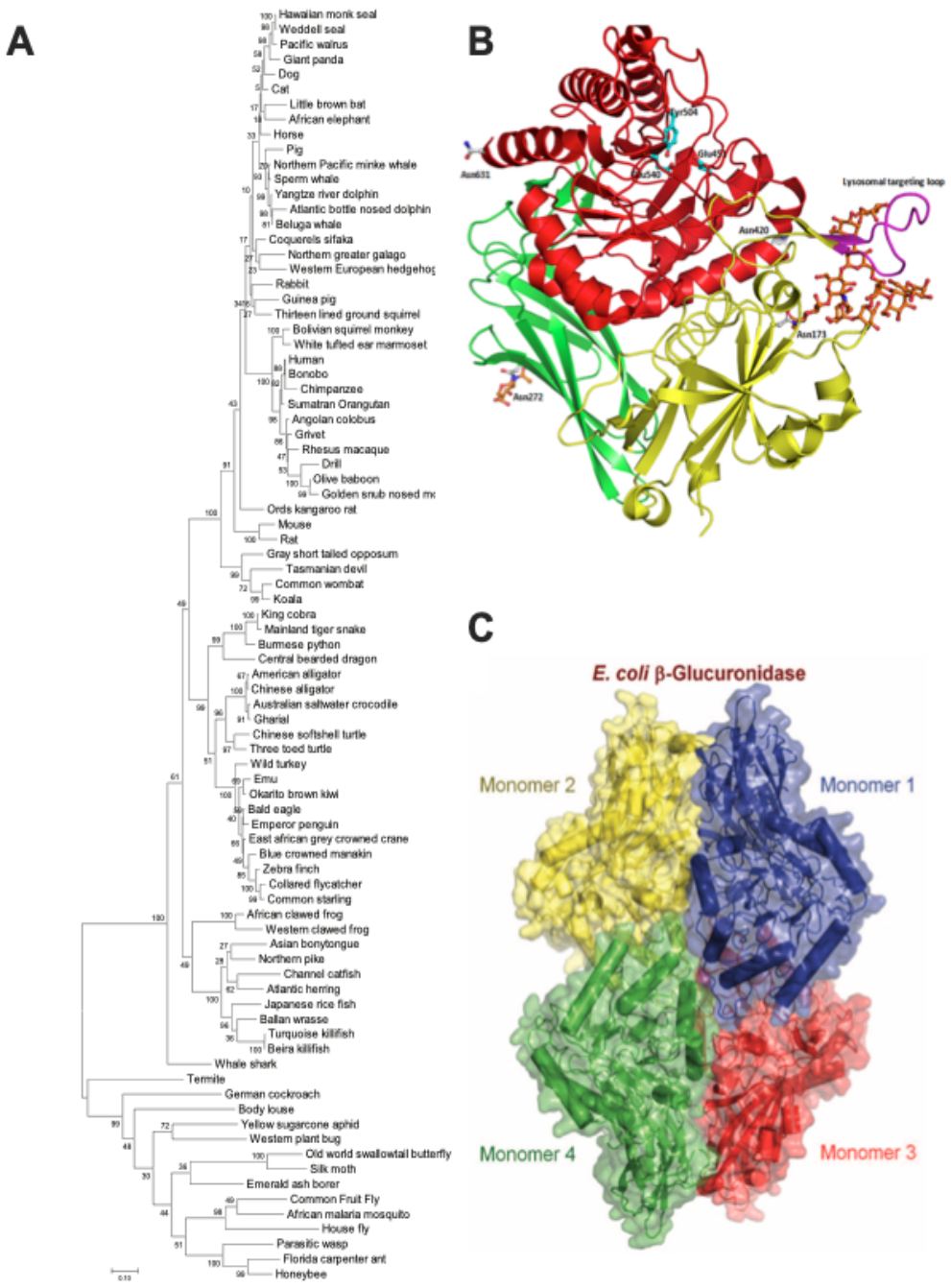

Figure 2.1: Structural differences and conserved nature of βG across the animal kingdom **(A)** Phylogenetic tree of the βG protein across the animal kingdom using insects as the outgroup. Tree produced using the Maximum Likelihood method based on the JTT matrix-based model (Jones *et al*., 1992). Bootstrap support is shown next to the branches. All positions with less than 95% site coverage were eliminated with a total of 552 positions in the final dataset. Evolutionary analyses were conducted in MEGA7 (Kumar *et al*., 2016) **(B)** Tetrameric structure of human βG with unique lysosomal targeting motif (Hassan *et al*., 2013). **(C)** *E. coli* βG structure is a tetramer characterized by distinct L1 loop structure near the active site (Wallace *et al*., 2010). Both figures are derived in original format with no modifications.

Glucuronide metabolism in the gut is likely due to both human and bacterial βG. Our research shows that the human version of the enzyme, at optimal pH, operates at comparable rates to some *E. coli* strains. Similar deconjugation rates helps support contributions to enterohepatic recycling being due, in part, to human βG. By investigating human intestinal βG activity, we have provided novel information on the role the eukaryotic enzyme may play in this recycling, as it is often overlooked by bacterial βG in species composing the gut microbiome. The inter-strain differences in βG activity at different pH values suggests that certain strains are more likely to contribute to enterohepatic recycling than others, especially in intestinal regions densely populated with microbes in a healthy gut (Figure 2.2A,B). The gut flora is not evenly distributed within the intestines as population density increases moving distally towards the large intestine (Gorbach, 1996).

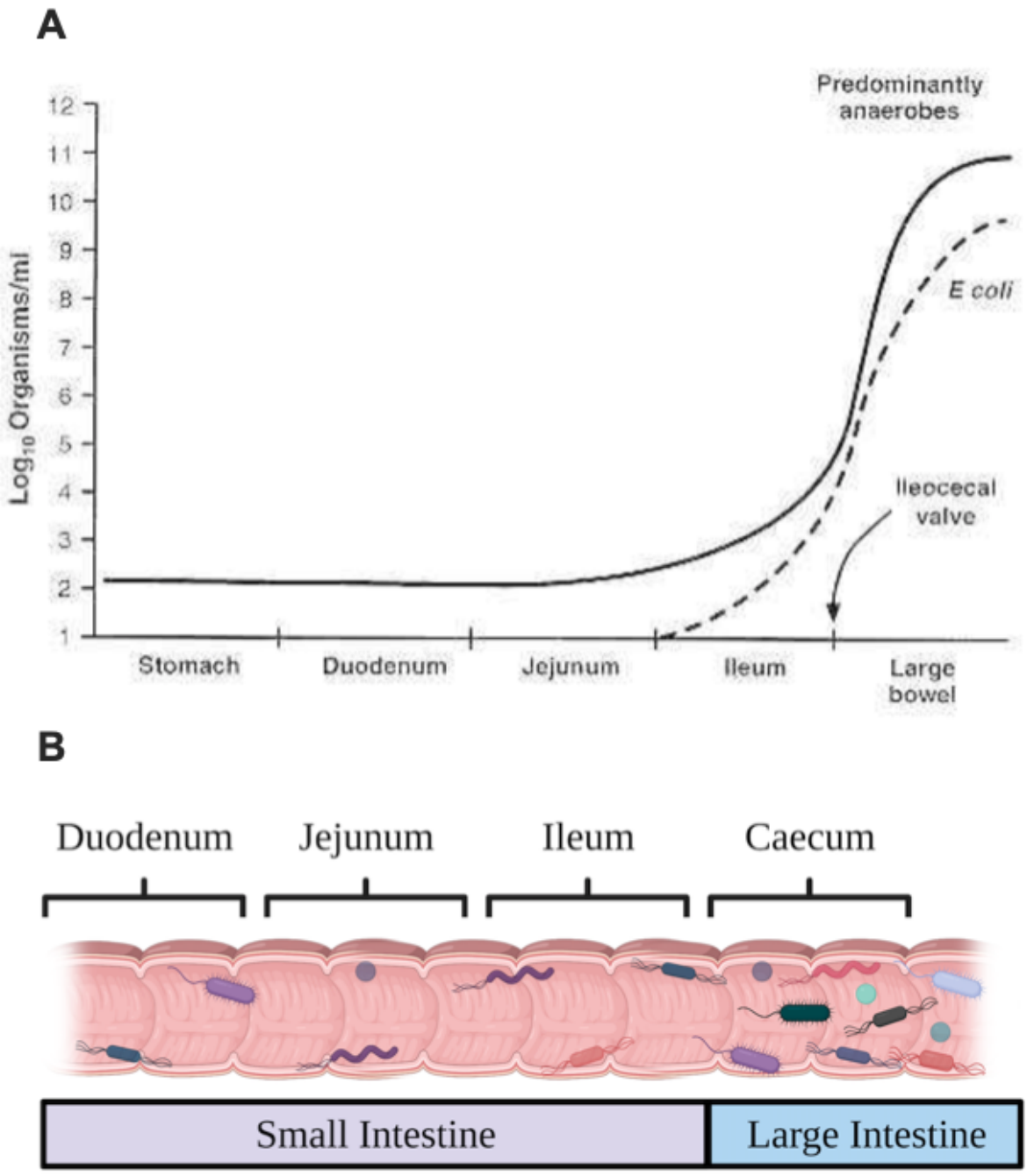

Figure 2.2: Intestinal microbes are densely populated in the caecum of a healthy gut
(A) Log scale for microbial populations residing in different intestinal regions. The upper GI tract including the stomach, duodenum and jejunum are scarcely populated with bacterial colonies. The caecum is rich with a diverse array of microbes, including *E. coli*, that thrive within this specific gut environment. Figure derived in original format with no modifications (Gorbach, 1996). **(B)** Visual representation showing the progressive increase in microbial density from the small intestine to proximal portion of the large intestine. Caecum represents the most densely populated region home to the most microbial diversity. Figure developed using BioRender.

Here we demonstrate that βG is differentially expressed and active across 14 distinct tissue types. An enzyme profile of the human body was developed using the following tissues: adrenal, alveoli, bronchus, caecum, duodenum, ileum, jejunum, kidney, liver, lymph node, placenta, pleura and prostate. Each tissue displayed unique UGT and βG activities resulting in a wide range of UGT:βG ratios. Of the 14 tissues studied, highest βG activity was observed in adrenal, caecum, liver and prostate. However, UGT activity remained 100-200 fold higher at pH 7.4, indicating that the metabolic equilibrium favoured conjugation in these tissues. Interestingly, the small intestine (duodeunum, jejunum and ileum) and proximal portion of the large intestine (caecum) showed lower UGT:βG activity, with the metabolic balance 7-17-fold in favour of conjugation at pH 7.4.

These results prompted further investigation of βG activity in the GI tract as a function of pH. Measuring enzyme activity at pH 7.4, 6.8 and 5.4, a 21-fold difference in βG activity was observed between certain strains, from levels comparable to the human enzyme in the SURE2 *E. coli* strain (230 pmol/min/mg) to levels 21-fold higher in the BigEasy TSA strain (4,854 pmol/min/mg) at optimal pH. Comparing βG activity at pH 7.4 and 5.4, human βG in intestinal tissue lysates increased 13-fold whereas *E. coli* βG increased less than 2-fold. Moreover, UGT:βG ratios, comparing UGT activity at pH 7.4 to βG activity at pH 5.4, were 1.2, 0.7, 1.2 and 0.8 for duodenum, jejunum, ileum and caecum respectively. These values suggest that the rate of elimination does not greatly exceed the rate of recycling in the GI tract. Jejunum and caecum are intestinal regions where kinetics favour βG activity and compound recycling. Increased recycling rates in intestinal regions may contribute to enterohepatic recycling, where βG activity in the gut regenerates active parent compounds with increased apparent half-life ($t_{1/2}$)

and decreased clearance. The extended presence of compounds retained in the body pose toxicity concerns and may require dosing alterations for certain drugs.

2.2 Materials and Methods

2.2.1 Chemicals and reagents

The following chemicals, reagents and supplies were used: 4-methylumbelliferone sodium salt (Cat#:A10337, Thermo Fisher, Ward Hill, MA, USA), 4-methylumbelliferyl-β-D-glucuronide (Cat#:M9130, Sigma Aldrich, Oakville, ON, CAN), alamethicin (Cat#:A4665, Sigma Aldrich, St. Louis, MO, USA), bovine liver βG (Cat#:G0251, Glucurase, Sigma Aldrich, St. Louis, MO, USA), uridine diphosphate-glucuronic acid (Cat#:U6751, Sigma Aldrich, St. Louis, MO, USA) and V79 cells (derived from Chinese hamster lung fibroblasts) (Sigma Aldrich, St. Louis, MO, USA) were used in fluorescent enzyme assays to determine total UGT and βG activity.

2.2.2 Human tissue samples and *E. coli* strains

All human tissue samples were derived from adults and were from healthy post-mortem donors. The majority (liver, spleen, lymph node, kidney, alveoli, bronchus, pleura, heart, placenta and adrenal) were obtained from the Hawai'i Biorepository (pools of n = 3). These samples were supplemented with commercial samples: brain (Cat#:NB820-59177, Novus Biologicals, Centennial, CO, USA), duodenum (Cat#:NB820-59257, Novus Biologicals, Centennial, CO, USA), jejunum (Cat#:NB820-59257, Novus Biologicals, Centennial, CO, USA), ileum (Cat#:NB820-59256, Novus Biologicals, Centennial, CO, USA), caecum (Cat#: NB820-59204, Novus Biologicals, Centennial, CO, USA) and prostate (Cat#:NBP2-47057,

Novus Biologicals, Centennial, CO, USA; Cat#:CP555253, OriGene Technologies, Rockville, MD, USA) were derived from single donors.

Non-surviving donors were consented into the Hawai'i Biorepository by next of kin, with approval for future research. Human ethics approval for use of all tissues used in this study was approved by The University of British Columbia Clinical Research Ethics Board (H14-00092).

BigEasy TSA and 10GF' strains were obtained from commercial vendor Lucigen (Middleton, WI, USA). The remaining *E. coli* strains (TOP10/P3, NEB10β, SURE2) were gifted by Dr. Peter Ruben from Simon Fraser University and collected from Dr. Tara Klassen's shuttered laboratory.

2.2.3 Western blot for βG in human tissue and bacterial lysates

Tissue lysates from individual human organs (20 μg for biorepository samples, 10 μg for commercial samples) and cell lysates from non-pathogenic *E. coli* strains (20 μg) were resolved on 6-12% sodium dodecyl sulfate-polyacrylamide gel electrophoresis (SDS-PAGE) under reducing conditions, transferred to polyvinylidene difluoride (PVDF) membranes with semi-dry transfer (Biorad, Hercules, CA, USA), then washed in Tris buffered saline with 0.5% tween-20 (TBS-T), pH 7.4. Membranes were immunoblotted with primary antibody (1:2500, 5% non-fat milk powder) against βG (Cat#:ab166904, Abcam, Cambridge, MA, USA) overnight at 4°C. Subsequently, membranes were washed with TBS-T before incubating with secondary antibody (1:3000-1:5000, 5% non-fat milk powder, 2% normal donkey serum (NDS)) for 1 hour at room temperature with gentle agitation. Membranes were rinsed in TBS-T to remove residual secondary antibody then incubated with Immobolin ECL Ultra Western horseradish peroxidase (HRP) Substrate (Millipore Corporation, Billerica, MA) for 2 minutes. Protein expression was

visualized using Alpha Innotech Fluorchem digital imaging system (San Leandro, CA, USA). Optical density analysis was performed using ImageJ software (NIH, Bethesda, MD, USA) as a means of quantifying target protein in each lane. Briefly, a drawing tool is used to construct a measurement area around each protein band to determine optical density. ImageJ software calculates the pixel density given for each lane and the resulting peaks are labelled as a percentage of total optical density. This analysis is applied to three separate membrane images where mean βG protein density for each tissue lysate (n=3) is reported. Optical density for each tissue lysate is normalized by total protein based on Coomassie blue stained gel protein bands and sample amount loaded.

Protein glycosylation differs between human and *E. coli* βG. Protein expression imaging shows human βG as a doublet whereas *E. coli* βG is present as a singlet. To investigate human βG glycosylation, samples were partially deglycosylated following incubation with endoglycosidase-H (EndoH). 20 µg of protein was combined with 0.5 µL denaturing buffer (New England Biolabs, Whitby, ON, CAN) and 3.5 µL mQH_2O in liver and adrenal samples. In prostate lysates, 8 µg of protein was combined with 0.5 µL denaturing buffer and 2.8 µL mQH_2O. Samples were denatured following heating at 100°C for 10 minutes before being centrifuged at 6000 revolutions per minute (RPM) and cooled for 7 minutes. Subsequently, samples were treated with 2 µL EndoH (New England Biolabs), 1 µL glycobuffer 3 and 2 µL mQH_2O. Control samples received additional 2 µL mQH_2O as substitute for EndoH. Samples were incubated at 37°C for 1 hour before being separated on 12% SDS-PAGE and western blotted as described above.

2.2.4 4MU assay – total UGT activity

Total UGT activity was determined by fluorescent biochemical assay (Collier *et al.*, 2000) with minor modifications. Briefly, 4MU is the fluorescent substrate metabolized by most human UGT isoforms using UDPGA as co-substrate. The assay is incompatible with UGT1A4 as 4MU is not a substrate and UDPGA is not a co-substrate for UGT3A1 (Uchaipichat *et al.*, 2004; Meech *et al.,* 2019). 1 µL alamethicin (0.050 mg/g tissue), 10 µL homogenized tissue lysate (0.5 mg/mL for adrenal and prostate, 5 mg/mL for all remaining samples), 10 µL 1mM 4MU and 69 µL 0.1 M Tris-HCl pH 7.4 containing 10 mM $MgCl_2$ were combined in a microplate well to a volume of 90 µL and pre-warmed to 37°C for 2 minutes. Activity assays were only performed at this pH level, which represents the cytosolic pH and optimal pH for UGT enzymes. The reaction was initiated with the addition of 10 µL 50 mM UDPGA for a final volume of 100 µL in each well. Reactions were continuously monitored at 37°C for 60 minutes at 355 nm excitation wavelength (λ_{exc}) and 460 nm emission wavelength (λ_{em}) using a FlexStation3 plate reader (Molecular Devices, Sunnyvale, CA). Samples were analyzed in triplicate on three separate occasions. Initial reaction velocities were calculated by least squares linear regression with substrate depletion, or decrease in fluorescence, serving as a marker for product formation. Fluorescence units (FU) were converted to concentrations by comparison to a 4MU standard curve. The intra- and inter assay coefficient of variation (CV) for the slopes of the standard curves were 4.9 and 13.4% respectively. Mean $R^2 = 0.995$. The assay was found to be linear between 42 – 47 µM 4MU per well using a 100 µL sample volume.

2.2.5 4MUG assay - βG activity

βG activity was assessed using a fluorescent biochemical assay with 4MUG as substrate (Trubetskoy and Shaw, 1999). Briefly, 10 µL homogenized tissue lysate (0.5 mg/mL for adrenal and prostate, 5 mg/mL for remaining samples) and 80 µL 0.1 M Tris-HCl with 10 mM $MgCl_2$ at either pH 7.4, pH 6.8, or pH 5.4 were added in a microplate well to study enzyme activity in increasingly acidic environments that more accurately represent the optimal pH of βG. Each solution was pre-warmed to 37°C for 2 minutes before reaction was initiated with addition of 10 µL 1mM 4MUG for a final volume of 100 µL in each well. Reactions were continuously monitored as described above using FlexStation 3 plate reader (Molecular Devices, Sunnyvale, CA). The intra- and inter assay CVs for the slopes of the standard curves were 7.6 and 11.2% respectively. Mean $R^2 = 0.995$. The assay was found to be linear between 1-10 µM 4MU per well using a 100 µL sample volume.

2.2.6 Statistical analysis

All values are shown as mean ± standard deviation (SD). βG and UGT activity results between samples were compared with Bonferroni's post hoc multiple comparison analysis using Prism 9.10 for MacOS X (Graph Pad Prism, San Diego, CA, USA). Assessing enzyme activity changes for the same sample at different pH levels was measured by two-way analysis of variance (ANOVA) whereas comparing enzyme activity of different samples at the same pH was analyzed using one-way ANOVA. Differences were considered statistically significant if $p < 0.05$.

2.3 Results

2.3.1 Expression profiles of βG in human tissue and bacterial cell lysates

Protein expression of βG was observed in all tissue lysate samples excluding brain and heart (Figure 2.3A,B). Protein expression was also determined in five non-pathogenic *E. coli* strains. Clear βG expression is shown in all cell lysates tested (Figure 2.3C).

Modifications to human βG glycan chains using EndoH were performed to investigate differential glycosylation and the detection of protein expression as a doublet band. Liver, adrenal and prostate lysates subject to EndoH partial deglycosylation showed a protein band around 75 kDa whereas control samples without the deglycosylation enzyme were depicted at 78 kDa (Figure 2.5). More specifically, the ability of EndoH to target and remove high mannose, simple N-linked glycans from asparagine residues on the βG protein results in protein appearance as a singlet, indicating that βG is post-translationally modified in human tissues by N-glycosylation.

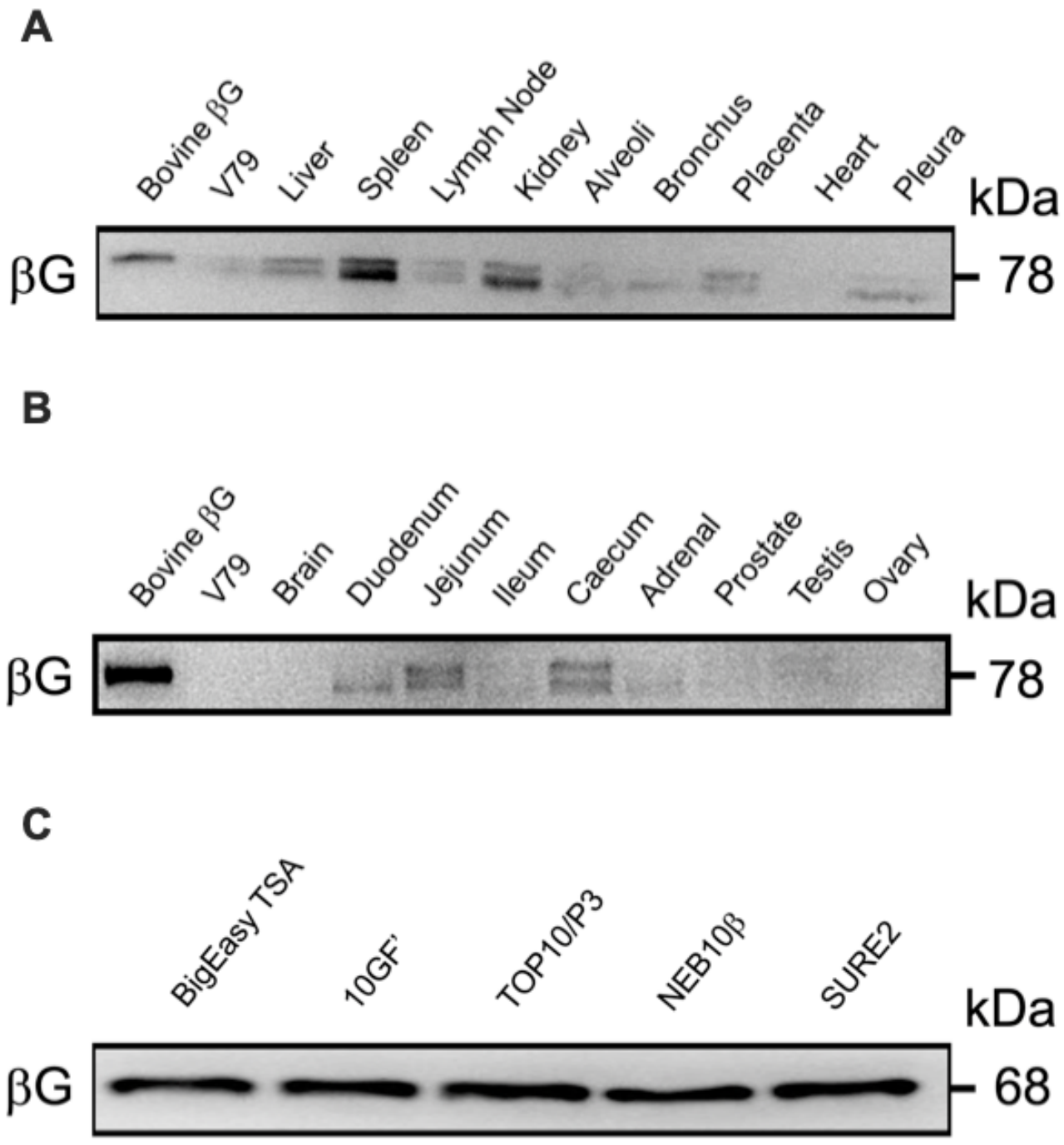

Figure 2.3: Human and *E. coli* βG expression across tissue and cell lysates
Western blot performed on human tissue and bacterial cell lysates to characterize expression of eukaryotic and prokaryotic βG. **(A,B)** βG expression in human tissue lysates **(C)** βG expression in non-pathogenic *E. coli* strains. Purified bovine βG and V79 cell lysates served as positive and negative controls.

Normalized optical density analysis showed βG expression was greatest in the spleen followed by in order: jejunum > liver > lymph node > caecum > lung pleura > placenta > duodenum > lung alveoli > kidney > lung bronchus > adrenal > ileum > prostate, with no detection in brain and heart lysates (Figure 2.4A). There were no significantly different changes ($p > 0.05$) in optical density when comparing βG expression across duodeunum, jejunum, ileum and caecum tissue lysates by one-way ANOVA. Moreover, in *E. coli* cell lysates, normalized optical density was greatest in SURE2 strain followed by TOP10/P3, NEB10β, 10GF' and BigEasy TSA. Analysis by one-way ANOVA with multiple comparisons showed that density differences in βG expression were not significantly different ($p > 0.05$) between SURE2 and any other *E. coli* strain (Figure 2.4B).

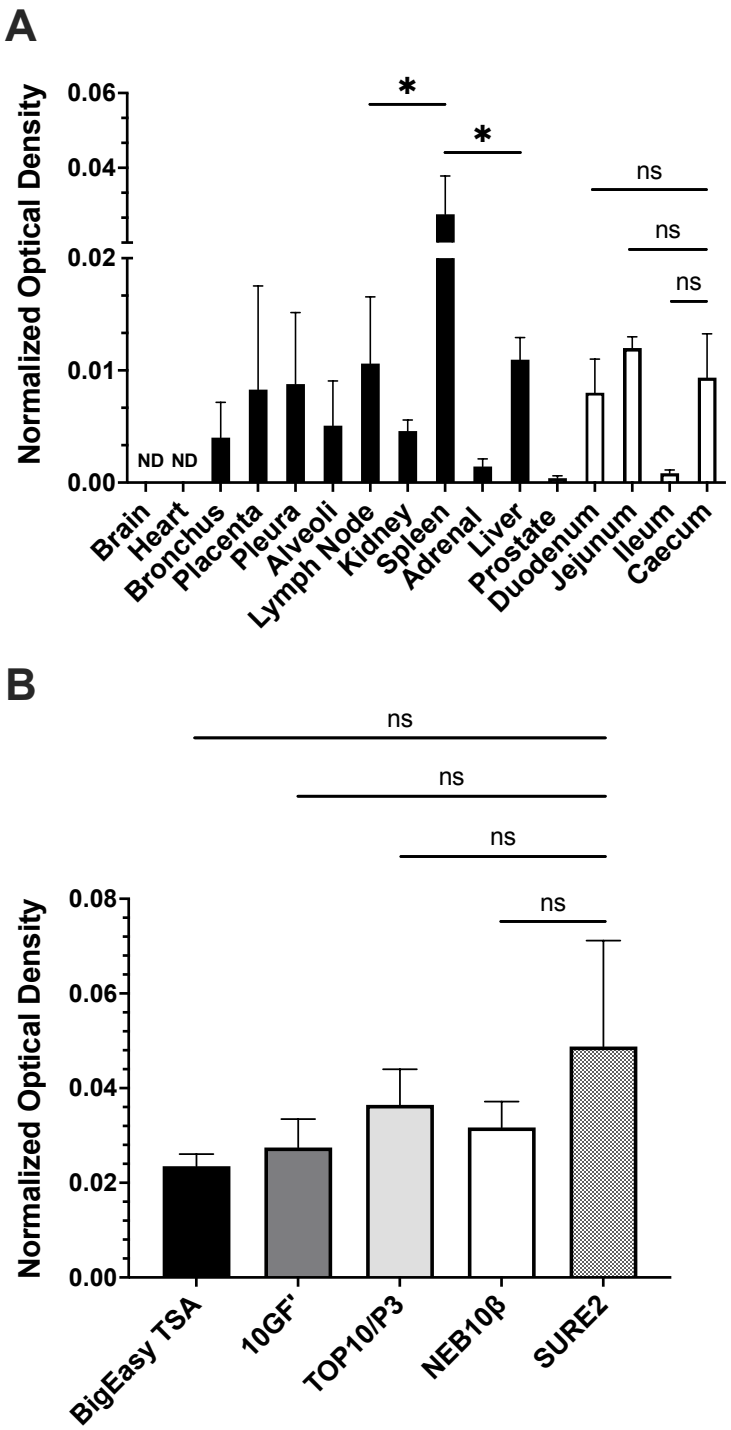

Figure 2.4: Normalized optical density of βG expression determined by western blot
Protein expression for each sample was normalized by total protein using ImageJ software. Analysis of each tissue or cell lysate was performed at n=3. **(A)** Normalized optical density of βG expression across all human tissue lysates. Density comparisons between intestinal tissue samples were not significant ($p>0.05$, one-way ANOVA). **(B)** Normalized optical density of bacterial βG expression in *E. coli* cell lysates. No significant difference in optical density were observed between bacterial strains ($p>0.05$, one-way ANOVA). Error bars are mean ± SD.

2.3.2 Post-translational modifications of βG protein in human tissue lysates

Investigation of βG glycosylation status using EndoH revealed differential appearance of singlet and doublet bands depending on the tissue. All samples show similar protein migration, where EndoH samples occur around 75 kDa and control samples at 78 kDa (Figure 2.5). The detection of a doublet occurs with each control sample, irrespective of tissue lysate used. However, observable differences between unique tissue types are shown in EndoH samples where protein bands in liver lysates occur as a singlet (Figure 2.5A). For both adrenal and prostate, βG bands retain the doublet at 75 kDa (Figure 2.5B,C). This data shows distinct glycosylation patterns across different tissues suggesting that βG glycosylation is driven by tissue-specific regulation.

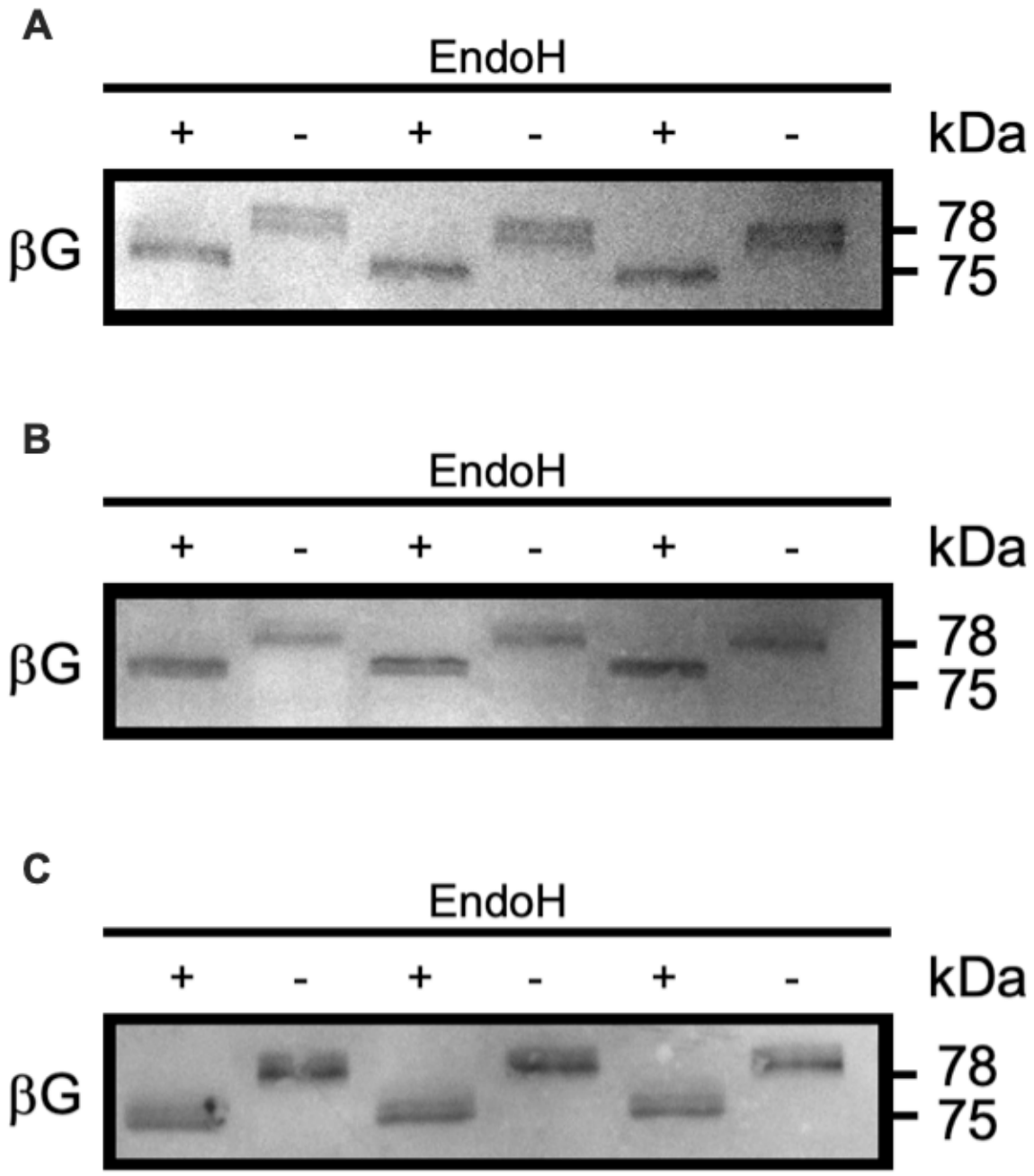

Figure 2.5: Investigation of βG glycosylation status across distinct tissue lysates
Samples were either incubated with EndoH or served as controls to investigate changes to βG glycan chains. Control samples are shown at 78 kDa and EndoH samples at 75 kDa. Liver and adrenal samples were run at n=3 whereas prostate samples are n=2. **(A)** Glycosylation studied using βG in human liver lysates treated with or without EndoH. Liver samples subject to EndoH appear as singlets whereas control samples are shown as doublets. **(B)** Glycosylation status of βG in adrenal lysates treated with or without EndoH. All samples are shown as doublets. **(C)** Investigation of βG glycosylation in prostate lysates with or without EndoH. Both positive and negative control samples appear as doublets.

2.3.3 Enzyme activity and comparison of UGT:βG in human tissue lysates at physiological pH

2.3.3.1 Total UGT activity across human tissue lysates at pH 7.4

Total UGT activity was determined across 16 distinct tissue types using 4MU as a fluorescent substrate. Greatest enzyme activity was observed in adrenal (2.29 ± 0.16 nmol/min/mg), followed by prostate (1.51 ± 0.17 nmol/min/mg), liver (1.24 ± 0.12 nmol/min/mg) and kidney (0.92 ± 0.24 nmol/min/mg) (Figure 2.6A). Adrenal UGT activity is significantly greater ($p < 0.0001$) than all other tissue samples tested. Excluding adrenal, prostate, liver, and kidney tissue lysates, UGT activity levels in the remaining 12 samples were not significantly different ($p > 0.05$) from each other. Moreover, differences in UGT activity for the intestinal tissue lysates (dudoenum, jejunum, ileum and caecum) were not significantly different ($p > 0.05$) (Figure 2.6A). An enzyme activity trend in the intestinal tissues was observed where UGT activity decreased moving distally through the small intestine before spiking in the caecum, the proximal portion of the large intestine. Statistical results were obtained using one-way ANOVA with Bonferroni post hoc test.

2.3.3.2 βG activity across human tissue lysates at pH 7.4

βG activity was calculated in unique tissue types using 4MUG as substrate in fluorescent assays. Highest enzyme activity was observed in the prostate (13.79 ± 1.80 pmol/min/mg), with slightly lower levels in the caecum (12.25 ± 1.17 pmol/min/mg), liver (12.15 ± 1.25 pmol/min/mg), adrenal (11.93 ± 0.67 pmol/min/mg), spleen (10.96 ± 0.78 pmol/min/mg) and kidney (10.42 ± 1.77 pmol/min/mg) (Figure 2.6B). βG activity in the prostate is not significantly different ($p > 0.05$) to the tissue samples described above. All remaining tissues, with the

exception of enzyme activity in the duodenum compared to ileum ($p < 0.05$), showed lower activity levels that were not significantly different from each other ($p > 0.05$). Compared to UGT activity, where data was reported for 16 distinct tissue types, βG activity was calculated for 14 unique tissue types where no activity was detected in brain or heart samples. Moreover, βG activity in the intestine progressively decreased along the small intestine before a sharp increase was observed in the caecum. This increase in caecum enzyme activity showed a significant difference in activity level when compared to jejunum ($p < 0.05$) and ileum ($p < 0.0001$), but did not show a significant difference when compared to duodenum ($p > 0.05$) (Figure 2.6B). All statistical analyses were performed using one-way ANOVA with Bonferroni post hoc test.

Next, we investigated the correlation between βG expression and activity across human tissue lysates. Optical density values obtained using ImageJ provided expression data whereas 4MUG assay results at pH 7.4 provided activity data. Our data suggest that βG expression and activity in 14 distinct tissue types is weakly correlated ($R^2 = 0.057$, $p = 0.129$) (Figure 2.6C).

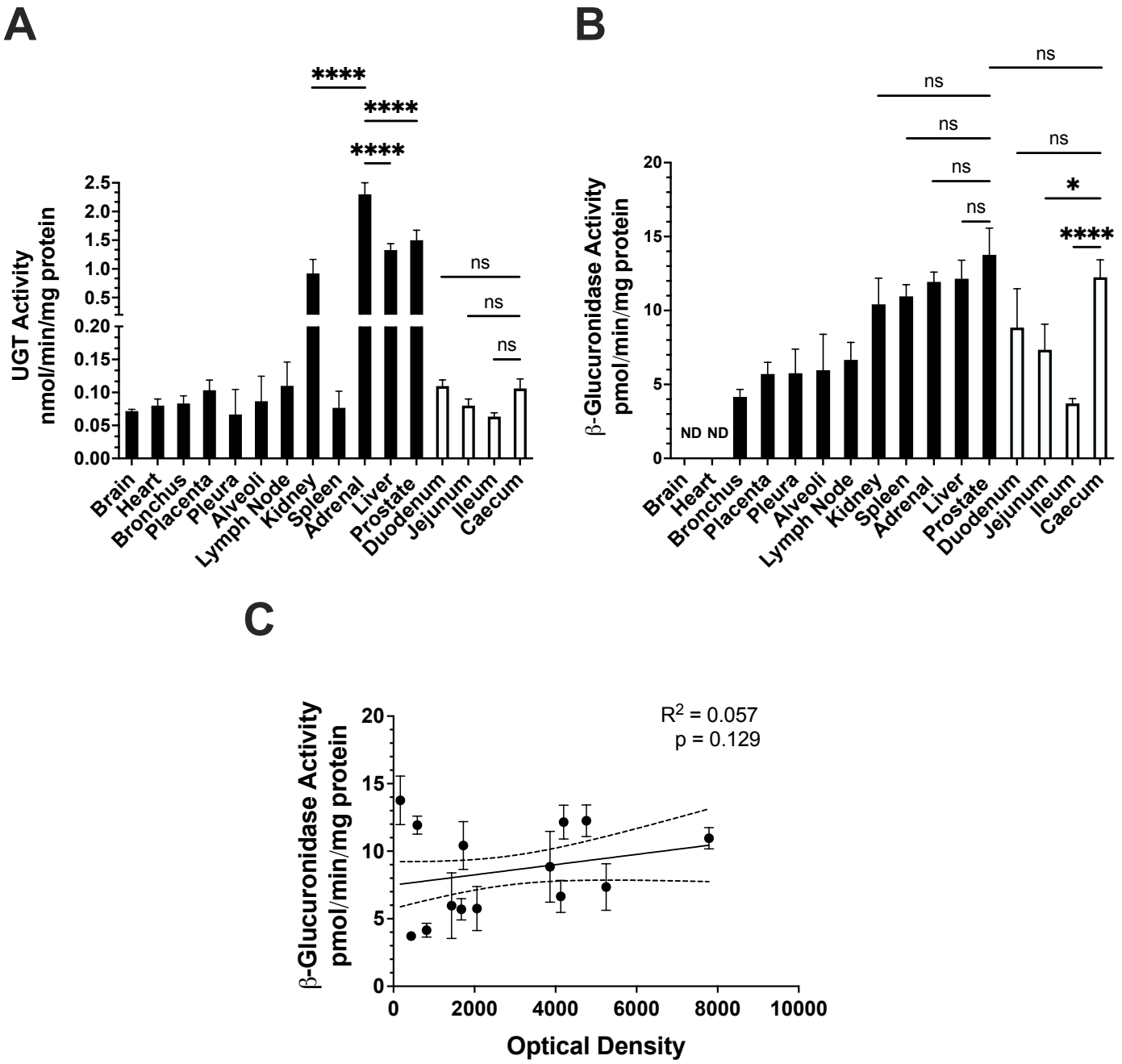

Figure 2.6: Human UGT and βG activity and correlation between expression and activity Fluorescent biochemical assays were conducted to determine **(A)** UGT activity in all 16 distinct tissue types at pH 7.4. There were no significant difference in UGT activity across the intestinal tissue samples. NS = not significant. **** = $p < 0.0001$. **(B)** βG activity across 14 unique tissue lysates at pH 7.4. Intestinal enzyme activity showed significant differences between caecum and both jejunum and ileum, but no significant difference when compared to duodenum. ND = not detected. NS = not significant. * = $p < 0.05$, **** = $p < 0.0001$. **(C)** βG activity plotted against protein expression for all tissue types excluding heart and brain. Expression and activity are weakly correlated. Solid line is regression and dotted line is 95% confidence interval.

2.3.3.3 Detoxification:recycling across all tissue lysates

Within each tissue, levels of endogenous and exogenous compounds are balanced through detoxification (UGT activity) and recycling (βG activity). The detoxification:recycling ratio describes metabolic balance between whether a compound undergoes conjugation, and is subsequently eliminated from the body, or may undergo recycling and be reabsorbed into the systemic circulation. UGT isoforms are more abundant and active than βG, suggesting that the metabolic equilibrium at pH 7.4 favours detoxification. Of 14 unique tissue types, it was determined that ratios differ broadly, ranging from 7-fold greater conjugation rate in the spleen to 192-fold greater conjugation in the adrenal gland at pH 7.4 (Table 2.1). All tissues show ratio values greater than 1 suggsting that the rate of detoxification exceeds the rate of recycling in each tissue. Classic metabolic tissues such as liver and kidney, in addition to adrenal gland and prostate, show the highest levels of both UGT and βG activities (Figure 2.6A,B) where the magnitude of UGT activity greatly outweighs βG activity and the rate of recycling at physiological pH.

Table 2.1: Detoxification:recycling ratios across unique human tissue types at pH 7.4

Tissue	Total UGT activity (pmol/min/mg)	βG activity (pmol/min/mg)	Detoxification:recycling
Brain	71.6	**ND**	-
Heart	80.0	**ND**	-
Spleen	76.7	11.0	7.0
Caecum	106.0	12.3	8.6
Jejunum	80.0	7.4	10.8
Pleura	66.7	5.8	11.5
Duodenum	109.6	8.8	12.5
Alveoli	86.7	6.0	14.5
Lymph Node	110	6.7	16.4
Ileum	63.3	3.7	17.1
Placenta	103.3	5.7	18.1
Bronchus	83.3	4.2	19.8
Kidney	920.0	10.4	88.5
Liver	1243.3	12.2	101.9
Prostate	1507.5	13.8	109.2
Adrenal	2287.4	11.9	192.2

Importantly, there is a disconnect between the highest levels of observed βG activity (prostate > caecum > liver > adrenal) and the levels of protein expression (jejunum > ileum > liver > lymph node); with only liver having highest expression and activity. This is not unprecedented in the glucuronidation field, where UGT protein expression seldom correlates to activity (Miyagi & Collier, 2007; Miyagi & Collier, 2011, Miyagi *et al*., 2012). Recent data from our laboratory and others suggests that post-translational modification via N-glycosylation [as shown here] (Liu 2021, *unpublished data*) as well as protein-protein interactions (Liu *et al*., 2020) may account for the mRNA/protein/activity disconnect.

2.3.4 The role of βG in enterohepatic recycling

2.3.4.1 Human βG activity in intestinal tissue lysates as a function of pH

The intestinal regions provide an interface between human and bacterial cells where βG activity may be due to both human and bacterial enzymes. More specifically, the optimal environments for which βG operates in eukaryotes and prokaryotes is different. In humans, βG resides within lysosomes of the cell, which provide more acidic environments than that of the cytosol. Understanding the contribution human βG may have on enterohepatic recycling requires investigating activity in intestinal tissue lysates at an optimal pH. To address this, we examined enzyme activity at three pH levels: pH 7.4, pH 6.8 and pH 5.4. The first value, pH 7.4, resembles the slightly alkaline environment of the cytosol, where activity data at this pH was previously reported above (Figure 2.6B). pH 6.8 represents the slightly acidic environment seen in the proximal portion of the small intestine (Evans *et al.*, 1999). Lastly, pH 5.4 represents the acidic environment within the lysosome and serves as the optimal pH for human βG (Weyel *et al.,* 2000).

Intestinal βG activity was compared at each unique pH level. Focusing on caecum, which shows greatest enzyme activity at each pH tested, no significant difference in enzyme activity was observed comparing values at pH 7.4 to pH 6.8 ($p > 0.05$). However, significant differences in activity were observed between pH 6.8 and pH 5.4 ($p < 0.0001$) and between pH 7.4 and pH 5.4 ($p < 0.0001$) (Figure 2.7A). This trend occurs in the other three intestinal tissues where the only non-significant difference in enzyme activity occurs between pH 7.4 and pH 6.8. Moreover, comparing enzyme activity across tissue samples at pH 7.4, βG activity was greatest in the caecum (12.3 ± 1.2 pmol/min/mg) followed by duodenum (8.8 ± 2.6 pmol/min/mg), jejunum (7.4 ± 1.7 pmol/min/mg) and ileum (3.7 ± 0.3 pmol/min/mg). Enzyme activity in the caecum was

significantly greater than the level in the jejunum ($p < 0.05$) and ileum ($p < 0.001$) (Figure 2.7B). Furthermore, caecum βG activity at pH 6.8 was highest (20.8 ± 3.1 pmol/min/mg) where activity decreased to jejunum (15.3 ± 4.1 pmol/min/mg), ileum (11.7 ± 1.7 pmol/min/mg) and lastly to duodenum (9.4 ± 4.5 pmol/min/mg). Enzyme activity in the caecum was significantly greater than that of duodenum and ileum ($p < 0.05$), but not when compared to jejunum ($p > 0.05$) (Figure 2.7C). Lastly, βG activity at pH 5.4 decreased from caecum (141.4 ± 14.3 pmol/min/mg) to jejunum (117.2 ± 9.1 pmol/min/mg) and duodenum (88.4 ± 23.3 pmol/min/mg), down to ileum (51.3 ± 4.2 pmol/min/mg). Enzyme activity in the caecum was significantly greater than duodeunum ($p < 0.01$) and ileum ($p < 0.001$), but not jejunum ($p > 0.05$) (Figure 2.7D). Analysis of enzyme activity in a specific tissue across multiple pH values was performed using two-way ANOVA with Bonferroni post hoc test. In contrast, one-way ANOVA with Bonferroni post hoc test was used to determine significant differences between tissue samples at same pH.

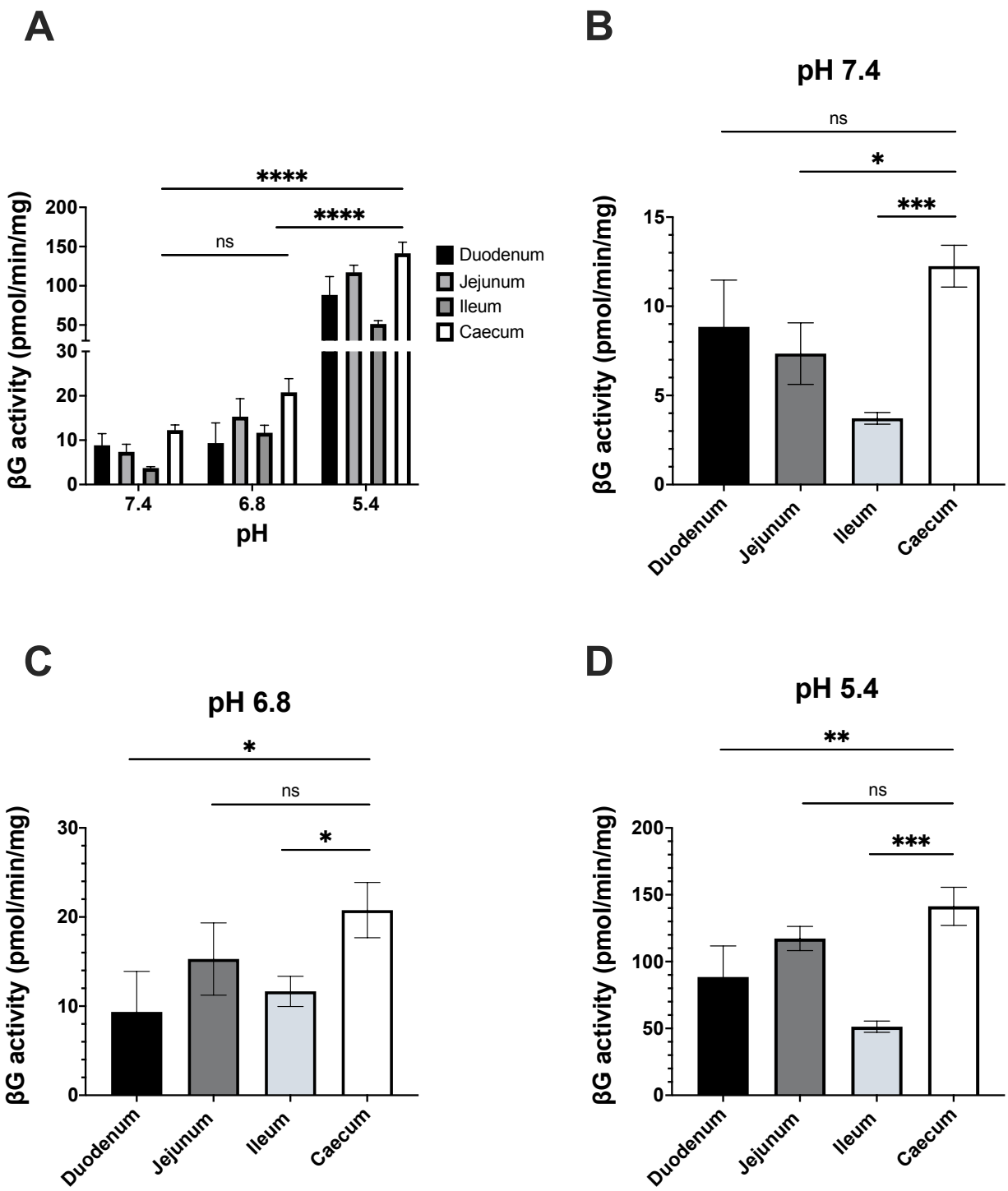

Figure 2.7: The effect of pH on human intestinal βG activity

4MUG fluorescent assays were run in triplicate on three separate occasions to determine **(A)** βG activity in intestinal tissue lysates measured at pH 7.4, 6.8 and 5.4. **(B)** Enzyme activity differences between intestinal tissues at pH 7.4. **(C)** Comparison of βG activity across intestinal tissues at pH 6.8. **(D)** Intestinal βG activity differences at optimal pH. NS = not significant. * = $p < 0.05$, ** = $p < 0.01$, *** = $p < 0.001$, **** = $p < 0.0001$.

The activity of βG in human intestinal tissue lysates increased as pH decreased. As enzyme activity approached optimal pH, detoxification:recycling ratios decreased. Compared to initial ratios at pH 7.4, βG activity increase at pH 6.8 resulted in 1-3 fold lower values for detoxification:recycling. Furthermore, ratio values decreased 10-15 fold when comparing UGT activity at pH 7.4 to βG activity at pH 5.4 (Table 2.2). The latter result compares both enzymes at their respective optimal pH. Detoxification:recycling ratios at pH 5.4 were 0.7 for jejunum and 0.8 for caecum suggesting that the metabolic equilibrium favours recycling in these intestinal regions.

Table 2.2: Detoxification:recycling ratios decrease with increasing βG activity at acidic pH (UGT is always pH 7.4)

	Tissue	Total UGT (pmol/min/mg)	βG (pmol/min/mg)	Detoxification:recycling
pH 7.4	Duodenum	109.6	8.8	12.5
	Jejunum	80.0	7.4	10.8
	Ileum	63.3	3.7	17.1
	Caecum	106.0	12.3	8.6
pH 6.8	**Tissue**	**Total UGT (pmol/min/mg)**	**βG (pmol/min/mg)**	**Detoxification:recycling**
	Duodenum	109.6	9.4	11.7
	Jejunum	80.0	15.3	5.2
	Ileum	63.3	11.7	5.4
	Caecum	106.0	20.8	5.1
pH 5.4	**Tissue**	**Total UGT (pmol/min/mg)**	**βG (pmol/min/mg)**	**Detoxification:recycling**
	Duodenum	109.6	88.4	1.2
	Jejunum	80.0	117.2	0.7
	Ileum	63.3	51.3	1.2
	Caecum	106.0	141.4	0.8

2.3.4.2 *E. coli* βG activity in cell lysates as a function of pH

βG activity in five non-pathogenic *E. coli* strains was determined at pH 7.4, pH 6.8 and pH 5.4 using 4MUG as substrate. Optimal pH for *E. coli* βG is pH 7.4, which differs from that of human βG. Across all pH levels tested, there was high variability in bacterial βG activity. BigEasy TSA strain showed greatest enzyme activity, being 11-12 fold higher on average than all other strains at each pH level. βG activity in BigEasy TSA was significantly different when comparing pH 6.8 to 5.4 ($p < 0.01$) and from pH 7.4 to 5.4 ($p < 0.001$). TOP10/P3 was the only other strain to show significant differences in enzyme activity from pH 6.8 to 5.4 and from pH 7.4 to 5.4 ($p < 0.05$). No strains showed significant differences in βG activity from pH 7.4 to 6.8 (Figure 2.8A). At pH 7.4, BigEasy TSA showed greatest enzyme activity (4853.7 ± 228.8 pmol/min/mg) followed by TOP10/P3 (1412.2 ± 406.7 pmol/min/mg), NEB10β (445.3 ± 161.7 pmol/min/mg), 10GF' (349.4 ± 138.2 pmol/min/mg) and SURE2 (229.5 ± 40.0 pmol/min/mg) (Figure 2.8B). βG activity in BigEasy TSA was significantly greater than all other strains for each pH level tested ($p < 0.0001$). Moreover, increasing acidity to pH 6.8 resulted in highest enzyme activity in BigEasy TSA (5250.4 ± 704.1 pmol/min/mg) before declining to TOP10/P3 (1481.5 ± 359.4 pmol/min/mg), NEB10β (508.7 ± 146.6 pmol/min/mg), 10GF' (450.4 ± 187.6 pmol/min/mg) and SURE2 (249.5 ± 37.3 pmol/min/mg) (Figure 2.8C). Lastly, βG activity at pH 5.4 decreased from BigEasy TSA (6179.8 ± 586.8 pmol/min/mg) to TOP10/P3 (2190.42 ± 544.1 pmol/min/mg), NEB10β (671.6 ± 188.6 pmol/min/mg), 10GF' (535.2 ± 214.6 pmol/min/mg), with lowest activity level in SURE2 (304.8 ± 34.1 pmol/min/mg) (Figure 2.8D). Analysis of βG activity in each distinct *E. coli* strain across multiple pH values was performed using two-way ANOVA with Bonferroni post hoc test. One-way ANOVA with Bonferroni post hoc test was used to determine significant differences between tissue samples at the same pH.

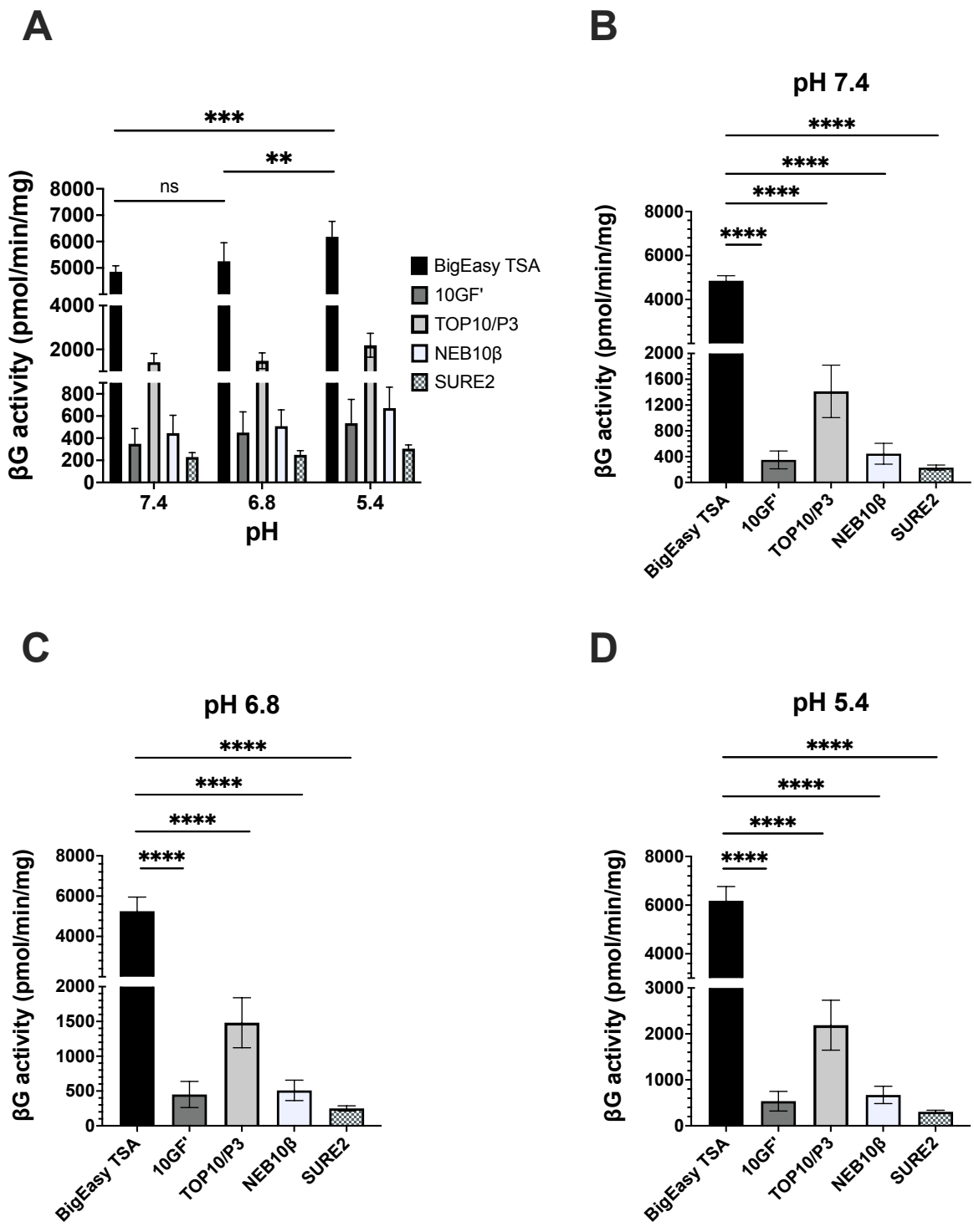

Figure 2.8: The effect of pH on *E. coli* βG activity

4MUG fluorescent assays were run in triplicate on three separate occasions to determine **(A)** βG activity in *E. coli* cell lysates measured at pH 7.4, 6.8 and 5.4. **(B)** *E. coli* βG activity at optimal pH. **(C)** Comparison of βG activity across *E. coli* strains at pH 6.8. **(D)** Enzyme activity differences between *E. coli* strains at pH 5.4. NS = not significant. ** = $p < 0.01$, *** = $p < 0.001$, **** = $p < 0.0001$.

2.3.4.3 Human and *E. coli* βG – pH differences and distinct changes in enzyme activity

The fold increase in enzyme activity between pH levels differed from human to *E. coli* βG. As pH decreased, *E. coli* βG showed progressively greater enzyme activity. In contrast, human βG showed greatest fold increase in enzyme activity between two pH levels. Moving from pH 7.4 to 6.8, human intestinal βG increased 1.2-3.2-fold compared to a smaller 1.1-1.3-fold increase in *E. coli* βG. Ileum, jejunum and caecum showed higher fold increases in enzyme activity compared to the top *E. coli* strain 10GF' (1.3-fold increase, Figure 2.9A). The same trend continued when comparing βG activity from pH 6.8 to 5.4. Human βG increased 4.5-13.1-fold whereas *E. coli* βG only increased by 1.2-1.5-fold. All intestinal tissue lysates showed greater increase in enzyme activity compared to any *E. coli* strain (Figure 2.9B). Additionally, human βG showed 11.0-16.7-fold and *E. coli* βG showed 1.3-1.6-fold increases in enzyme activity when comparing values at pH 7.4 and 5.4 (Figure 2.9C). With increasing acidity, human βG operated closer to optimal pH and greater fold increases in enzyme activity were observed compared to *E. coli* βG, which has an alkaline optimal pH. Overall, human βG averaged a 2.0-fold increase from pH 7.4 to 6.8, 8.2-fold increase from pH 6.8 to 5.4 and 13.3-fold increase from pH 7.4 to 5.4. Over the same pH ranges, *E. coli* βG averaged 1.1, 1.3 and 1.5-fold increases in enzyme activity. Human βG fold increase in activity was significantly greater than *E. coli* βG from pH 7.4 to 6.8 ($p < 0.05$), pH 6.8 to 5.4 ($p < 0.01$) and from pH 7.4 to 5.4 ($p < 0.0001$) by unpaired t-test (Figure 2.9D). These results are not surprising and are indicative of human tissue βG being lysosomal (optimal pH 5.4) but *E. coli* βG being cytosolic (pH 7.4).

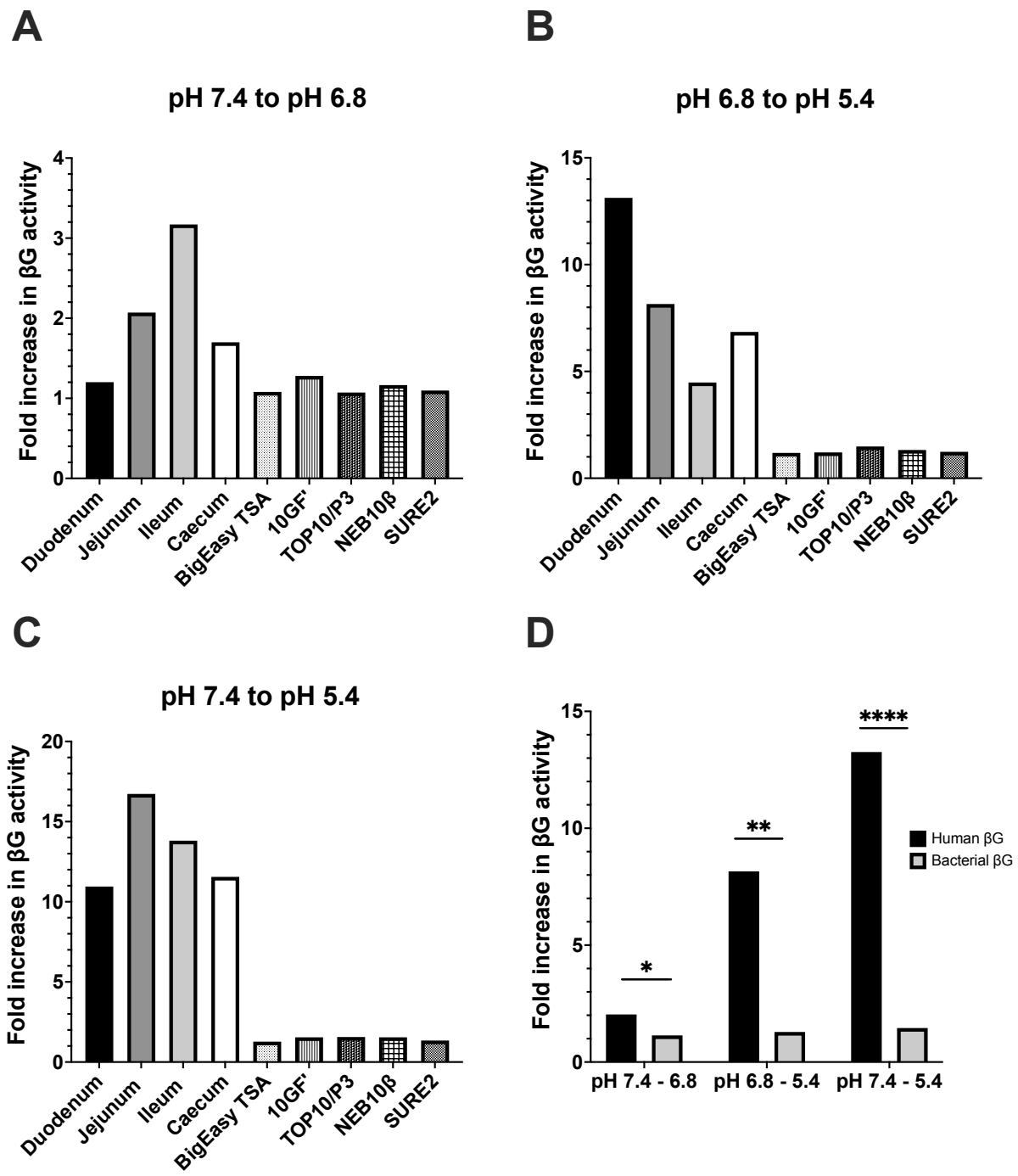

Figure 2.9: Fold increase in human and *E. coli* βG activity at different pH levels
(A) Human and *E. coli* βG differ in fold increase of enzyme activity moving from pH 7.4 to 6.8. **(B)** Human βG shows greater magnitude increase in enzyme activity from pH 6.8 to 5.4 as *E. coli* βG increases are more consistent. **(C)** The fold increase in βG activity gap widens as human βG functions at optimal pH. The lowest increase in human βG activity from pH 7.4 to 5.4 is 5-fold greater than the largest increase in activity from any *E. coli* strain. **(D)** Human βG shows significantly greater fold increase in enzyme activity compared to *E. coli* βG over the same pH ranges. * = $p < 0.05$, ** = $p < 0.01$, **** = $p < 0.0001$.

2.4 Discussion

These results showed that βG is differentially expressed and active across distinct, healthy human tissues. Western blot and activity assay data supported the hypothesis that each tissue would display unique enzyme expression and activity levels based on local metabolic demand. In addressing the research question, the first comprehensive expression and activity profile of βG in the human body was developed. Additionally, the role of glycosylation was investigated in tissue types that showed elevated enzyme activity but poor protein expression. Our data suggests that βG in liver, adrenal and prostate tissues may be differentially glycosylated and subject to tissue-specific regulation.

Glycan chains on βG play a key role in coordinating enzyme transport from the rough endoplasmic reticulum to the lysosome (Jain *et al*., 1996). As a functional glycoprotein, the βG monomer contains four asparagine sites for N-linked glycosylation where phosphorylation of certain mannose residues provides the key recognition signal for delivery to the lysosome (Shipley *et al*., 1993). The high mannose oligosaccharide chains are suitable targets for EndoH, which specifically cleaves between the innermost N-acetylglucosamine residues (GlcNAc) leading to partial deglycosylation (Freeze & Kranz, 2010). Glycan chain degradation results in decreased βG molecular weight and an improved ability to migrate during gel electrophoresis. The EndoH data shows that all treated samples appear 2-3 kDa lower than the fully glycosylated protein suggesting the partial removal of oligosaccharides. Interestingly, βG in liver lysate appears as a singlet whereas adrenal and prostate βG is shown as a doublet. The observed difference may indicate that carbohydrate chain composition is unique to certain human tissues and EndoH treatment may result in different degradation, with innermost GlcNAc retained. While the possibility of tissue-specific regulation for βG glycosylation has not been extensively

studied, future research investigating potential tissue differences in humans may further elucidate the role of carbohydrate moieties in organelle targeting and function of lysosomal hydrolases.

Future studies should start with peptide:N-glycosidase F (PNGase F) degradation of N-linked oligosaccharide chains in adrenal and prostate – the major differences between EndoH and PNGase F being the specific glycosidic linkage cleavage site and substrate selectivity. PNGase F is much less selective, catalyzing complete deglycosylation whereas EndoH partially deglycosylates the glycan chain of high mannose and some hybrid carbohydrate types leaving the innermost GlcNAc linked to an asparagine residue (Norris *et al*., 1994; Depetris *et al*., 2012). All N-linked carbohydrates, excluding those with the innermost GlcNAc covalently linked to an α1-3 fucose residue, are sensitive to PNGase F, but only some types are sensitive to EndoH (Norris *et al*., 1994). Therefore, investigating βG glycosylation in different tissues using EndoH may not work due to the selectivity of targeting specific carbohydrate types. The data shows both singlet and doublet bands for EndoH treated samples in liver, adrenal and prostate lysates suggesting that tissue-specific glycosylation involves different oligosaccharide types, some of which are not targets for EndoH. Importantly, EndoH use allows for potentially detecting different N-linked glycan chains as PNGase F, with its broad substrate selectivity, would cleave all glycan chains irrespective of tissue and carbohydrate type. In addition to determining the role of glycosylation in protein expression, its role across human body tissues, eukaryotic and prokaryotic enzyme activity was also assessed as a function of pH.

Activity data showed βG increased in tissue and bacterial cell lysates with an increase in acidity. However, the fold change in enzyme activity was greater in human tissue lysates as increasing acidity brought human βG closer to its optimal pH of 5.4. Intestinal UGT:βG ratios

show regions where the rate of recycling exceeds the rate of conjugation suggesting that the contributions from human βG to enterohepatic recycling are region-specific.

These findings help address the lack of comparative βG data in human tissues and allow for the determination of detoxification:recycling across 14 distinct tissue types (Sperker *et al.*, 1997). Comparing UGT:βG activity locally provides a more accurate metabolic picture than previous glucuronidation studies where βG was routinely inhibited using saccharolactone, hence the resulting glucuronidation rate may have been overestimated due to the inactivation of the recycling pathway (Oleson & Court, 2008). Besides saccharolactone, additional compounds including butyrolactone derivatives, L-aspartic acid, thiadazole derivatives, oxadiazole coupled-thaidiazole derivatives, and piperazine-based compounds have been developed to serve as βG inhibitors (Haroon *et al*., 2013; Kreamer *et al.*, 2001; Salar *et al.*, 2016; Taha *et al*., 2019; Pellock *et al*., 2018). Early interest in βG inhibition focused on preventing the recirculation of bilirubin leading to neonatal jaundice, whereas recent research targets intestinal βG and its role in enterohepatic recycling contributing to dose-limiting toxicity (Gourley *et al*., 1986; Bhatt *et al*., 2020). Many inhibitors designed today show improved potency compared to the original βG inhbitor, D-saccharic acid 1,4-lactone (Zhou *et al*., 2020). Additionally, differences in enzyme kinetics between UGT isoforms and βG may suggest an insignificant contribution for the rate of recycling. Analysis of first trimester placentas showed that UGT activity operates 3 orders of magnitude above βG activity at pH 7.4 (Collier *et al.*, 2002). UGT specific activity is calculated in nmol/min/mg protein whereas βG is reported in pmol/min/mg protein. Our results at pH 7.4 confirm that UGT activity operates orders of magnitude greater than βG activity in the same tissue, at that pH. However, in light of our findings using the more appropriate lysosomal pH of 5.4, some of these conclusions may need to be reconsidered. In highly metabolic organs such as

kidney and liver, where βG activity is elevated, detoxification:recycling ratios at pH 7.4 are 88.5 and 101.9 respectively, suggesting that the conjugation rate is 88.5-101.9-fold greater than recycling. Once again, revisiting this in light of the correct lysosomal pH may be advisable. Although metabolism favours conjugation at pH 7.4, the intestinal tissues provide a unique environment where βG activity from both human and bacteria contribute to parent compound regeneration and enterohepatic recycling. Importantly, this study provided a unique opportunity to reconsider the pH of tissue lysates and their relationship to real *in vivo* βG activities, one of the major findings presented in this thesis.

The gut provides a dynamic interface between human and bacterial cells. Each intestinal region offers a unique physical and chemical environment (Berg, 1996). The critical factor for investigating whether intestinal βG was differentially active was by measuring enzyme activity at different pH levels. These experiments furthered our understanding of βG, in two distinct forms, by measuring activity at optimal pH. More specifically, pH 7.4 served as the optimal pH for *E. coli* βG and pH 5.4 for human βG (Pollet *et* al., 2017; Weyel *et al*., 2000). The range between these pH values represents the unique pH environments within the intestines (Abuhelwa *et al.*, 2016). Our results show that pH has a considerable effect on βG activity in intestinal tissue lysates, where decreases in pH lead to increases in enzyme activity. Given the elevated βG activity in a more acidic environment, detoxification:recycling ratios decrease such that certain intestinal regions metabolically favour the rate of recycling over conjugation. Specifically, jejunum and caecum are suggested sites for enterohepatic recycling by human βG. Uncertainty surrounding this phenomenon, which draws clinical attention to βG, remains as contributions from enzyme activity, human and bacterial, is not fully understood.

Enterohepatic recycling is understood in pharmacological sciences as the systemic recirculation of compounds that have primarily been conjugated in the liver, followed by intestinal deconjugation (Roberts *et al*., 2002). Glucuronides formed by UGT enzymes in the liver are transported to the duodenum in bile via the common bile duct and progress distally towards the caecum. Within the intestines, βG activity may regenerate active compounds and reverse the inactivation by phase II metabolism in the liver. In the context of drugs, this recycling extends drug half-life and alters its pharmacokinetic profile (Malik *et al*., 2016). Clinical concerns have focused on the enterohepatic recycling of the anti-cancer drug Irinotecan and NSAIDs as prolonged drug half-life is associated with intestinal damage and dose-limiting toxicity (Bhatt *et al*., 2020; Wallace *et al*., 2010; Saitta *et al*., 2014). Inhibition of enzyme activity, which helps to alleviate these conditions, targets primarily bacterial βG. Of the changing microbial populations that occupy our gut, *Bacteroidetes* and *Firmicutes* are the dominant phyla found in adults, followed by lesser detection of *Actinobacteria*, *Proteobacteria*, and *Verrucomicrobia* (Eckburg *et al*., 2005). Our studies focus on bacterial βG from *E. coli*, a species found within the *Proteobacteria* phylum. While *E. coli* represents only a subset of species found within the gut microbiome it is a thorougly studied bacteria characterized by a well-defined βG crystal structure with a L1 structure near the active site (as shown in Figure 2.1C above). The presence of L1 reduces the active site space suggesting that *E. coli* βG is more optimized for metabolizing smaller glucuronide substrates over larger carbohydrates (Pollet *et al.*, 2017). Moreover, *E. coli* possess a GUS operon specific for the detection and metabolism of glucuronides passing through the gut (Little *et al*., 2018). The ability to efficiently metabolize glucuronide substrates provides intestinal *E. coli* with glucuronic acid, a carbon source, which can be shuttled through the Entner-Doudoroff pathway to generate pyruvate (Pellock & Redinbo,

2017). Given this efficiency in processing glucuronide substrates, *E. coli* βG activity in all five strains was greater than the corresponding enzyme activity in intestinal tissue lysates at each pH level measured. Additionally, there was a large variation in *E. coli* βG activity from 4854 pmol/min/mg in BigEasy TSA to 230 pmol/min/mg in SURE2 (21-fold difference) at optimal pH. Despite this, pH changes had a negligible effect on bacterial βG, as would be expected since *E. coli* βG is a cytosolic enzyme. Additionally, human βG enzyme activity in the caecum is comparable to that observed in the SURE2 strain at optimal pH suggesting that more acidic environments may lead to greater contributions from human βG to enterohepatic recycling. As clearly demonstrated above, the relative contributions of human:bacterial βG will depend on the intestinal localization of the human enzyme and the composition of the gut microbiome. The microbial populations occupying a healthy gut are not evenly distributed. Microbial density is fairly sparse in the duodenum (10^1-10^3 bacterical cells/mL of intestinal content), rises in the jejunum and ileum (10^4-10^7 bacterial cells/mL of intestinal content), and becomes most densely populated in the caecum (10^{11} bacterial cells/mL of intestinal content) (O'Hara & Shanahan, 2006). Also, previous estimates on bacterial:human cells in the body have been revised by orders of magnitude down from either 100:1 or 10:1 to 1.3:1 (Sender *et al*., 2016). This suggest that enterohepatic recycling, and contributions from human βG activity, may be more likely in certain intestinal regions where human cells are not as outnumbered by bacteria as previously reported. Our findings suggest that enterohepatic recycling of active compounds in the intestine is due, at least in part, to human βG. This is an important and novel finding that helps address a long-standing argument in pharmacology and toxicology as to the contribution (or not) of human βG to the recycling process as compared to the gut bacteria.

Future studies should focus on βG activity across a diverse range of microbes that occupy the gut. Understanding how differences in gut microbiome composition, compared to differential human βG activities in the intestine, may affect rate and extent of enterohepatic recycling is important for providing clarity as to which enzyme, human or bacterial, may make a contribution in a given intestinal region. To this end, enzyme activity should be assessed in bacterial strains outside of *Proteobacteria*, particularly in *Bacteriodetes* and *Firmicutes*, the dominant phyla in adults. Understanding the activity of βG across a range of diverse bacterial strains would allow for comparison of unique active site loop structures and the testing of strains with unique optimal pH (Pollet *et al*., 2017). Better understanding of microbiome dynamics can help with understanding of endo- and xenobiotic balance. Furthering our understanding of human and bacterial βG in the gut will also provide novel insights into xenobiotic safety, efficacy and toxicity. This will also provide clarity as to drug dosing and/or drug and chemical toxicity in the face of changing diets and gut environments, facilitating better uses of personalized medicine approaches.

Chapter 3: Beta-glucuronidase in prostate cancer: Evidence for a role in prostate cancer progression, and comparison of cell lines as appropriate *in vitro* models for mechanistic investigation

3.1 Introduction

Cancer etiology, progression and detection can all be associated with the presence or absence of certain enzymes. The role of βG in malignant tissues has been investigated for more than 60 years, where increases in enzyme activity were first observed in 1947 (Fishman & Anlyan, 1947). Elevated βG activity in certain bodily fluids are detected in a variety of cancer types including bladder, colorectal, lung, ovarian and pancreatic (Boyland *et* al., 1957; Waszkiewicz *et al*., 2015; Mürdter *et al*., 1997; Beratis *et al*., 2005; Sperker *et al*., 2000). Our lab wanted to investigate the relationship between βG and prostate cancer, focusing on how enzyme expression and activity may change with disease progression – since we found unexpectedly high levels of expression and activity of βG in normal prostate tissues (Chapter 2).

Development of PCa is hormone-dependent and influenced by androgens (Higgins, 1975; Huggins & Hodges, 1941). Specifically, testosterone and dihydrotestosterone (DHT) bind the androgen receptor (AR) leading to ligand-receptor dimerization, translocation to the nucleus and transcriptional activation of certain genes. Around 80-90% of early stage PCa is androgen-driven where cancer progression occurs through abnormal AR activation and signalling which stimulates excessive cell proliferation and inhibits apoptosis (Heinlein & Chang, 2004; Matsumoto *et al*., 2013). As androgens are critical to cancer development, a common treatment approach called ADT aims to reduce systemic circulating androgen levels. ADT includes both surgical and chemical approaches ranging from bilateral orchiectomy to the use of LHRH agonists and antagonists, CYP17 antagonists and anti-androgens that block the AR (Crawford *et al*., 2019). However, while ADT is initially effective, disease relapse is common (Ceder *et al*.,

2016). PCa progresses into CRPC characterized by increasing PSA in a low testosterone environment (Parimi *et al*., 2014). Treatments focus heavily on targeting androgen production, not androgen recycling. Our study aims to investigate βG and its role in androgen recycling (and/or the recycling of other endobiotics), providing the tumour with a local supply of testosterone and DHT, which may influence disease progression in a castration environment. Specifically, these studies aimed to understand if βG expression and activity changes using *in vitro* and *ex vivo* models representing different stages of prostate cancer.

The recycling ability of βG was assessed using prostate cell lines and tissue lysates, representing varying stages of PCa progression. We investigated βG expression and activity using five prostate cell lines that are either androgen-dependent or androgen-independent and serve as models for normal prostate, PCa, and CRPC. Our *in vitro* studies used PNT1A, 22Rv1, LNCaP, C4-2 and PC3 cell lines to characterize changes in βG expression and activity with cancer progression. Beyond cell lines, our *ex vivo* approach involved the use of benign and malignant prostate tissue lysates including normal, benign prostatic hyperplasia (BPH), adenoma and adenocarcinoma. These studies investigated βG enzyme behaviour and its importance in providing a local, circulating supply of androgens to aid tumour growth. It is notable that some of these cell lines and tissues represent androgen-independent stages of PCa, so increased βG recycling of other as-yet unidentified endobiotics may also be a mechanism of PCa progression.

UGT activity and androgen elimination plays a key role in the prostate. Understanding androgen metabolism in prostate cancer progression requires investigating the expression and activity of certain UGT isoforms. In the prostate, UGT2B15 and 2B17 eliminate androgens through glucuronidation (Grosse *et al*., 2013; Gauthier-Landry *et al*., 2015). More specifically, testosterone and DHT are metabolized into glucuronide products that are biologically inactive

and more readily eliminated from the body. UGT2B17 shows greatest capacity to metabolize testosterone whereas UGT2B15 shows moderate capacity to catalyze the glucuronidation of DHT (Gauthier-Landry *et al*., 2015). We investigated UGT2B15 and 2B17 expression and activity across all prostate cell line and tissue lysate samples. Another laboratory project led by Summer Student Blair MacDonald, using these same PCa cell lines, performed western blotting for major human UGT isoforms (UGT1A1, 1A3, 1A4, 1A6 and 2B7) which showed that these isoforms were not present in the PCa cell lines (*data not shown*). However, we cannot be sure whether the lack of protein expression in these cell lines differs from that of non-cancerous and cancerous prostate tissue. While UGT2B7, 2B15 and 2B17 are known to metabolize androgens, only 2B15 and 2B17 are expressed in the prostate (Gauthier-Landry *et* al., 2015). It was decided to focus on UGT2B15 and 2B17 isoforms in prostate tissues and cell lines with respect to their roles in androgen inactivation and elimination, as compared to βG recycling.

Our findings show that βG activity increased with prostate cancer progression in our *in vitro* and *ex vivo* models suggesting steroid deconjugation and androgen recycling may play a role in disease progression. Normal prostate epithelium was represented by androgen-dependent PNT1A cells, while 22Rv1, an androgen-responsive cell line derived from a primary tumour expressing low levels of AR and PSA, served as the PCa model (Avancès *et al*., 2001; Sramkoski *et al*., 1999; Attardi *et al*., 2004). Disease progression to CRPC was studied using three cell lines: LNCaP, C4-2, and PC3. LNCaP cells are androgen-sensitive and express AR whereas C4-2, a LNCaP subline, is androgen-independent (Horoszewicz *et al*., 1983; Zhau *et al*., 1996; Wu *et al*., 1994). Lastly, PC3 is an AR- and PSA-null androgen-independent cell line resembling small cell neuroendocrine carcinoma (SCNC) that shows greatest metastatic potential (Tai *et al*., 2011). Enzyme activity was greatest in the PC3 cell lysate at pH 7.4, 6.8 and 5.4,

followed by C4-2 and LNCaP CRPC cell lysates. A similar trend was observed in the prostate tissue lysates where adenocarcinoma showed highest βG activity at each pH level tested. Moreover, clear βG expression was observed in the adenocarcinoma lysate and UGT2B17 was the more commonly expressed isoform in prostate cell lines. Our results provide a better understanding of androgen metabolism, the elimination and recycling of testosterone and DHT, and how tumours may upregulate βG to ensure a local supply of androgens with cancer progression.

3.2 Materials and Methods

3.2.1 Chemicals and reagents

The following chemicals, reagents, and supplies were used: 4-methylumbelliferone sodium salt (Cat#:A10337, Thermo Fisher, Ward Hill, MA, USA), 4-methylumbelliferyl-β-D-glucuronide (Cat#:M9130, Sigma-Aldrich, Oakville, ON, CAN), alamethicin (Cat#:A4665, Sigma-Aldrich, St. Louis, MO, USA), bovine liver βG (Cat#:G0251, Glucurase, Sigma-Aldrich, St. Louis, MO, USA), uridine diphosphate-glucuronic acid (Cat#:U6751, Sigma-Aldrich, St. Louis, MO, USA) and V79 cells (derived from Chinese hamster lung fibroblasts) (Sigma-Aldrich, St. Louis, MO, USA) were used in fluorescent enzyme assays to determine total UGT and βG activity.

3.2.2 Human prostate cell lines and tissue lysates

PNT1A cell line was obtained from American Type Culture Collection. 22Rv1, LNCaP, C4-2 and PC3 cells were gifted by Dr. Michael Cox from Vancouver Prostate Centre and bulk cultured by Manrose Mann in our laboratory. The following prostate tissue lysates were obtained

from commercial vendors: normal prostate (Cat#:NBP2-47064, Novus Biologicals, Centennial, CO, USA), benign prostatic hyperplasia (Cat#:NBP2-47056, Novus Biologicals, Centennial, CO, USA), adenoma (Cat#:NBP2-47065, Novus Biologicals, Centennial, CO, USA) and adenocarcinoma (Cat#:CP555253, OriGene Technologies, Rockville, MD, USA). All commercial tissue samples were derived from single donors.

3.2.3 Western blot for βG, UGT2B15 and 2B17 in prostate cell line and tissue lysates

To determine βG expression, prostate cell lysates (20 μg) and tissue lysates (10 μg) were resolved on 6-12% SDS-PAGE under reducing conditions, transferred to PVDF membranes with semi-dry transfer (Biorad, Hercules, CA, USA), then washed with TBS-T, pH 7.4. Membranes were immunoblotted with primary antibody (1:2500 for prostate cell lysates, 1:2000 for prostate tissue lysates, 5% non-fat milk powder) against βG (Cat#:ab166904, Abcam, Cambridge, MA, USA), against UGT2B15 (1:250 for prostate cell and tissue lysates) (Cat#:SAB1411383, Sigma-Aldrich, Oakville, ON, Canada) and against UGT2B17 (1:300 for prostate cell and tissue lysates) (Cat#:SAB1301563, Sigma-Aldrich, Oakville, ON, Canada) overnight at 4°C. Following primary antibody incubation, membranes were subsequently washed with TBS-T before adding donkey α-rabbit horseradish peroxidase (HRP) secondary antibody (βG: 1:5000; UGT2B15: 1:3000; UGT2B17: 1:3000) with 5% non-fat milk powder and 2% NDS for 1 hour at room temperature with gentle agitation. Membranes were further rinsed with TBS-T to remove residual secondary antibody and incubated with Immobolin ECL Ultra Western HRP Substrate (Millipore Corporation, Billerica, MA) for 2 minutes. Protein expression was visualized using Alpha Innotech Fluorchem imaging system (San Leondro, CA, USA). Densitometry analysis was performed using ImageJ software (NIH, Bethesday, MD, USA). Briefly, membrane images were

analyzed by first selecting a target area including the protein band for each individual lane. Next, the optical density in each lane is plotted and peaks are labelled to provide a measure of optical density for each lane as a percentage of the total optical density calculated for the membrane. This analysis is performed on three separate membrane images to provide an average optical density value for each cell and tissue lysate at n=3. Lastly, optical density calculated for unique samples were normalized by total protein based on Coomassie blue stained gel protein bands and sample amount loaded.

3.2.4 4MU assay – total UGT activity

Total UGT activity was determined in prostate cell and tissue lysates using the fluorescent assay method described previously (Collier *et al*., 2000). 1 µL alamethicin (0.050 mg/g cell or tissue lysate), 10 µL homogenized prostate cell or tissue lysate (0.5 mg/mL for prostate tissue lysate, 1 mg/mL for cell lysates), 10 µL 1mM 4MU and 69 µL 0.1M Tris-HCl pH 7.4 containing 10 mM $MgCl_2$ were combined in a microplate well to a volume of 90 µL. UGT activity was only assessed at pH 7.4, as this pH value corresponded to the optimal pH of the enzyme. Each solution was pre-warmed to 37°C for 2 minutes. The reaction was initiated with the addition of 10 µL 50 mM UDPGA for a final volume of 100 µL in each well. Reactions were continuously tracked at 37°C for 60 minutes at λ_{exc} = 355 nm and λ_{em} = 460 nm using a FlexStation3 plate reader (Molecular Devices, Sunnyvale, CA). Samples were analyzed in triplicate on three separate occasions. Initial reaction velocities were calculated by least squares linear regression with substrate depletion, or decrease in fluorescence, serving as a marker for product formation. The FU were converted to concentrations by comparison to a 4MU standard curve. The intra- and inter-assay CVs for the slopes of the standard curves were 4.4 and 26.4%

respectively. Mean $R^2 = 0.991$. The assay was found to be linear between 45–50 μM 4MU per well using a 100 μL sample volume.

3.2.5 4MUG assay - βG activity

βG activity was assessed in prostate cell and tissue lysates using the fluorescent assay with 4MUG as substrate described previously (Trubetskoy & Shaw, 1999). In a microplate well, 10 μL homogenized cell or tissue lysate (0.5 mg/mL for prostate tissue lysate, 1 mg/mL for cell lysate) and 80 μL 0.1M Tris-HCl with 10 mM $MgCl_2$ at either pH 7.4, pH 6.8 or pH 5.4 were combined to study enzyme activity in differing pH environments. Each solution was pre-warmed to 37°C for 2 minutes before 10 μL 1mM 4MUG was added to initiate the reaction. Final volume in each well was 100 μL. Reactions were continuously monitored as described above using FlexStation 3 plate reader (Molecular Devices, Sunnyvale, CA) to record changes in fluorescence with reaction progress. The intra- and inter assay CVs for the slopes of the standard curves were 11.9 and 12.1% respectively. Mean $R^2 = 0.992$. The assay was found to be linear between 1-10 μM 4MU per well using a 100 μL sample volume.

3.2.6 Statistical analysis

All values are shown as mean ± SD. βG and UGT activity results between samples were compared with Bonferroni's post hoc multiple comparison analysis using Prism 9.10 for MacOS X (Graph Pad Prism, San Diego, CA, USA). Assessing enzyme activity changes for the same sample at different pH levels was measured by two-way ANOVA whereas comparing enzyme activity of different samples at the same pH was analyzed using one-way ANOVA. Differences were considered statistically significant if $p < 0.05$.

3.3 Results

3.3.1 Protein expression profiles in prostate cell and tissue lysates

3.3.1.1 βG, UGT2B15 and UGT2B17 expression profiles in prostate cell lysates

Protein expression of βG was clearly observed in C4-2 and LNCaP prostate cell lysates, with little to no detection in 22Rv1, PC3 and PNT1A. The positive control, bovine βG, shows a clear protein band around 78 kDa whereas no protein is detected in the V79 cell lysate negative control (Figure 3.1A). Moreover, UGT2B15 protein expression was determined in the prostate cell lysates. Clear protein expression is observed in LNCaP cell lysate and positive controls, XT200 and liver lysate. Little to no protein is detected in any other prostate cell lysate (Figure 3.1B). Lastly, UGT2B17 protein expression was clearly expressed across all prostate cell lysates, suggesting this is the most common UGT isoform found in the prostate (Figure 3.1C). Other UGT isoforms were previously blotted in our laboratory with recombinant controls and PCa cell lines were negative (*Blair Macdonald, unpublished data*).

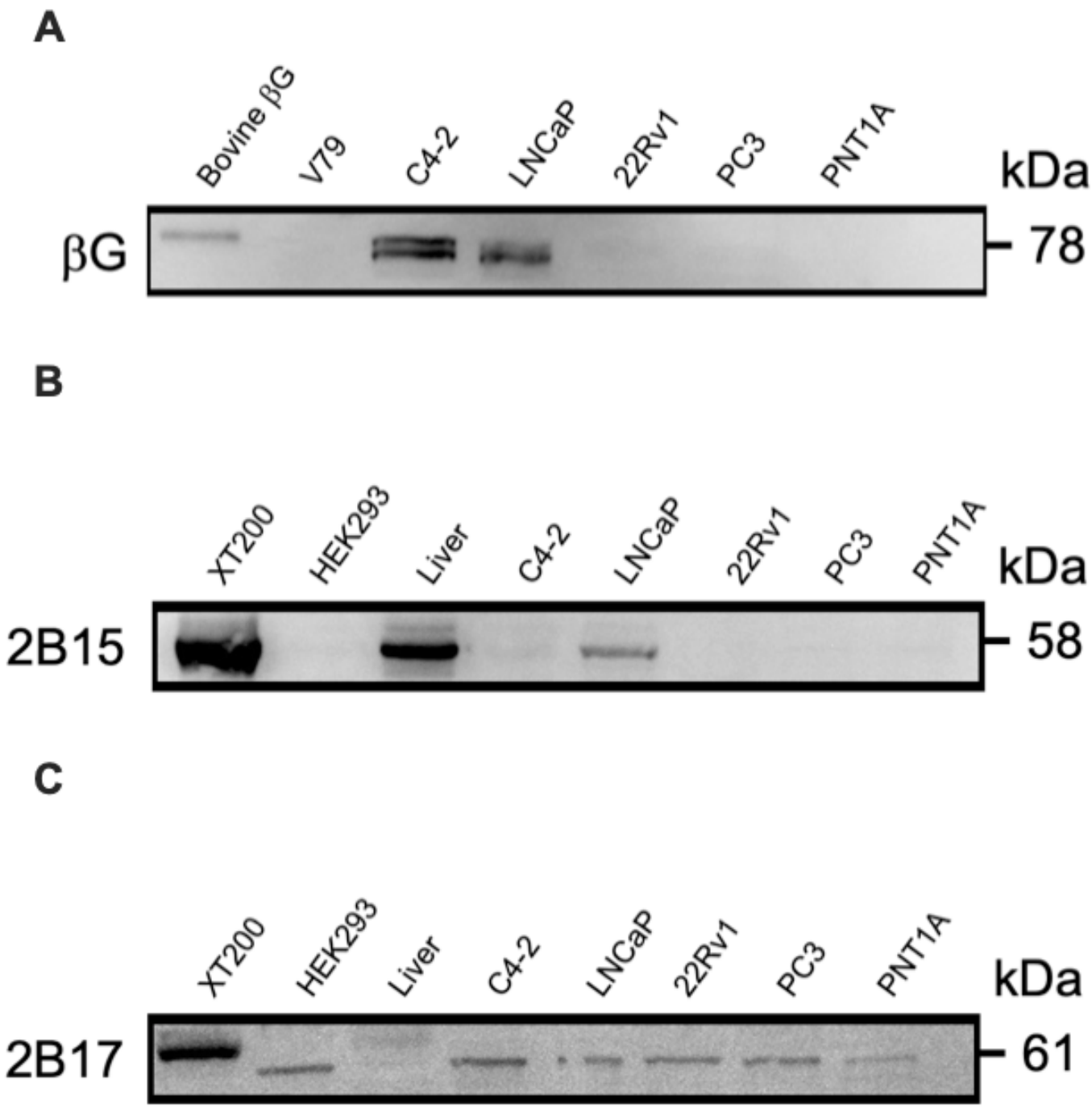

Figure 3.1: Protein expression of βG, UGT2B15 and 2B17 across prostate cell lysates
Western blot performed to characterize **(A)** βG expression in prostate cell lysates. Purified bovine βG and V79 cell lysates served as positive and negative controls. **(B)** UGT2B15 expression across all prostate cell lysates. XT200 microsomes and HEK293 cell lysates served as positive and negative controls. **(C)** UGT2B17 expression is observed in all prostate cell lysates. XT200 microsomes and HEK293 cell lysates served as positive and negative controls.

Normalized optical density of protein expression in prostate cell lysates was determined using ImageJ software. Firstly, density analysis showed βG expression was greatest in the C4-2 cell lysate followed in order by: purified bovine βG > LNCaP > 22Rv1 > PNT1A > PC3 > V79 (Figure 3.2A). Optical density for C4-2 was not significantly greater than LNCaP, purified bovine βG, or any remaining sample ($p > 0.05$). Additionally, there was no difference in normalized optical density between LNCaP and purified bovine βG ($p > 0.05$).

UGT2B15 optical density was normalized across prostate cell lysates. Greatest protein density was observed in XT200 microsomes followed closely by: liver > LNCaP > C4-2 > PC3 > HEK293 > 22Rv1 > PNT1A (Figure 3.2B). Normalized optical density in XT200 was significantly greater than C4-2, 22Rv1, PC3 and PNT1A cell lysates ($p < 0.05$). No significant difference in optical density was observed between XT200 and LNCaP cell lysate ($p > 0.05$). Moreover, LNCaP showed greatest UGT2B15 protein density of all prostate cell lysates, but did not show any significant differences in density compared to any other sample ($p > 0.05$).

Lastly, normalized UGT2B17 optical density was determined across all five prostate cell lysates. Greatest protein density was shown in XT200 microsomes followed by: PC3 > C4-2 > 22Rv1 > HEK293 > LNCaP > PNT1A > liver (Figure 3.2C). Protein density in XT200 was significantly greater than levels found in PNT1A and liver lysates ($p < 0.05$). Although normalized optical density in prostate cell lysates was highest in PC3, there was no significant difference in protein level when compared to other samples ($p > 0.05$).

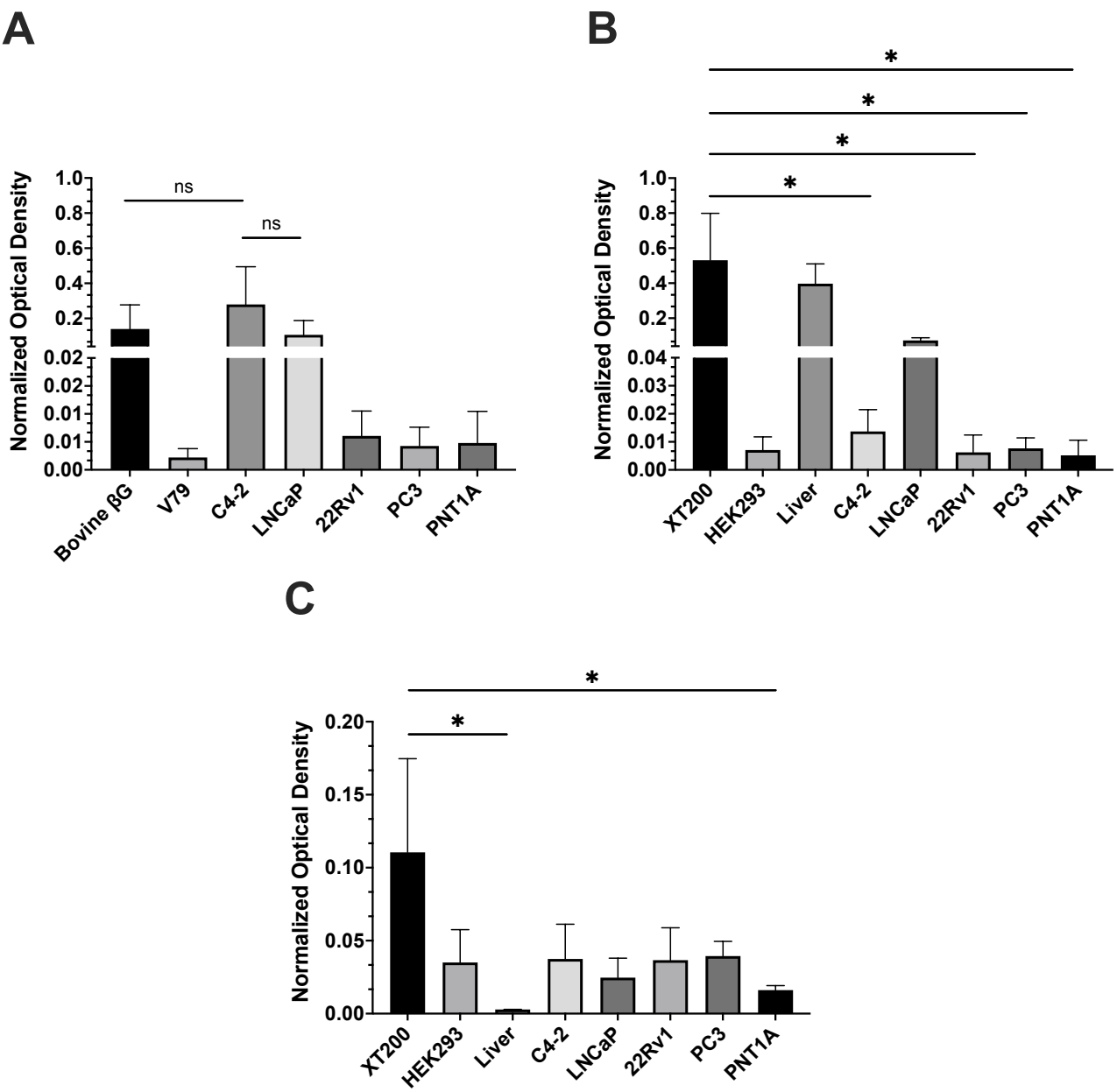

Figure 3.2: Normalized optical density of βG, UGT2B15 and 2B17 expression across prostate cell lysates

Protein expression optical density was determined using ImageJ software and normalized by total protein. Western blot experiments for each cell lysate were performed at n=3. **(A)** Normalized optical density of βG expression across prostate cell lysates. C4-2 showed greatest optical density, but was not significantly different from LNCaP or bovine βG. NS = not significant. **(B)** UGT2B15 optical density normalized across all prostate cell lysates. XT200 showed greatest UGT2B15 density that was significantly greater than C4-2, 22Rv1, PC3 and PNT1A cell lysates. * = $p < 0.05$. **(C)** UGT2B17 optical density normalized across prostate cell lysates. XT200 protein density was significantly greater than liver and PNT1A lysates. * = $p < 0.05$. Error bars are mean ± SD.

3.3.1.2 βG, UGT2B15 and UGT2B17 expression profiles in prostate tissue lysates

Among the prostate tissue lysates, clear βG expression was observed in the adenocarcinoma sample. Fainter protein bands were also detected for normal prostate, adenoma and liver lysates. A clear protein band is observed in the purified bovine βG positive control sample, whereas no protein was detected for V79 cell lysate negative control (Figure 3.3A). Furthermore, UGT2B15 protein expression is observed across all tissue lysates with greatest abundance in hyperplasia and adenoma samples. Clear protein expression is shown in positive controls, XT200 and liver lysate, at 78 kDa with no detection of HEK293 negative control (Figure 3.3B). Lastly, UGT2B17 is clearly expressed in hyperplasia and adenoma samples with lower expression in normal prostate. Little to no expression is seen in the metastatic adenocarcinoma sample. Protein detection is shown for both positive controls, where a clear protein band appears in XT200 and a faint band in liver lysate. Similar to UGT2B17 expression in prostate cell lines (Figure 3.1), a faint protein band is detected in HEK293 negative control that appears at a molecular weight below 61 kDa. It is not clear whether the band detection corresponds to 2B17 or a protein artifact (Figure 3.3C).

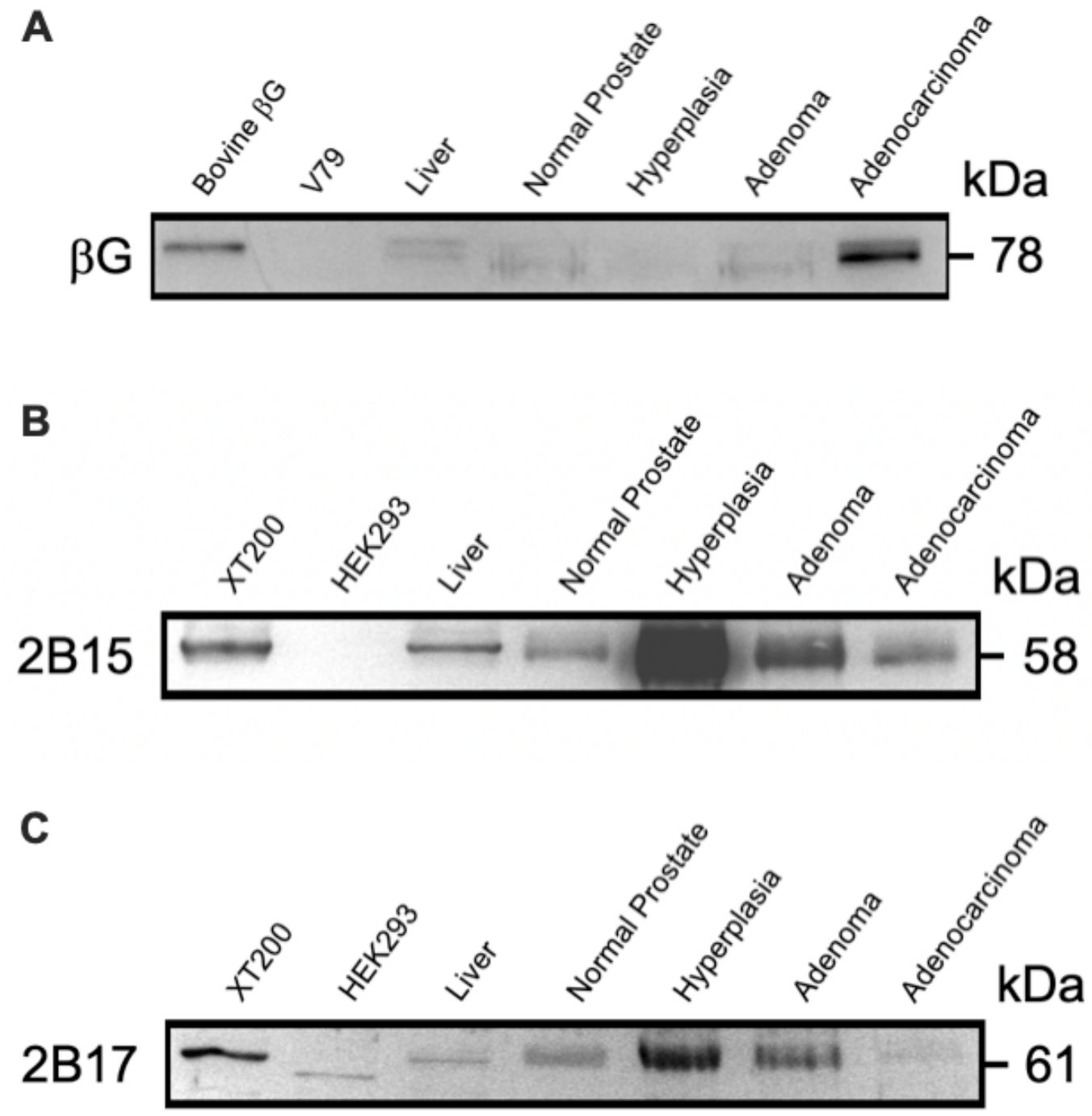

Figure 3.3: Protein expression of βG, UGT2B15 and 2B17 across prostate tissue lysates
Western blot performed to characterize **(A)** βG expression in prostate tissue lysates. Purified bovine βG and V79 cell lysates served as positive and negative controls. **(B)** UGT2B15 protein expression is observed across all prostate tissue lysates. XT200 microsomes and liver lysate served as positive controls whereas HEK293 cell lysate served as negative control. **(C)** UGT2B17 expression across all prostate cell lysates. XT200 microsomes and liver lysate served as positive controls, HEK293 cell lysate as negative control.

Normalized optical density analysis showed greatest βG expression in the adenocarcinoma tissue lysate followed closely by: purified bovine βG > liver > adenoma > normal prostate > hyperplasia > V79. Protein density levels were not significantly different between adenocarcinoma and purified bovine βG ($p > 0.05$). However, significant differences in normalized optimal density were observed when comparing adenocarcinoma to all other prostate tissue lysates ($p < 0.0001$) (Figure 3.4A).

Across all prostate tissue lysates, greatest UGT2B15 expression was observed in the hyperplasia sample followed in order by: adenoma > normal prostate > liver > XT200 > adenocarcinoma > HEK293. Hyperplasia showed significantly greater normalized optical density when compared to XT200, liver and adenocarcinoma tissue lysate ($p < 0.05$). Additionally, significant differences in optical density were shown between hyperplasia and negative control HEK293 ($p < 0.001$), and between adenoma and HEK293 ($p < 0.05$) (Figure 3.4B).

Normalized optical density of UGT2B17 was greatest in hyperplasia, followed by adenoma. In the remaining samples, greatest UGT2B17 optical density listed in order was: normal prostate > XT200 > adenocarcinoma > HEK293 > liver. Hyperplasia showed significantly greater protein expression when compared to adenocarcinoma, liver and HEK293 lysates ($p < 0.05$), but not against normal prostate or adenoma samples ($p > 0.05$). When compared to XT200 positive control, normalized UGT2B17 optical density in hyperplasia was not significantly greater ($p > 0.05$). Lastly, no significant difference in optical density was observed between normal prostate and adenoma tissue lysates ($p > 0.05$) (Figure 3.4C).

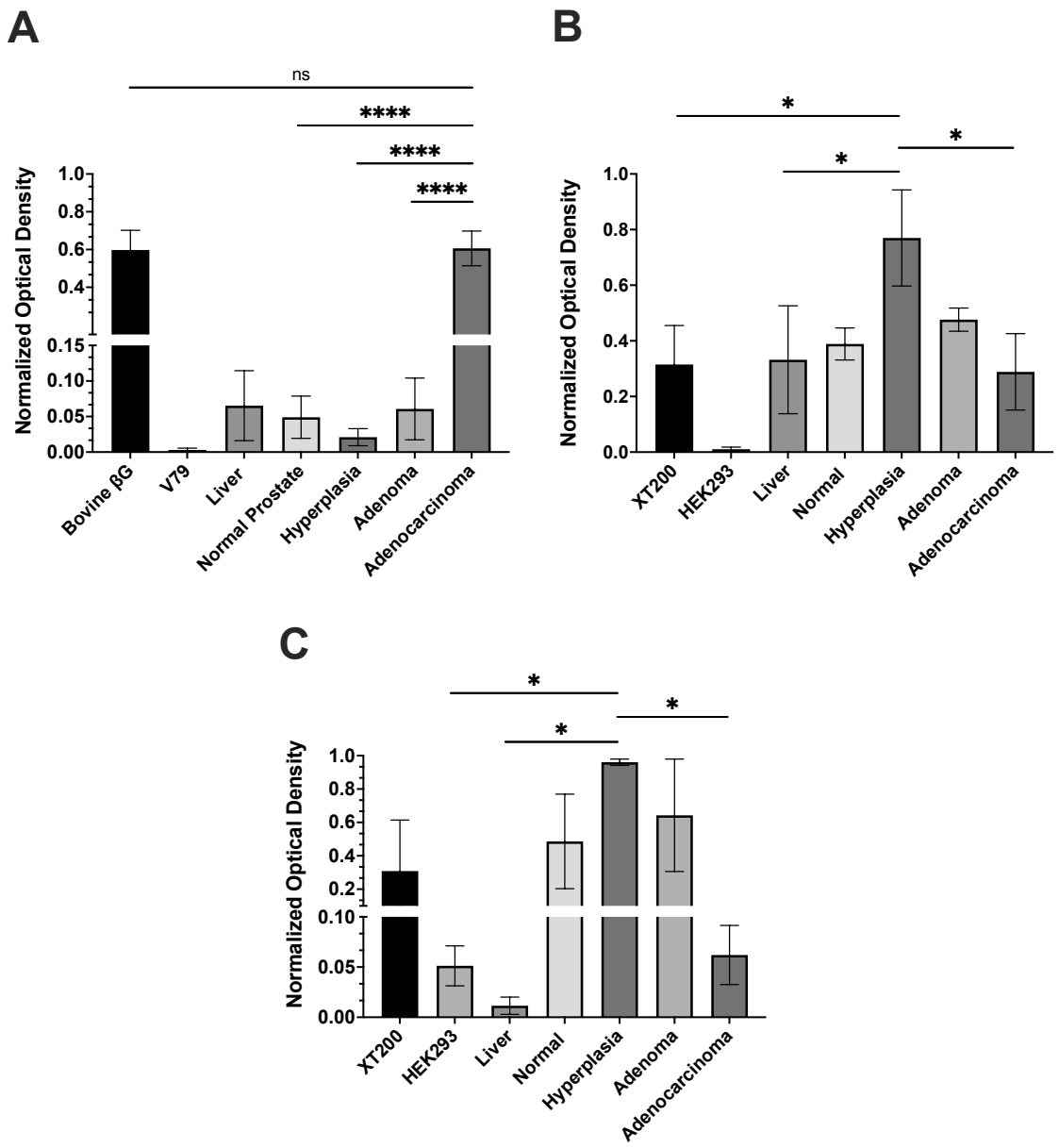

Figure 3.4: Normalized optical density of βG, UGT2B15 and 2B17 expression in prostate tissue lysates

ImageJ software was used to calculate protein expression across all prostate tissue samples. Protein expression was determined by western blot with each tissue being analyzed at n=3. Optical density for each tissue lysate was normalized by total protein. (**A)** Optical density of βG expression normalized across prostate tissue lysates. Adenocarcinoma protein density was significantly greater than all other prostate tissue samples. NS = not significant. **** = $p < 0.0001$. **(B)** Normalized UGT2B15 optical density determined across all prostate tissue samples. Hyperplasia showed highest 2B15 protein expression that was significantly greater than XT200, liver and adenocarcinoma samples. * = $p < 0.05$. **(C)** UGT2B17 optical density normalized across prostate tissue lysates. Greatest protein expression was shown in hyperplasia and significantly differed from optical density reported in HEK293, liver and adenocarcinoma lysates. * = $p < 0.05$. Error bars are mean ± SD.

3.3.2 Enzyme activity and UGT:βG comparison in prostate cell lysates as a function of pH

3.3.2.1 UGT activity across prostate cell lysates at pH 7.4

Total UGT activity was determined across five distinct prostate cell lysates using the 4MU fluorescence assay. Greatest enzyme activity was observed in PNT1A (303.2 ± 71.5 pmol/min/mg) followed in order by: 22Rv1 (303.6 ± 62.8 pmol/min/mg), PC3 (301.5 ± 29.1 pmol/min/mg), LNCaP (254.0 ± 61.1 pmol/min/mg) and C4-2 (235.4 ± 34.1 pmol/min/mg) (Figure 3.5A). There were no significant differences in enzyme activity between the different prostate cell lysates ($p > 0.05$) measured at pH 7.4. UGT activity studied at this pH level corresponds to the optimal pH for the enzyme. Statistical analysis was performed using one-way ANOVA with Bonferroni post hoc test.

3.3.2.2 βG activity across prostate cell lysates at distinct pH levels

Prostate cancer development and shifts in cellular metabolism alter the local pH environment. As cancer progresses, the tumour microenvironment (TME) becomes more acidic as lactate and excess protons accumulate. Understanding how βG activity changes from a normal to cancerous setting requires measuring enzyme activity at unique pH levels. Specifically, βG activity from five distinct prostate cell lysates was assessed at three pH levels: pH 7.4, pH 6.8 and pH 5.4. The most alkaline environment, pH 7.4, represents the cytosolic environment whereas pH 6.8 corresponds to the slighly acidic TME (Feng *et al*., 2018). This pH level has been used in previous studies to investigate enzyme activity in prostate cancer cells (Zhunussova *et al*., 2015). The most acidic pH, pH 5.4, represents the lysosomal environment and optimal pH for βG (Weyel *et al*., 2000).

Enzyme activity in prostate cell lysates was assessed using 4MUG assay at physiological pH. Greatest βG activity was observed in the PC3 cell lysate (15.7 ± 1.7 pmol/min/mg), with next highest activity detected in the CRPC cell line models C4-2 (7.1 ± 0.5 pmol/min/mg) and LNCaP (6.7 ± 0.4 pmol/min/mg). Lowest enzyme activity was found in PNT1A (0.6 ± 0.2 pmol/min/mg) and 22Rv1 (0.5 ± 0.3 pmol/min/mg) (Figure 3.5B). Cell line models of CRPC, LNCaP, C4-2 and PC3, showed significantly greater enzyme activity when compared to normal prostate epithelium cell line, PNT1A ($p < 0.0001$). There was not a significant difference in enzyme activity between PNT1A and 22Rv1 ($p > 0.05$). Moreover, the βG activity trend continues as pH becomes more acidic, reflecting the TME. Highest enzyme activity occurs in PC3 (46.6 ± 4.7 pmol/min/mg) followed in order by: LNCaP (13.8 ± 2.0 pmol/min/mg), C4-2 (11.2 ± 3.9 pmol/min/mg), PNT1A (6.4 ± 1.0 pmol/min/mg) and 22Rv1 (4.9 ± 3.5 pmol/min/mg) (Figure 3.5C). Enzyme activity at pH 6.8 is significantly greater in PC3 when compared to PNT1A ($p < 0.0001$). All other comparisons of βG activity between prostate cell lines are not significant ($p > 0.05$). Lastly, at pH 5.4, greatest βG activity was observed in PC3 (286.8 ± 68.0 pmol/min/mg) followed by decreased enzyme activity in: C4-2 (143.7 ± 29.5 pmol/min/mg), LNCaP (97.9 ± 4.4 pmol/min/mg), PNT1A (18.4 ± 6.1 pmol/min/mg) and 22Rv1 (10.7 ± 5.7 pmol/min/mg) (Figure 3.5D). Enzyme activity levels in C4-2 and PC3 cell lysates were significantly greater than PNT1A at pH 5.4 ($p < 0.01$ and $p < 0.0001$, respectively). There were no significant differences in βG activity in 22Rv1 and LNCaP when compared to PNT1A ($p > 0.05$). Importantly, elevated enzyme activity in each prostate cell lysate was observed with increasing acidity. Statistical analysis of βG activity in prostate cell lysates at a specific pH was performed using one-way ANOVA with Bonferroni post hoc test.

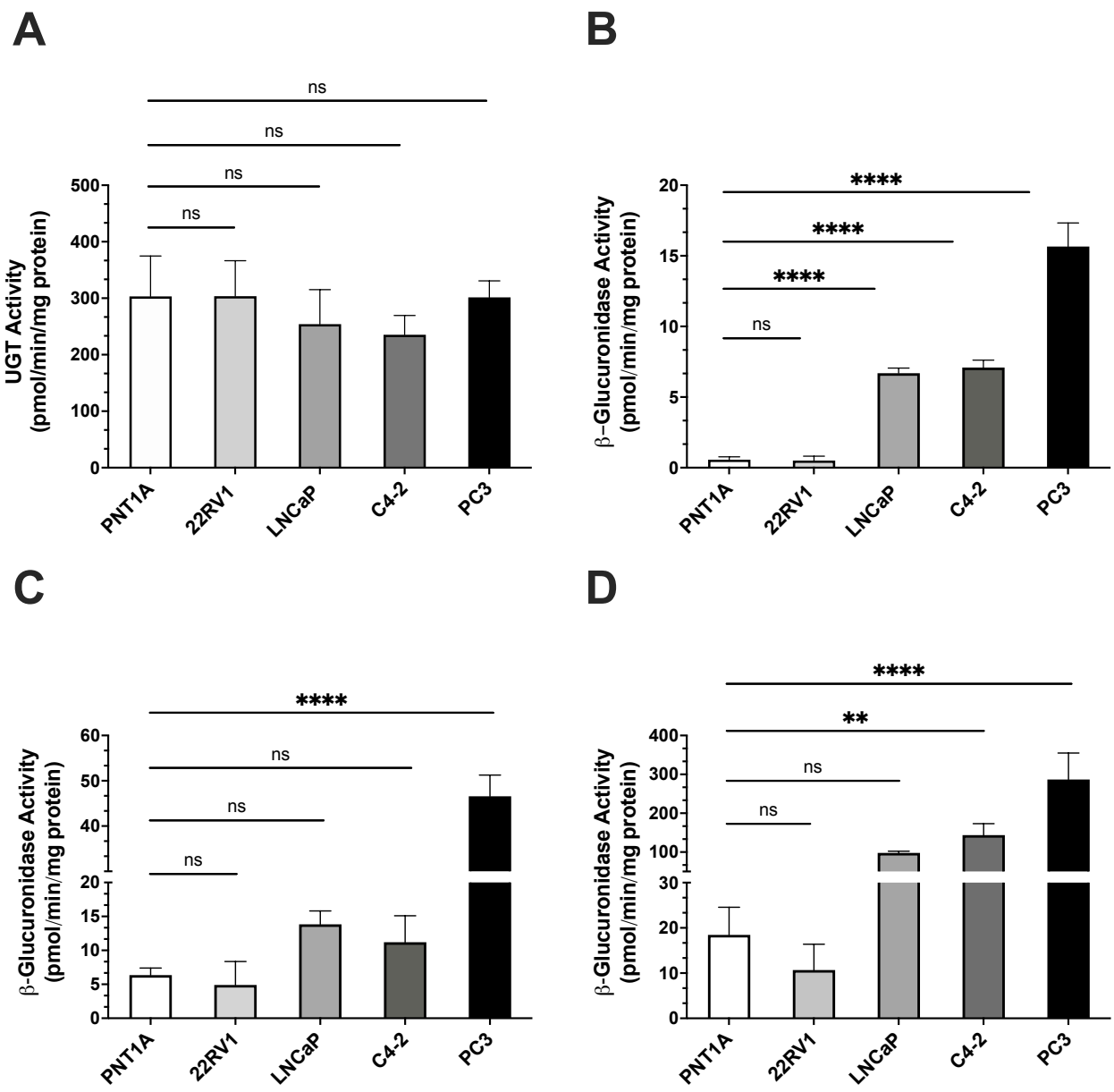

Figure 3.5: The effect of pH on UGT and βG activity in prostate cell lysates
4MU and 4MUG fluorescent assays were run in triplicate on three separate occasions to determine **(A)** Total UGT activity across all prostate cell lysates at optimal pH. No significant differences in enzyme activity was observed when compared to PNT1A. NS = not significant. **(B)** Differences in βG activity across prostate cell lysates at pH 7.4. LNCaP, C4-2 and PC3 showed significantly greater enzyme activity compared to PNT1A. NS = not significant. **** = $p < 0.0001$. **(C)** Prostate cell lysate βG activity at pH 6.8, which represents the tumour microenvironment. PC3 cell lysate shows highest and significantly greater enzyme activity when compared to PNT1A. NS = not significant. **** = $p < 0.0001$. **(D)** Enzyme activity differences between prostate cell lysates at optimal pH. Highest activity is observed in PC3 and C4-2 cell lysates which show significantly greater enzyme activity compared to PNT1A. NS = not significant. ** = $p < 0.01$, **** = $p < 0.0001$.

3.3.2.3 Detoxification:recycling across all prostate cell lysates as function of pH

Elevated enzyme activity in prostate cell lysates at acidic pH contributed to decreased detoxification:recycling ratios. At pH 7.4, optimal pH for UGT enzymes, the ratios for each prostate cell lysate favoured detoxification as rate of glucuronidation exceeded the rate of recycling by 19-604-fold. However, measuring βG activity in more acidic environments led to increased activity. When compared to the intial ratios at physiological pH, elevated enzyme activity at pH 6.8 resulted in 2-11-fold lower ratio values. The decrease in detoxification:recycling becomes more pronounced at pH 5.4, the optimal pH for βG. When comparing both UGT and βG activity at their respective optimal pH values, detoxification:recycling ratios range from 1.1-28.4. These results indicate a 15-33-fold decrease from the initial ratio values comparing both enzymes at pH 7.4 (Table 3.1). In PC3, C4-2 and LNCaP cell lysates, the rate of glucuronidation only slightly exceeds the rate of recycling suggesting that some of the local androgen supply may be recycled rather than eliminated.

Table 3.1: Detoxification:recycling ratios decrease with elevated βG activity at acidic pH

pH 7.4	Cell Lysate	Total UGT (pmol/min/mg)	βG (pmol/min/mg)	Detoxification:recycling
	PC3	301.6	15.7	19.3
	C4-2	235.4	7.1	33.2
	LNCaP	254.0	6.7	38.0
	PNT1A	303.2	0.6	534.7
	22Rv1	303.6	0.5	603.5
pH 6.8	**Cell Lysate**	**Total UGT (pmol/min/mg)**	**βG (pmol/min/mg)**	**Detoxification:recycling**
	PC3	301.6	46.6	6.5
	LNCaP	254.0	13.8	18.4
	C4-2	235.4	11.2	21.0
	PNT1A	303.2	6.4	47.7
	22Rv1	303.6	4.9	61.9
pH 5.4	**Cell Lysate**	**Total UGT (pmol/min/mg)**	**βG (pmol/min/mg)**	**Detoxification:recycling**
	PC3	301.6	286.8	1.1
	C4-2	235.4	143.7	1.6
	LNCaP	254.0	97.9	2.6
	PNT1A	303.2	18.4	16.4
	22Rv1	303.6	10.7	28.4

3.3.3 Enzyme activity and UGT:βG comparison in prostate tissue lysates as function of pH

3.3.3.1 UGT activity across prostate tissue lysates at pH 7.4

Total UGT activity was determined across four distinct prostate tissue lysates using 4MU fluorescence assay. Enzyme activity was assessed at pH 7.4, the optimal pH for UGT enzymes. These results provide a better understanding of the glucuronidation rate in non-cancerous and cancerous prostate tissue samples. Of the four tissue lysates studied, greatest UGT activity was observed in the adenocarcinoma lysate (677.7 ± 207.5 pmol/min/mg) followed by: prostatic hyperplasia (538.5 ± 70.3 pmol/min/mg), adenoma (524.2 ± 101.3 pmol/min/mg) and normal prostate (509.6 ± 24.7 pmol/min/mg) (Figure 3.6A). Although highest enzyme activity was shown in the adenocarcinoma sample, it was not significantly greater than enzyme activity observed in normal prostate or any other prostate tissue lysate tested ($p > 0.05$). Statistical results were obtained using one-way ANOVA with Bonferroni post hoc test.

3.3.3.2 βG activity across prostate tissue lysates at distinct pH levels

Enzyme activity was determined in prostate tissue lysates at pH 7.4, 6.8, and 5.4 using 4MUG fluorescence assay. Non-cancerous and cancerous prostate samples were investigated to characterize how βG activity changes in response to the alkaline environment of the cytosol (pH 7.4), tumour microenvironment (pH 6.8) and lysosomal environment (pH 5.4). At physiological pH, greatest enzyme activity was shown in adenocarcinoma (211.7 ± 14.7 pmol/min/mg) before decreasing to normal prostate (53.8 ± 8.0 pmol/min/mg), adenoma (23.9 ± 8.2 pmol/min/mg) and prostatic hyperplasia (19.7 ± 1.4 pmol/min/mg) (Figure 3.6B). Activity level of βG in normal prostate was significantly greater than that of prostatic hyperplasia ($p < 0.01$) and adenoma ($p <$

0.05), but significantly less than activity found in adenocarcinoma ($p < 0.0001$). Moreover, at the pH representing the TME, highest βG activity was observed in adenocarcinoma (274.3 ± 40.5 pmol/min/mg) followed by: normal prostate (84.6 ± 39.3 pmol/min/mg), adenoma (79.4 ± 24.2 pmol/min/mg) and prostatic hyperplasia (39.9 ± 12.7 pmol/min/mg) (Figure 3.6C). Each tissue showed elevated enzyme activity at pH 6.8 compared to 7.4. Furthermore, enzyme activity in adenocarcinoma lysate showed a significantly greater difference compared to normal prostate ($p < 0.001$). No other significant differences in βG activity was observed between other prostate tissue lysates ($p > 0.05$). Lastly, in the most acidic environment, enzyme activity was greatest in adenocarcinoma (2596.9 ± 57.1 pmol/min/mg) with activity decreasing to: adenoma (750.4 ± 71.6 pmol/min/mg), normal prostate (363.6 ± 28.2 pmol/min/mg) and prostatic hyperplasia (212.9 ± 40.7 pmol/min/mg) (Figure 3.6D). Activity levels of βG in adenocarcinoma and adenoma were significantly greater than that of normal prostate ($p < 0.0001$). Additionally, enzyme activity in normal prostate was significantly greater than prostatic hyperplasia ($p < 0.05$). Statistical results investigating enzyme activity differences at distinct pH values were determined by one-way ANOVA with Bonferroni post hoc test.

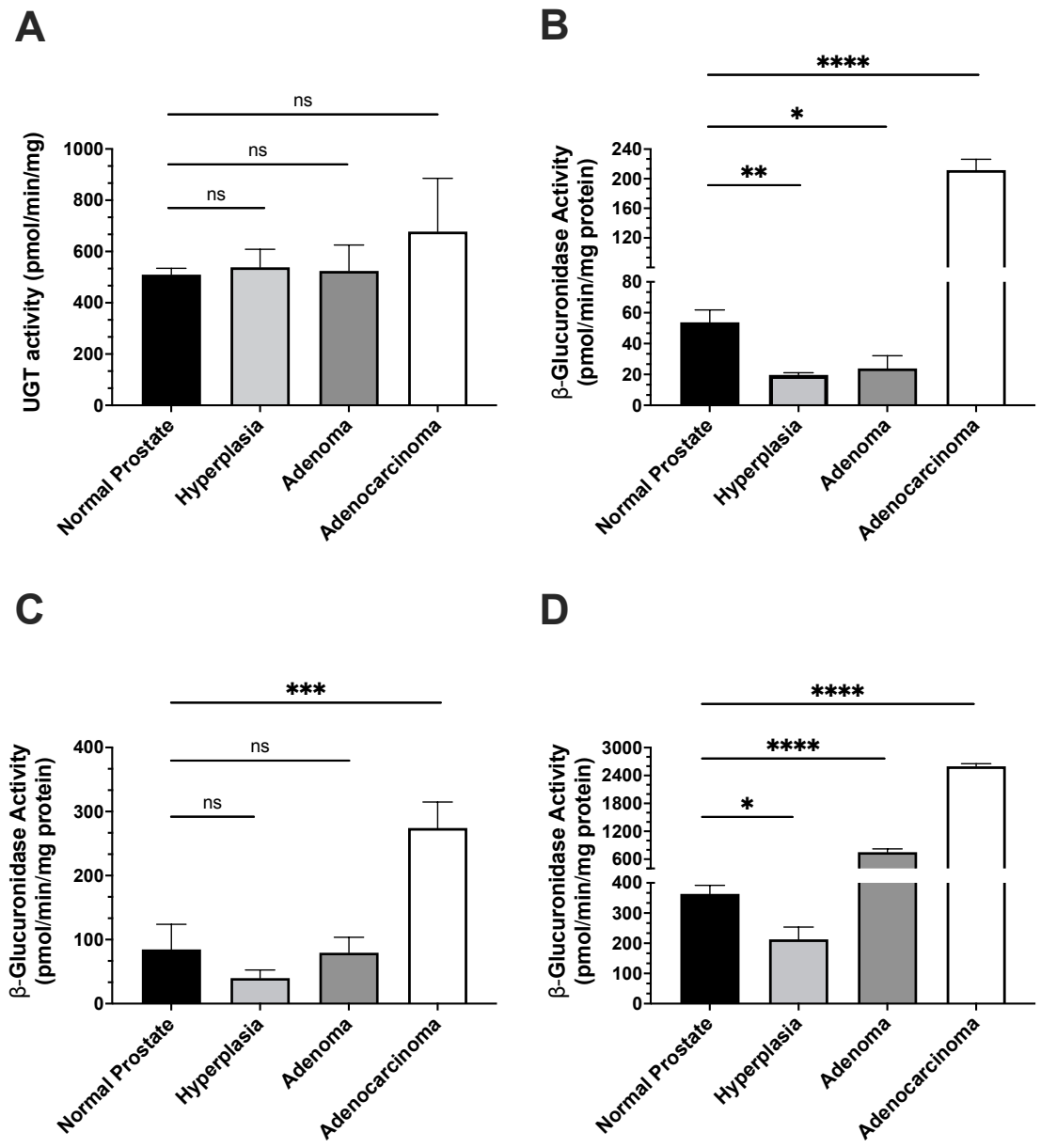

Figure 3.6: UGT and βG activity in prostate tissue lysates as a function of pH
4MU and 4MUG fluorescent assays were run in triplicate on three independent experiments to determine **(A)** Total UGT activity for all prostate tissue lysates at pH 7.4. No significant differences in enzyme activity were observed when comparing level in normal prostate to the other tissue samples. NS = not significant. **(B)** Enzyme activity differences across prostate tissue lysates at pH 7.4. Adenocarcinoma and adenoma lysates showed significantly greater βG activity when compared to normal prostate. * = $p < 0.05$, ** = $p < 0.01$, **** = $p < 0.0001$. **(C)** Activity of βG in prostate tissue samples at pH representing tumour microenvironment, pH 6.8. Only adenocarcinoma shows significantly greater enzyme activity compared to normal prostate. NS = not significant. *** = $p < 0.001$. **(D)** Enzyme activity differences across prostate tissue lysates at optimal pH for βG, pH 5.4. Adenocarcinoma and adenoma lysates show significantly greater enzyme activity compared to normal prostate. * = $p < 0.05$, **** = $p < 0.0001$.

3.3.3.3 Detoxification:recycling across all prostate tissue lysates as function of pH

Increased acidity contributed to elevated βG activity and decreased detoxification:recycling ratios across prostate tissue lysates. The initial ratios, which compare UGT:βG activity at pH 7.4, showed 4-27-fold greater glucuronidation rate in prostate tissue samples suggesting that local metabolism favours androgen elimination rather than androgen recycling. As pH became more acidic, βG activity increased. At pH 6.8, ratio values decreased 1-3-fold when compared to initial recycling rates at physiological pH. At optimal pH for βG, detoxification:recycling decreased by the greatest magnitude resulting in 7-31-fold lower ratio values (Table 3.2). Importantly, when comparing UGT and βG at their respective optimal pH levels, two prostate tissue samples showed a ratio value below 1. Adenocarcinoma and adenoma lysate samples were reported at 0.3 and 0.7 respectively, suggesting that the rate of recycling exceeds the rate of glucuronidation and may promote androgen recycling in these tissues.

Table 3.2: UGT:βG ratios decreased in prostate tissue lysates with increased acidity (UGT is always pH 7.4)

pH 7.4	Tissue Lysate	Total UGT (pmol/min/mg)	βG (pmol/min/mg)	Detoxification:recycling
	Prostatic Adenocarcinoma	677.7	211.7	3.2
	Normal Prostate	509.6	53.8	9.5
	Prostatic Adenoma	524.2	23.9	21.9
	Prostatic Hyperplasia	538.5	19.7	27.4
pH 6.8	**Tissue Lysate**	**Total UGT (pmol/min/mg)**	**βG (pmol/min/mg)**	**Detoxification:recycling**
	Prostatic Adenocarcinoma	677.7	274.3	2.5
	Normal Prostate	509.6	84.6	6.0
	Prostatic Adenoma	524.2	79.4	6.6
	Prostatic Hyperplasia	538.5	39.9	13.5
pH 5.4	**Tissue Lysate**	**Total UGT (pmol/min/mg)**	**βG (pmol/min/mg)**	**Detoxification:recycling**
	Prostatic Adenocarcinoma	677.7	2596.9	0.3
	Prostatic Adenoma	524.2	750.4	0.7
	Normal Prostate	509.6	363.6	1.4
	Prostatic Hyperplasia	538.5	212.9	2.5

3.4 Discussion

Our results provide evidence that βG expression and activity is upregulated in both *in vitro* and *ex vivo* models representing prostate cancer progression. It was shown that enzyme activity increased from non-cancerous to cancerous cell line and prostate tissue lysate where samples with the highest metastatic potential, PC3 cell lysate and adenocarcinoma tissue lysate, showed greatest overall activity. Importantly, βG activity was upregulated across all cell line and prostate tissue lysates as pH became more acidic. The pH shift more accurately represented the lysosomal environment that houses βG, which differs from the more alkaline conditions in microsomes where UGTs reside. This elevated activity, especially when considering activity values at optimal pH, suggests that the metabolic balance between androgen biosynthesis and elimination is not overwhelmingly driven by the glucuronidation rate. In fact, certain prostate cell and tissue lysates show either similar or greater rates of recycling over glucuronidation when comparing UGT activity at pH 7.4 and βG activity at pH 5.4 suggesting that steroid recycling may provide a local supply of androgens to fuel cancer growth. The decreased pH in the prostate between normal and pathophysiological conditions shows that βG activity is elevated in diseases like cancer where the acidity of the tumour microenvironment promotes increased acid hydrolase activity.

The purpose of this research builds on discoveries that βG activity is elevated in a broad range of cancer tissues (Fishman & Anylan, 1947). Our finding of βG activity being elevated with cancer progression in prostate tissue lysates is supported by previous work that found enzyme activity to be roughly 4-fold greater in prostatic carcinoma when compared to benign prostatic hyperplasia (Pearson *et al*., 1989). In the prostate, upregulated βG is believed to provide a localized supply of androgens through steroid recycling. In hormone-dependent cancers,

especially breast cancer, the role of βG in cancer progression was believed to occur as a consequence of regenerating active steroid hormones capable of further initiating downstream proliferation and anti-apoptotic signals (Fishman & Anylan, 1947). Where early development of breast cancer depends on estrogen signalling through the estrogen receptor, so to does prostate cancer development with androgens stimulating signalling via the AR. At the stage where prostate cancer is androgen-dependent, and disease progression is driven by AR transcription of target genes, ADT is commonly used to reduce or suppress circulating androgen levels and free AR binding sites. Importantly, while ADT consistently reduces systemic androgen levels, not all androgen sources are accounted for. While surgical and chemical approaches inhibit testosterone production in the testes from reaching the prostate, adrenal androgens, specifically DHEA, can be metabolized into testosterone (Matsumoto *et al*., 2013; Suzuki *et al*., 2007). Studies have shown that expression of enzymes required for the biotransformation of DHEA into testosterone are elevated in castration-resistant metastatic tumours when compared to untreated primary tumours (Montgomery *et al*., 2008). Besides testosterone production from adrenal androgens, prostate tumours show an ability to produce an androgen supply locally. The activity data of βG provides support that both *in vitro* and *ex vivo* models of prostate cancer produce androgens locally through a steroid recycling pathway, especially in CRPC models. Although PCa progression contributes to altered androgen metabolism, with increased androgen recycling, the role of UGT2B isoforms and androgen elimination is not fully understood.

Androgen inactivation and elimination is modulated by UGT isoforms. Specifically, UGT2B7, 2B15 and 2B17 are capable of metabolizing androgens into glucuronides. However, in the prostate, only 2B15 and 2B17 are expressed (Gauthier-Landry *et al*., 2015). Each isoform shows unique substrate specificity toward androgens where modifications to protein expression

and activity disrupt androgen inactivation and may promote prostate cancer progression (Shafiee-Kermani *et al*., 2021). Previous work reported detection of lower levels of DHT metabolite glucuronides where *UGT2B17* deletion contributed to a reduction in 3α-diol-17 glucuronide and the $UGT2B15^{D85Y}$ polymorphism resulted in decreased formation of 3α-diol-3-glucuronide (Olsson *et al*., 2011). The $UGT2B15^{D85Y}$ polymorphism is a risk factor for prostate cancer suggesting that an inability to effectively remove androgens from the prostate may provide a sufficient local supply to stimulate prolonged AR signalling (Grant *et al*., 2013).

Previous research suggests that different racial groups display unique *UGT2B17* genotype frequencies, some of which may increase prostate cancer risk (Park *et al*., 2006). Compared to *UGT2B15* mRNA expression, which is more influenced by methylation and epigenetic control, *UGT2B17* expression is more associated with the presence of the del/del genotype (Oeser *et al*., 2018). The *UGT2B17* null genotype is most commonly observed in Asian populations where *UGT2B17* mRNA levels were significantly lower compared to Caucasians (Nadeau *et al*., 2011; Oeser *et al*., 2018). In a study comparing *UGT2B17* polymorphisms between Korean and Swedish men, the deletion genotype was 7 times more common among Koreans and these men showed low or undetectable urinary testosterone levels (Jakobsson *et al*., 2006). Similarly, Japanese men showed significantly lower levels of androgen glucuronides compared to Caucasian and African American subjects (Ross *et al*., 1992). The association between *UGT2B17* del/del genotype and PCa risk remains unclear as meta-analyses report conflicting results (Kpoghomou *et al*., 2013; Deng *et al*., 2014). Further investigation studying race and the *UGT2B17* null genotype is warranted as Asians show lowest PCa incidence with greatest del/del genotype frequency, whereas Caucasians with this genotype show increased PCa risk and African Americans are unaffected (Nadeau *et al.*, 2011; Park *et al*., 2006).

Upregulated *UGT2B17* gene expression is shown in CRPC metastases compared to primary PCa tumours (Montgomery *et al*., 2008; Li *et al*., 2016). Detection of overexpressed *UGT2B17* mRNA transcripts and elevated protein expression were found in CRPC samples relative to primary tumours (Lévesque *et al*., 2020). These findings are aligned with my data for 2B15 and 2B17 expression in prostate cell lines. The more commonly expressed UGT isoform is 2B17, where clear protein expression is observed in all cell lines representing CRPC (Figure 3.1B,C). Normal prostate epithelium, PNT1A, shows lowest UGT2B17 expression by normalized optical density analysis. Moreover, the presence of androgens and certain growth factors may contribute to decreased expression of UGT isoforms, even in CRPC models. Multiple studies investigating CRPC using LNCaP cells showed that DHT and growth factors, such as EGF, were capable of downregulating UGT2B15 and 2B17 expression and decreasing levels of DHT metabolite glucuronides (Guillemette *et al*., 1997; Shafiee-Kermani *et al*., 2021). The binding of EGF to the epidermal growth factor receptor (EGFR) and subsequent signalling events promoting prostate tumour growth highlights the importance of alternative signalling mechanisms in CRPC that are capable of inducing AR target genes driving further cancer growth and proliferation.

Investigating protein expression in prostate tissue lysates showed upregulated βG in cancerous tissue. Compared to non-cancerous samples (normal prostate, BPH, adenoma) clear protein expression is observed in adenocarcinoma suggesting that the role of androgen recycling in providing intratumoural androgens may be important to fuel cancer growth. Moreover, UGT2B15 expression is detected across all prostate tissue samples, with greatest expression in BPH tissue. Although 2B15 is capable of metabolizing androgens and associated metabolites, 2B17 is the predominant isoform for androgen inactivation (Meech *et al*., 2019). Expression data

shows 2B17 is more commonly found in BPH and adenoma samples, with less detection in normal prostate and little to no detection in adenocarcinoma (Figure 3.3C). As testosterone and DHT glucuronidation are primarily driven by UGT2B17 in the prostate, lack of this enzyme may lead to less efficient processing by other isoforms, particularly 2B15. Interestingly, as seen in adenocarcinoma, elevated βG expression is associated with little to no 2B17 expression. Previous work has shown that the presence of local androgens in prostate cancer models may result in the reduction of 2B15 and 2B17 expression (Bao *et al*., 2008). In other words, the role of recycling in maintaining a circulating androgen supply may stimulate the suppression of enzymes capable of inactivating and eliminating androgens. In prostate cancer, androgen homeostasis is dysregulated towards favouring androgen production.

Treatment of prostate cancer shows reduced effectiveness following AR modifications and the emergence of alternative signalling pathways in cancer progression. The transition from PCa to CRPC involves modifications to the AR, or its coregulators, that allow AR signalling to continue despite castration levels of circulating androgens. Specifically, AR overexpression, receptor mutations producing a truncated protein without a LBD and upregulation of certain coactivators enable further cancer progression at the CRPC stage (Coutinho *et al*., 2016). However, prostate cancer growth is stimulated by other steroid hormone receptors besides the AR.

Previous studies have shown the ability of estrogen in metastatic PCa to induce transcription of AR target genes through downstream signalling events following ligand binding to either the progesterone receptor or estrogen receptor alpha (Bonkhoff *et al*., 2001; Setlur *et al*., 2008). Additionally, glucocorticoid receptor signalling promotes AR target gene expression in drug resistant-tumours providing another alternative signalling mechanism where AR signalling

is inhibited following anti-androgen treatment (Arora *et al*., 2013). Other androgen-independent signalling mechanisms involving the overexpression of Src family kinases and activation of STAT3 by pro-inflammatory cytokine IL-6 are shown in the literature to stimulate prostate cancer growth (Fizazi, 2007; Chen *et al*., 2000). Moreover, AR antagonists with increased potency are contributing to higher frequency of new metastatic PCa phenotypes that operate through elevated mitogen-activated protein kinase (MAPK) and fibroblast growth factor receptor (FGFR) signalling (Bluemn *et al.*, 2017). One particular area of interest is the role of glycosaminoglycans (GAGs) in cancer biology.

Heparan sulfate (HS), existing freely or bound to proteins to form HS proteoglycans, act as a co-receptor with FGFR to bind fibroblast growth factors (FGFs) as ligands to induce downstream activation of MAPK signalling cascades leading to further cell growth and proliferation (Mao *et al.*, 2016). Of the androgen-independent signalling mechanisms outlined above, the function of HS in cancer progression is most important for my research project as it represents a common substrate for a variety of glycosidases. Previous studies have shown that heparanase, a specific endo-β-D-glucuronidase, is commonly overexpressed in a variety of malignancies (Jayatilleke & Hulett, 2020; Coombe & Gandhi, 2019). Heparanase cleaves the specific glycosidic linkage between glucuronic acid and a sulfated glucosamine resulting in the degradation of the extracellular matrix (ECM) and basement membrane (BM) promoting tumour cell invasion and the colonization of secondary tumours from the primary site (Elgundi *et al*., 2020; Vlodavsky *et al*., 2011). Additionally, the breakdown of HS may release growth factors like FGF that are free to bind to their respective receptors and activate downstream signalling cascades (Elgundi *et al*., 2020). The upregulation and extracellular secretion of heparanase for tumour invasion was observed in the malignant PCa cell line, PC3 (Kosir *et al*., 1997). The

ability of heparanase to degrade the ECM and BM extends to other glycosidases, specifically βG. This exoglycosidase, which catalyzes the removal of a terminal GlcA from the non-reducing end of an oligosaccharide chain, is found in the ECM of different tumour types and may play a degradative role in the breakdown of GAGs and the growth of tumours (Bernacki *et al*., 1985).

These findings provide support for the 4MUG data observed in the prostate cell lysates. Specifically, greatest βG activity being observed in PC3 at all pH levels may be due to the enzyme's role in heparan sulfate degradation and release of FGF or other growth factors, not androgen recycling. A cell line representing SCNC, which is AR-null, likely does not advance by recycling testosterone and DHT to activate the AR signalling axis. However, the role of βG in recycling steroid glucuronides may extend to the activation of compounds capable of binding estrogen receptor alpha and the progesterone receptor to bypass AR signalling and promote transcription of AR target genes. Therefore, in advanced metastatic PCa, βG activity may contribute to a variety of functions beyond androgen recycling that stimulate androgen-independent signalling pathways for disease progression. In contrast, βG activity in CRPC cell lines that express AR, C4-2 and LNCaP, likely plays a role in maintaining local tumoural androgen supply for driving cancer growth through AR signalling.

Future work should investigate changes in βG tissue distribution and activity using normal, benign and malignant tissue samples. Immunohistochemistry (IHC) using prostate tissue slides should provide useful information on how enzyme expression and location change from non-cancerous to cancerous samples. Additionally, changes in βG expression and activity should be studied in treatment naïve and ADT-treated tumours. The use of ADT-treated samples will address the role of βG in contributing to alternative signalling mechanisms for prostate cancer progression that bypass AR signalling. Lastly, quantitation of steroid and steroid metabolites

using liquid chromatography-mass spectrometry (LC-MS) extracted from patient serum and tissue lysates should be further investigated. Steroid level differences between normal and PCa patients provides a better understanding of the disconnect between detected levels in the serum and tissues, and helps address if compounds other than androgens are elevated in cancer patients. Further investigations into the role of glycosidases in cancer biology, especially where functions may change with emergence of more aggressive cancer phenotypes, may confirm βG as a novel biomarker in PCa and promote development of potent inhibitors to either reduce or suppress cancer growth. To improve treatment in patients with metastatic CRPC, a better understanding of glycosidase mechanisms of action and how tumour cells upregulate these enzymes to perform diverse functions at different stages of disease progression is required.

As prostatic adenocarcinoma may be androgen-insensitive, the potential role of βG in recycling other non-steroidal endobiotics, that enable cancer progression and/or activation of metastatic pathways, should be investigated. Suggestions for future work include either ribonucleic acid (RNA)-sequencing or untargeted proteomics with machine learning approaches to more accurately identify the mechanistic pathways in which βG is participating. These network approaches would be followed up with laboratory experiments in the cell lines representing CRPC (LNCaP, C4-2 and PC3), using UGT and βG knock out (short hairpin RNA, clustered regularly interspaced short palindromic repeats), as well as V79 (hamster lung fibroblast) or HEK293 (human embryonic kidney cell line) which are βG and UGT null respectively. Additionally, conducting overexpression experiments upregulating βG and UGT enzymes levels may determine their effects on growth, invasion and viability assays.

The data presented in this thesis represent novel insights into βG expression and activity with prostate cancer progression using *in vitro* and *ex vivo* models. Elevated enzyme activity is

likely contributing to PCa development through both androgen-dependent and androgen-independent mechanisms depending on which substrates are being recycled. The upregulation of βG across distinct cancers types, particularly PCa, suggests it may be a useful cancer biomarker. While additional research is needed to elucidate the role of βG across all signalling pathways stimulating metastasis, this thesis provides support that a previously understudied recycling enzyme may play a larger role in cancer progression than initially thought. The significance of our research highlights the multi-functional impact βG may have in driving cancer growth from PCa to CRPC through intratumoural androgen production and stimulation of androgen-independent alternative signalling mechanisms.

Chapter 4: Discussion, conclusions and future work

4.1 Discussion and conclusions

Metabolic recycling plays a fundamental role in balancing compound levels in the body. Recycling enzymes catalyze deconjugation reactions, often serving as the obligate partners to a host of phase II drug metabolizing enzyme families that function in eliminating compounds through improving hydrophilicity of substrates (Meech *et al*., 2019). This thesis focuses on βG, the recycling enzyme reversing the most common phase II reaction, glucuronidation, catalyzed by the UGT enzyme superfamily (Jančová *et al*., 2010). The importance of UGT function contributing to the detoxification and removal of endo- and xenobiotics is well documented in the drug metabolism literature (Jančová & Šiller, 2012; Tukey & Strassburg, 2000; Meech *et al*., 2019). However, the historical interest in compound elimination has often undermined the biological importance of recycling in health and disease. The evolutionarily conserved nature of βG suggests that compound recycling plays a key physiological role in balancing chemical equilibrium through the removal of glucuronic acid and regeneration of lipophilic parent molecules (Lalley *et al*., 1970; Sperker *et al*., 1997; Henrissat, 1991).

Although not extensively studied, βG is implicated in multiple diseases often involving the build up of certain hormones or polysaccharides. Interestingly, both reduced and elevated enzyme activity contribute to disease with the accumulation of bilirubin and GAGs manifesting clinically as hyperbilirubinemia and Sly Syndrome respectively due to genetic defects in βG expression (Sirota *et al*., 1992; Gourley & Arend, 1986; Sly *et al*., 1973). Additionally, βG has been linked to HIV and several cancer types, of which prostate cancer is most relevant to this research (Saha *et al*., 1991; Pearson *et al*., 1989). Based on the available evidence, this thesis

intended to contribute to the growing literature of βG in health and disease by first addressing the lack of available data on enzyme expression and activity in healthy human tissues.

In order to address the lack of comparative βG data across distinct tissue types described in Sperker *et al.*, Chapter 2 involved constructing the first comprehensive body map of protein expression and activity. This research comprised my first Aim, in which βG expression and activity was determined across 14 unique tissues. Enzyme activity was initially calculated at pH 7.4 according to a previously validated fluorescent assay (Trubetskoy & Shaw, 1999). Additionally, total UGT activity was assessed using a similar fluorescent assay to generate UGT: βG ratios providing a measure for local metabolism at pH 7.4 in each tissue (Collier *et al*., 2000). Of 14 tissues analyzed, greatest βG expression at pH 7.4 was found in prostate, followed closely by: caecum, liver, and adrenal. However, with the exception of caecum, these tissues showed greater UGT activity such that the resulting UGT:βG values favoured the rate of conjugation by 102-192-fold at pH 7.4.

Low UGT:βG in the intestinal tissues prompted further investigation into βG activity and the role it may play in enterohepatic recycling. Given that a healthy GI tract contains unique pH environments, enzyme activity was assessed at three pH levels: (1) pH 7.4 representing the cytosolic pH and served as optimal pH for human UGT and *E. coli* βG activity, (2) pH 6.8 corresponding to the slightly acidic environment found within the proximal small intestine and may reflect the environment in intestinal lysates where all organelles are lysed together and (3) pH 5.4 representing the lysosomal environment and optimal pH for human βG (Evans *et al.,* 1999; Fallingborg, 1999; Awolade *et al*., 2020; Weyel *et al.*, 2000). Across all intestinal tissues, βG activity increased from pH 7.4, to pH 6.8 and to pH 5.4, the optimal pH. Caecum showed greatest enzyme activity at all three pH levels which peaked interest as this region is most

densely populated with microbes (Gorbach, 1996). *E. coli* βG from five non-pathogenic strains was assessed at the same three pH levels. A 21-fold difference in enzyme activity was reported between BigEasy TSA and SURE2 at optimal pH, pH 7.4 (Awolade *et al*., 2020). In comparison to human βG at pH 5.4, enzyme activity was greater in *E. coli* strains. Although highest enzyme activity was observed in *E. coli*, the overall increase in enzyme activity from pH 7.4 to 5.4 was 13-fold in human and only 2-fold in bacteria, as expected because bacterial βG is cytosolic, not lysosomal.

These results may be partly explained based on the substrates for which both eukaryotic and prokaryotic βG are optimized. Specifically, *E. coli* possess a GUS operon making them sensitive to the presence of certain glucuronides and are structurally optimized to metabolize smaller glucuronides, such as 4MUG, based on a L1 structure near the active site which restricts available space at the active site (Little *et al*., 2018; Pollet *et al.*, 2017). On the other hand, the active site of human βG is not sterically hindered by the L1 structure and is capable of degrading larger polysaccharides. Despite these differences, both enzyme versions are capable of contributing to enterohepatic recycling. Human βG is associated with recirculating endobiotics such as bilirubin and bile acids whereas bacterial βG is implicated in xenobiotic metabolism, particularly the use of drugs that raise clinical concerns with the emergence of intestinal ulcers and dose-limiting toxicity (Bhatt *et al*., 2020; Wallace *et al*., 2010). Despite this, as our probe substrate is a coumarin derivative, clear evidence for human βG involvement in xenobiotic metabolism is presented.

Importantly, measuring βG as a function of pH allowed for the determination of enzyme activity at pH 5.4, the native lysosomal pH. The assessment of enzyme activity in more acidic environments deviated from the original method outlined by Trubetskoy and Shaw at pH 7.4,

which does not accurately reflect human βG in the lysosome. The reaction product, coumarin derivative 4MU, is intensely fluorescent and shows a consistent emission spectrum from pH 2-11, well within the acidic pH levels tested (Fink & Koehler, 1970). All experiments monitored λ_{em} at 460 nm, the peak emission for 4MU within the target pH range, and λ_{exc} at 355 nm. Although the emission spectrum did not deviate with pH change in these studies, shorter excitation wavelengths should be applied to more acidic pH profiles. Excitation wavelength remained at 355 nm for measurements at both pH 6.8 and pH 5.4 where some literature suggests detecting excitation at either 320 or 330 nm below pH 6 (Zhi *et al*., 2013; Fink & Koehler, 1970). Changes in excitation wavelength result in changes to the Stokes shift. Given that pK_a of the 7-hydroxyl proton of 4MU is 7.85 ± 0.03, the neutral species is most likely to be present across all pH levels tested, pH 7.4, 6.8 and 5.4 (Zhi *et al*., 2013).

The expression profile of βG across human tissues showed weak correlation with activity. Of particular interest were prostate and adrenal, two tissues with elevated enzyme activity but weak protein detection in initial western blot experiments. To address this, additional experiments using EndoH were conducted to investigate the role of glycosylation and determine whether partial removal of glycan chains may allow for proper detection of βG in expression studies. Liver, adrenal and prostate lysates showed clear band detection in both EndoH treated and control samples, with glycosylation accounting for a 2-3 kDa difference. Interestingly, EndoH treated samples appeared as a singlet in liver lysate and a doublet in adrenal and prostate lysates suggesting βG may be differentially glycosylated. Protein glycosylation is likely driven by tissue-specific regulation.

The second portion of this thesis focused on βG and its potential role in prostate cancer progression. Chapter 3 investigated enzyme activity and expression using *in vitro* and *ex vivo*

models. Similar to pH experiments conducted in Chapter 2, βG activity was assessed at three pH levels: (1) pH 7.4 corresponding to the cytosolic pH and optimal pH for UGT enzymes, (2) pH 6.8 representing the slightly acidic tumour microenvironment and (3) pH 5.4 as the lysosomal pH and optimal pH for human βG (Feng *et al*., 2018; Weyel *et al*., 2000). Our findings demonstrate enzyme upregulation with cancer progression, where PC3 cells and adenocarcinoma tissue displayed greatest enzyme activity across all pH levels tested. The UGT:βG ratios, considering UGT activity at pH 7.4 and βG activity at pH 5.4, showed lower values in more metastatic cell lines and malignant tissues. These results suggest the importance of recycling in stimulating further cancer growth through maintaining a local supply of androgens and other signalling compounds required by tumours. Given that enzyme activity is upregulated in an androgen-sensitive and androgen-insensitive context, βG may be multi-functional, playing roles in recirculating hormones for subsequent AR binding and degrading GAGs in the ECM to promote tumour invasion (Bernacki *et al*., 1985). Although the exact mechanisms are not identified in this thesis, the elucidation of alternative signalling pathways stimulating metastasis remains an ongoing area of research.

Expression studies in prostate cell lines and tissue lysates show clear βG expression in models of advanced disease. Specifically, protein expression is greatest in C4-2 and LNCaP cells and adenocarcinoma tissue, and appears as a doublet. Of the UGT isoforms found in the prostate, UGT2B17 was expressed in all prostate cell lines and 2B15 only in LNCaP. At the tissue level, 2B15 is detected in each sample and 2B17 is present in all tissues excluding adenocarcinoma. These results, particularly those observed for 2B17 in prostate cell lines, are supported by previous findings that show *UGT2B17* gene and protein expression are upregulated in CRPC compared to primary tumours (Montgomery *et al*., 2008; Li *et al*., 2016; Lévesque *et al*., 2020).

Overall, the results of Chapter 2 characterize βG expression and activity in healthy tissues, with novel findings relating to the human enzyme likely contributing to enterohepatic recycling. To continue with investigating βG in disease, Chapter 3 focuses on the enzyme's role in prostate cancer and the importance of recycling as an understudied mechanism by which tumours can sustain growth and proliferation signalling through the potential reuse of signalling molecules. The major findings presented in this thesis were that:

- βG is differentially expressed and active across 14 distinct tissue types suggesting that recycling varies in each tissue according to local metabolic demands.
- Both human and bacterial βG are likely to contribute to enterohepatic recycling of endo- and xenobiotics, being optimized to metabolize substrates with different affinities.
- Accurate assessment of βG activity at native pH 5.4 was assessed in intestinal tissues where the recycling rate was shown to exceed the glucuronidation rate in the jejunum and caecum.
- βG is differentially glycosylated across tissues suggesting the glycoprotein is subject to tissue-specific regulation.
- Upregulated βG activity is associated with prostate cancer progression and highest in prostate cell lines representing CRPC and SCNC (C4-2, LNCaP and PC3) and malignant prostate tissues from adenocarcinoma.
- Enzyme activity increases in more acidic environments suggesting that secreted βG operates efficiently in acidic tumour microenvironments.
- βG contribution to prostate cancer is likely multi-faceted, with recycling of hormones and other signalling molecules and degradation of larger

polysaccharides playing roles in progression of both androgen-sensitive and androgen-insensitive cancer types.

- UGT isoforms in the prostate, UGT2B15 and UGT2B17, are differentially expressed in cell lines and tissue lysates with 2B17 more commonly expressed in cell lines and 2B15 in prostate tissues.
- LNCaP, C4-2, and PC3 cells were shown to be valid *in vitro* CRPC and SCNC models based on elevated βG activity and UGT2B17 expression, which is commonly upregulated in CRPC samples (Lévesque *et al*., 2020). The absence of UGT2B17 expression in adenocarcinoma suggests that this tissue, while still useful as an *ex vivo* cancer model, does not accurately represent CRPC based on UGT expression profile.
- LNCaP, C4-2 and PC3 cells provide systems of advanced disease that are both androgen-sensitive, LNCaP, and androgen-insensitive, C4-2 and PC3.

The greatest strengths of the presented research are: (1) first constructed βG expression and activity profile in the human body to provide comparative data between healthy tissues, (2) accurate assessment of βG activity at its native, optimal pH in the lysosome, (3) the novel finding that enterohepatic recycling is likely due to both eukaryotic and prokaryotic forms of βG, where active sites are optimized to handle different substrates with high affinity and (4) the upregulation of βG activity in prostate cancer development using both androgen-sensitive and androgen-insensitive models suggesting a multi-functional contribution to disease progression. Although the results presented in this thesis provide new insights into drug metabolism and cancer biology, certain limitations of the research are acknowledged. Firstly, all activity assays

assessing βG activity were conducted using only one substrate, 4MUG, which cannot precisely describe the range of kinetics for other glucuronides, particularly testosterone and DHT glucuronides. Secondly, assessing enterohepatic recycling using bacterial βG only involved the study of non-pathogenic *E. coli*, which represents a subset of all microbial species that occupy the gut and are subject to change. A variety of bacterial βG with unique active site structures exist, suggesting that larger molecules not optimized for *E. coli* may be suitable substrates for other microbes. Lastly, samples of duodenum, jejunum, ileum, caecum, brain, normal prostate, benign prostatic hyperplasia, adenoma and adenocarcinoma were all dervied from different single donors. Pooled samples, or those derived from several separate donors, should be assessed to determine genetic diversity that can accurately translate to the population level.

4.2 Future directions

4.2.1 Immunohistochemistry of βG in non-cancerous and cancerous prostate tissues to determine tissue distribution

Building on previous protein expression studies, enzyme distribution among normal, benign and malignant tissues should be assessed by IHC. These experiments will identify potential changes in βG tissue distribution using normal, benign, neoplasia and adenocarcinoma prostate tissue slides. Of particular interest is identifying protein localization differences between non-cancerous and cancerous samples, in addition to observing whether the distribution pattern among malignant samples is consistent or variable. Our laboratory possesses the required tissue samples and commercially validated antibodies for accurate detection.

4.2.2 Investigation of βG and UGT2B15/2B17 expression and activity in treatment naïve and ADT prostate tumours

Since androgens play a key role in the early development of prostate cancer through AR signalling, use of ADT-treated samples may confirm the role of βG in alternative signalling mechanisms stimulating cancer growth. Importantly, the study of human tumours, with or without androgen deprivation, provides another model to investigate the potential association between βG and disease progression which can be compared to prior *in vitro* and *ex vivo* work. If protein activity and expression are upregulated in ADT-treated samples compared to naïve tumours, further support for βG as a prostate cancer biomarker will be established.

Analysis of UGT isoform expression and activity in tumour samples provides an overview on glucuronidation and how it may be altered with androgen deprivation. Previous literature shows that UGT2B17 may be downregulated in CRPC and that DHT may play a negative feedback role in reducing *UGT2B17* transcripts (Montgomery *et al*., 2008; Guillemette *et al*., 1997). Comparison of UGT2B15 and UGT2B17 in naïve and ADT-treated tumours will address how the presence or absence of androgens affect expression and activity differences *in vivo*.

Overall, upregulated or constant protein expression and activity among ADT-treated samples may confirm βG as a useful survival mechanism leveraged by tumours. The addition of assessing UGT2B15/2B17 changes in naïve and ADT-treated samples provides a clear metabolic picture regarding the dominant metabolic pathway, compound elimination or recycling, in these prostate tumours.

4.2.3 Quantification of steroid glucuronides and metabolites in patient serum and tissue lysates using LC-MS

Detection of steroids and associated metabolites provide insights into metabolic differences between matched serum and tissue samples from normal, PCa and CRPC patients. As prostate cancer advances, the detection of steroid glucuronides should decrease due to either elevated βG activity or downregulated UGT2B15/2B17. Quantifying testosterone and DHT is important in an androgen-sensitive context whereas the detection of other steroids, such as estrogen and progesterone, may indicate activation of androgen-insensitive pathways fueling cancer growth.

Given the sensitivity and limit of detection using this method, an accurate picture of the metabolome can be constructed for serum and tissue samples from non-cancerous and cancerous sources. These experiments may support previous work detailing βG and UGT2B15/2B17 activity based on the detection of certain compounds known to be enzyme products in the associated deconjugation and conjugation reactions respectively. The balance between steroids and their glucuronides, in samples from different patients, may provide a useful measure for distinguishing between health and disease.

In conclusion, this thesis characterizes βG expression and activity in health and disease, detailing the potential roles in enterohepatic recycling and prostate cancer progression, thus showing that recycling pathways may contribute to clinically relevant conditions. These novel findings are applicable to the fields of drug metabolism and oncology, but future work is necessary to confirm exact βG mechanisms and investigate glucuronide metabolism in depth.

Bibliography

Abehouse, A. *et al.* The molecular taxonomy of primary prostate cancer. *Cell* **163**, 1011-1025 (2015).

Abuhelwa, A.Y., Foster, D.J.R., & Upton, R.N. A quantitative review of meta-models of the variability and factors affecting oral drug absorption – part I: Gastrointestinal pH. *AAPS J.* **18**(5):1309-1321 (2016).

Adlercreutz, H., Martin, F., Järvenpää, P., & Fotsis, T. Steroid absorption and enterohepatic recycling. *Contraception* **20**(3), 201-223 (1979).

Allanson, J.E., Gemmill, R.M., Hecht, B.K., Johnsen, S., & Wenger, D.A. Deletion mapping of the beta-glucuronidase gene. *Am. J. Med Genet.* **29**(3), 517-522 (1988).

Arcaro, A. Targeting the insulin-like growth factor-1 receptor in human cancer. *Front. Pharmacol.* 4**,** 30 (2013).

Arora, V.K., Schenkein, E., Murali, R., Subudhi, S.K., Wongvipat, J., Balbas, M.D., Shah, N., Cai, L., Efstathiou, E., Logothetis, C., Zheng, D., & Sawyers, C.L. Glucocorticoid receptors confers resistance to antiandrogens by bypassing androgen receptor blockade. *Cell* **155**, 1309-1322 (2013).

Attardi, B.J., Burgenson, J., Hild, S.A, & Reel, J.R. Steroid hormonal regulation of growth, prostate specific antigen secretion, and transcription meditated by the mutated androgen receptor in CWR22Rv1 prostate carcinoma cells. *Mol Cell Endocrinol*. **222**(1-2), 121-132 (2004).

Avancès, C., Georget, V., Térouanne, B., Orio, F., Cussenot, O., Mottet, N., Costa, P., & Sultan, C. Human prostatic cell line PNT1A, a useful tool for studying androgen receptor transcriptional activity and its differential subnuclear localization in the presence of androgens and antiandrogens. *Molecular and Cellular Endocrinology* **184**, 13-24 (2001).

Awolade, P., Cele, N., Kerru, N., Gummidi, L, Oluwakemi, E., & Singh, P. Therapeutic significance of β-glucuronidase activty and its inhibitors: A review. *European Journal of Medicinal Chemistry* **187**, 111921-111921 (2020).

Baker, M.E. Albumin, steroid hormones and the origin of vertebrates. *J. Endocrinol.* **175**(1), 121-127 (2002).

Barbieri, C.E., *et al*. Exome sequencing identifies recurrent SPOP, FOXA1, and MED12 mutations in prostate cancer. *Nat Genet.* **44**(6), 685-689 (2012).

Bélanger, A., Pelletier, G., Labrie, F., Barbier, Ol, Chouinard, S. Inactivation of androgens by UDP-glucuronosyltransferase enzymes in humans. *Trends Endocrinol. Metab.* **14**, 473-479 (2003).

Bennett, N.C., Gardiner, R.A., Hooper, J.D., Johnson, D.W., & Gobe, G.C. Molecular cell biology of androgen receptor signalling. *Int. J. Biochem. Cell Biol.* **42**, 813-827 (2010).

Beratis, N.G., Kaperonis, A., Eliopoulou, M.I., Kourounis, G., Tzingounis, V.A. Increased activity of lysosomal enzymes in the peritoneal fluid of patients with gynecologic cancers and pelvic inflammatory disease. *J Cancer Res Clin Oncol*. **131**(6), 371-376 (2005).

Berg, R.D. The indigenous gastrointestinal microflora. *Trends Microbiol.* **4**(11), 430-435 (1996).

Bernacki, R.J., Niedbala, M.J., & Korytnyk, W. Glycosidases in cancer and invasion. *Cancer Metastatis Rev*. **4**, 81-101 (1985).

Bhatt, A.P., Pellock, S.J., Biernat, K.A., Walton, W.G., Wallace, B.D., Creekmore, B.C., Letertre, M.M., Swann, J.R., Wilson, I.D., Roques, J.R., Darr, D.B., Bailey, S.T., Montgomery, S.A., Roach, J.M., Azcarate-Peril, M.A., Sartor, R.B., Gharaibeh, R.Z., Bultman, S.J., & Redinbo, M.R. Targeted inhibition of gut bacterial β-glucuronidase activity enhances anticancer drug efficacy. *PNAS* **117**, 7374-7381 (2020).

Biernat, K.A., Pellock, S.J., Bhatt, A.P., *et al.* Structure, function, and inhibition of drug reactivating human gut microbial β-glucuronidases. *Sci Rep.* **9**, 825 (2019).

Bill-Axelson, A., Holmberg, L., Garmo, H., Taari, K., Busch, C., Nordling, S., Häggman, M., Andersson, S.O., Andrén, O., Steineck, G., Adami, H.O., Johansson, J.E. Radical prostatectomy or watchful waiting in prostate cancer – 29-year follow-up. *N. Engl. J. Med.* **379**, 2319-2329 (2018).

Bluemn, E.G., Coleman, I.M., Lucas, J.M., Coleman, R.T., Hernandez-Lopez, S., Tharakan, R., Bianchi-Frias, D., Dumpit, R.F., Kaipainen, A., Corella, A.N., Yang, Y.C., Nyquist, M.D., Mostaghel, E., Hsieh, A.C., Zhang, X., Corey, E., Brown, L.G., Nguyen, H.M., Pienta, K., Ittmann, M., Schweizer, M., True, L.D., Wise, D., Rennie, P.S., Vessella R.L., Morrissey, C., & Nelson, P.S. Androgen receptor pathway-independent prostate cancer is sustained through FGF signaling. *Cancer Cell* **32**(4), 474-489 (2017).

Body, J.J., Casimiro, S., & Costa, L. Targeting bone metastases in prostate cancer: improving clinical outcome. *Nat. Rev. Urol.* **12**, 340-356 (2015).

Bonkhoff, H., Fixemer, T., Hunsicker, I., & Remberger, K. Progesterone receptor expression in human prostate cancer: correlation with tumor progression. *Prostate* **48**(4), 285-291 (2001).

Boyland, E., Gasson, J.E., & Williams, D.C. Enzyme activity in relation to cancer. *Br J Cancer*. **11**(1), 120-129 (1957).

Burchell, B., Brierley, C.H., & Rance, D. Specificity of human UDP-glucuronosyltransferases and xenobiotic glucuronidation. *Life Sci.* **57**, 1819-1831 (1995).

Canadian Cancer Society's Advisory Committee on Cancer Statistics. Canadian Cancer Society 2021. (Toronto, ON, 2021).

Catimel, G., Chabot, G.G., Guastalla, J.P., Dumortier, A., Cote, C., Engel, C., Gouyette, A., Mathieu-Boué, A., Mahjoubi, M., & Clavel, M. Phase I and pharmacokinetic study of irinotecan (CPT-11) administered daily for three consective days every three weeks in patients with advanced solid tumors. *Ann. Oncol.* **6**(2), 133-140 (1995).

Ceder, Y., Bjartell, A., Culig, Z., Rubin, M.A., Tomlins, S., & Visakorpi, T. The molecular evolution of castration-resistant prostate cancer. *Eur Urol Focus.* **2**(5), 506-513 (2016).

Centers for Disease Control (CDC). Kaposi's sarcoma and Pneumocystis pneumonia among homosexual men. *Morb. Mortal. Wkly. Rep.* **30**(25), 305-308 (1981).

Cheever, M.A., & Higano, C.S. PROVENGE (Sipuleucel-T) in prostate cancer: The first FDA-approved therapeutic cancer vaccine. *Clin. Cancer Res.* **17**, 3520-3526 (2011).

Chen, T., Wang, L.H., & Farrar, W.L. Interleukin 6 activates androgen receptor-mediated gene expression through a signal transducer and activator of transcription 3-dependent pathway in LNCaP prostate cancer cells. *Cancer Res.* **60**(8), 2132-2135 (2000).

Collier, A., Tingle, M., Keelan, J., Paxton, J., & Mitchell, M. A highly sensitive fluorescent microplate method for the determination of UDP-glucuronosyltransferase activity in tissues and placental cell lines. *Drug Metab. Dispos.* **28**, 1184-1186 (2000).

Collier, A., Tingle, M., Paxton, J., Mitchell, M., & Keelan, J. Metabolizing enzyme localization and activities in the first trimester human placenta: the effect of maternal and gestational age, smoking and alcohol consumption. *Human Reproduction* **17**, 2564-2572 (2002).

Coombe, D.R., & Gandhi, N.S. Heparanase: A challenging cancer drug target. *Front Oncol.* **9**, (2019).

Cooper, G.M. The cell: A molecular approach. 2nd edition. 2000.

Coutinho, I., Day, T.K., Tilley, W.D., & Selth, L.A. Androgen receptor signaling in castration-resistant prostate cancer: a lesson in persistence. *Endocrine-Related Cancer* **23**, 179-197 (2016).

Crawford, E.D. Understanding the epidemiology, natural history, and key pathways involved in prostate cancer. *Urology* **73**(5), S4-S10 (2009).

Crawford, E.D., Heidenreich, A., Lawrentschuk, N., Tombal, B., Pompeo, A.C.L., Mendoza-Valdes, A., Miller, K., Debruyne, F.M.J., & Klotz, L. Androgen-targeted therapy in men with prostate cancer: evolving practice and future considerations. *Prostate Cancer and Prostatic Diseases* **22**, 24-38 (2019).

Culig, Z., Hobisch, A., Cronauer, M.V., Radmayr, C., Trapman, J. Hittmair, A., Bartsch, G., & Klocker, H. Androgen receptor activation in prostatic tumor cell lines by insulin-like growth factor-1, keratinocyte growth factor, and epidermal growth factor. *Cancer Res.* **54**(20), 5474-5478 (1994).

Culp, M.B., Soerjomataram, I., Efstathiou, J.A., Bray, F., & Jemal, A. Recent global patterns in prostate cancer incidence and mortality rates. *Eur. Urol.* **77**(1), 38-52 (2020).

Cunha, G.R., Vezina, C.M., Isaacson, D., Ricke, W.A., Timms, B.G., Cao, M., Franco, O., & Baskin, L.S. Development of the human prostate. *Differentiation* **103**, 24-45 (2018).

Dahms, N.M., Lobel, P., & Kornfield, S. Mannose 6-phosphate receptors and lysosomal enzyme targeting. *J. Biol. Chem.* **264**, 12115-12118 (1989).

Dall'Era, M.A., Albertsen, P.C., Bangma, C., Carroll, P.R., Carter, H.B., Cooperberg, M.R., Freedland, S.J. Klotz, L.H., Parker, C., & Soloway, M.S. Active surveillance for prostate cancer: a systematic review of the literature. *Eur. Urol.* **62**, 976-983 (2012).

D'Amico, A.V. US food and drug administration approval of drugs for the treatment of prostate cancer: a new era has begun. *J. Clin. Oncol.* **32**(4), 362-364 (2014).

Davey, R.A., & Grossmann, M. Androgen receptor structure, function and biology: from bench to bedside. *Clin Biochem Rev.* **37**(1), 3-15 (2016).

Dehm, S.M., Tindall, D.J. Androgen receptor structural and functional elements: role and regulation in prostate cancer. *Mol. Endocrinol.* **21**, 2855-2863 (2007).

Deng, X., Cheng, Y., Yang, X., Li, S., Zhao, R., Liu, K., Liu, J., Cao, Q., Qin, C., Shao, P., Meng, X., Li, J., Lu, Q., & Yin, C. Meta-analysis reveals a lack of association between UGT2B17 deletion polymorphism and tumor susceptibility. *PLoS One* **9** (2014).

Depetris, R.S., Julien, J.P., Khayat, R., Lee, J.H., Pejchal, R., Katpally, U., Cocco, N., Kachare, M., Massi, E., David, K.B., Cupo, A., Marozsan, A.J., Olson, W.C., Ward, A.B., Wilson, I.A., Sanders, R.W., & Moore, J.P. Partial enzymatic deglycosylation preserves the structure of cleaved recombinant HIV-1 envelope glycoprotein trimers. *J. Biol. Chem.* **287**, 24239-24254 (2012).

Dobrinska, M.R. Enterohepatic circulation of drugs. *J. Clin. Pharmacol.* **29**(7), 577-580 (1989).

Duggan, D.E., Hooke, K.F., Noll, R.M., & Kwan, K.C. Enterohepatic circulation of indomethacin and its role in intestinal irritation. *Biochem. Pharmacol.* **24**(19), 1749-1754 (1975).

Duve, C.D., Gianetto, R., Appelmans, F., Wattiaux, R. Enzymic content of the mitochondrial fraction. *Nature* **172**, 1143-1144 (1953).

Eckburg, P.B, Bik, E.M., Bernstein, C.N., Purdom, E., Dethlefsen, L., Sargent, M., Gill, S.R., Nelson, K.E., & Relman, D.A. Diversity of the human intestinal microbial flora. *Science* **308**(5728), 1635-1638 (2005).

Elgundi, Z., Papanicolaou, M., Major, G., Cox, T.R., Melrose, J., Whitelock, J.M., & Farrugia, B.L. Cancer metastasis: the role of the extracellular matrix and the heparan sulfate proteoglycan perlecan. *Front Oncol.* **9**, (2020).

Evans, D.F., Pyek G., Bramley, R., Clark, A.G., Dyson, T.J., & Hardcastle, J.D. Measurement of gastrointestinal pH profiles in normal ambulant human subjects. *Gut* **29**(8), 1035-1041 (1988).

Fallingborg, J. Intraluminal pH of the human gastrointestinal tract. *Dan Med Bull.* **46**(3), 183-186 (1999).

Fay, E.K., & Graff, J.N. Immunotherapy in prostate cancer. *Cancers* **12**(7), 1752 (2020).

Feng, L., Dong, Z., Tao, D., Zhang, Y., & Liu, Z. The acidic tumour microenvironment: a target for smart cancer nano-theranostics. *Natl. Sci. Rev.* **5**, 269-286 (2018).

Ferlay, J., Colombet, M., Soerjomataram, I., Mathers, C., Parkin, D.M., Piñeros, M., Znaor, A., & Bray, F. Estimating the global cancer incidence and mortality in 2018: GLOBOCAN sources and methods. *Int. J. Cancer* **144**(8), 1941-1953 (2019).

Fink, D.W., & Koehler, W.R. pH effects on fluorescence of umbelliferone. *Analytical Chemistry* **42**, 990-993 (1970).

Fishman, W.H., & Anlyan, A.J. Beta-glucuronidase activity in human tissues; some correlations with processes of malignant growth and with the physiology of reproduction. *Cancer Res*. **7**(12), 808-817 (1947).

Fishman, W.H., & Farmelant, M.H. Effects of androgens and estrogens on β-glucuronidase in inbred mice. *Endocrinology* **52**, 536-545 (1953).

Fizazi, K. The role of Src in prostate cancer. *Ann Oncol.* **18**(11), 1765-1773 (2007).

Freeze, H.H., & Kranz, C. Endoglycosidase and glycoamidase release of N-linked glycans. *Curr Protoc Mol Biol*, (2010).

Fujiwara, R., Yokoi, T., & Nakajima, M. Structure and protein-protein interactions of human UDP-glucuronosyltransferases. *Front Pharmacol.* **7**, (2016).

Gianetto, R., & Duve, C.D. Comparative study of the binding of acid phosphatase, β-glucuronidase and cathepsin by rat-liver particles. *Biochem. J.* **59**, 433-438 (1955).

Gorbach, S.L. Microbiology of the gastrointestinal tract. *Medical Microbiology* **4**, (1996).

Goyal, J., & Antonarakis, E.S. Bone-targeting radiopharmaceuticals for the treatment of prostate cancer with bone metastases. *Cancer Lett.* **323**, 135-146 (2012).

Grino, P.B., Griffin, J.E., & Wilson, J.D. Testosterone at high concentrations interacts with the human androgen receptor similarly to dihydrotestosterone. *Endocrinology* **126**(2), 1165-1172 (1990).

Gregory, C.W., He, B., Johnson, R.T. Ford, O.H., Mohler, J.L., French, F.S., & Wilson, E.M. A mechanism for androgen receptor-mediated prostatte cancer recurrence after androgen deprivation therapy. *Cancer Res.* **61**(11), 4315-4319 (2001).

Guillemette, C., Lévesque, E., Beaulieu, M., Turgeon, D., Hum, D.W., & Bélanger, A. Differential regulation of two uridine diphospho-glucuronosyltransferases, UGT2B15 and UGT2B17, in human prostate LNCaP cells. *Endocrinology* **138**, 2998-3005 (1997).

Gauthier-Landry, L., Bélanger, A., & Barbier, O. Multiple roles for udp-glucuronosyltransferase (UGT)2B15 and UGT2B17 enzymes in androgen metabolism and prostate cancer evolution. *J. Steroid Biochem. Mol. Biol.* **145**, 187-192 (2015).

Gourley, G.R., & Arend, R.A. β-glucuronidase and hyperbilirubinemia in breast-fed and formula-fed babies. *The Lancet* **327**, 644-646 (1986).

Grant, D.J., Hoyo, C., Oliver, S.D., Gerber, L., Shuler, K., Calloway, E., Gaines, A.R., McPhail, M., Livingston, J.N., Richardson, R.M., Schildkraut, J.M., & Freedland, S.J. Association of uridine diphosphate glucuronosyltransferase 2B gene variants with serum glucuronide levels and prostate cancer risk. *Genet. Test. Mol. Biomark.* **17**, 3-9 (2013).

Grasso, C.S., Wu, Y.M., Robinson, D.R., Cao, X., Dhanasekaran, S.M., Khan, A.P., Quist, M.J., Jing, X., Lonigro, R.J., Brenner, J.C., Asangani, I.A., Ateeq, B., Chun, S.Y., Siddiqui, J., Sam, L., Anstett, M., Mehra, R., Prensner, J.R., Palanisamy, N., Ryslik, G.A., Vandin, F., Raphael, B.J., Kunju, L.P., Rhodes, D.R., Pienta, K.J., Chinnaiyan, A.M., & Tomlins, S.A. The mutational landscape of lethal castration-resistant prostate cancer. *Nature* **487**(7406),239-243 (2012).

Hadd, H.E., & Blickenstaff, R.T. The preparation and renal β-glucuronidase response of testosterone glucuronide. *Steroids* **4**(4), 503-513 (1964).

Halkidou, K., Gnanapragasam, V.J., Mehta, P.B., Logan, I.R., Brady, M.E., Cook, S., Leung, H.Y., Neal, D.E., & Robson, C.N. Expression of Tip60, an androgen receptor coactivator, and its role in prostate cancer development. *Oncogene* **22**, 2466-2477 (2003).

Hanahan, D., & Weinberg, R.A. The hallmarks of cancer. *Cell* **100**, 57-70 (2000).

Hanahan, D., & Weinberg, R.A. Hallmarks of cancer: the next generation. *Cell* **144**(5), 646-674 (2011).

Haroon, M.H, Premaratne, S.R., Choudhry, M.I., & Dharmaratne, H.R. A new β-glucuronidase inhibiting butyrolactone from the marine endophytic fungus Aspergillus terreus. *Nat Prod Res.* **27**(12), 1060-1066 (2013).

Harris, W.P., Mostaghel, E.A., Nelson, P.S., & Montgomery, B. Androgen deprivation therapy: progress in understanding mechanisms of resistance and optimizing androgen depletion. *Nat. Clin. Pract. Urol.* **6**, 76-85 (2009).

Hassan, M.I., Waheed, A., Grubb, J.H., Klei, H.E., Korolev, S., & Sly, W.S. High resolution crystal structure of human β-glucuronidase reveals structural basis of lysosome targeting. *PLOS ONE* **8**, (2013).

Heinlein, C.A., & Chang, C. Androgen receptor in prostate cancer. *Endocrine Reviews* **25**(2), 276-308 (2004).

Henrissat, B. A classification of glycosyl hydrolases based on amino acid sequence similarities. *Biochem. J.* **280**, 309-316 (1991).

Henrissat, B., Callebaut, I., Fabrega, S., Lehn, P., Mornon, J.P., & Davies, G. Conserved catalytic machinery and the prediction of a common fold for several families of glycosyl hydrolases. *Proc. Natl. Acad. Sci.* **92**, 7090-7094 (1995).

Higgins, I.T.T. The epidemiology of cancer of the prostate. *J Chronic Dis.* **28**, 343-348 (1975).

Hillman, E.T., Lu, H., Yao, T., & Nakatsu, C.H. Microbial ecology along the gastrointestinal tract. *Microbes Environ.* **32**, 300-313 (2017).

Hopkins, M.J., Sharp, R., & Macfarlane, G.T. Age and disease related changes in intestinal bacterial populations assessed by cell culture, 16S rRNA abundance, and community cellular fatty acid profiles. *Gut* **48**, 198-205 (2001).

Horoszewicz, J.S., Leong, S.S., Kawinski, E., Karr, J.P, Rosenthal, H., Chu, T.M., Mirand, E.A, & Murphy, G.P. LNCaP model of human prostatic carcinoma. *Cancer Res.* **43**, 1809-1818 (1983).

Hu, J., Zhang, Z., Shen, W.J., & Azhar, S. Cellular cholesterol delivery, intracellular processing and utilization for biosynthesis of steroid hormones. *Nutr. Metab.* **7**, 47 (2010).

Huggins, C., & Hodges, C.V. Studies on prostatic cancer. The effect of castration, of estrogen and of androgen injection on serum phosphatases in metastatic carcinoma of the prostate. *Cancer Res*. **1**(4), 293-297 (1941).

Islam, M.R., Tomatsu, S., Shah, G.N., Grubb, J.H., Jain, S., & Sly, W.S. Active site residues of human β-glucuronidase. *Journal of Biological Chemistry* **274**, 23451-23455 (1999).

Iyanagi, T. Moelcular mechanism of phase I and phase II drug-metabolizing enzymes: implications for detoxification. *Int. Rev. Cytol.* **260**, 35-112 (2007).

Jain, S., Drendel, W.B., Chen, Z.W., Mathews, F.S., Sly, W.S., & Grubb, J.H. Structure of human β-glucuronidase reveals lysosomal targeting and active-site motifs. *Nat. Struct. Mol. Biol.* **3**, 375-381 (1996).

Jakobsson, J., Ekström, L., Inotsume, N., Garle, M., Lorentzon, M., Ohlsson, C., Roh, H.K., Carlström, K., & Rane, A. Large differences in testosterone excretion in Korean and Swedish men are strongly associated with a UDP-glucuronosyl transferase 2B17 polymorphism. *J. Clin. Endocrinol. Metab.* **91**, 687-693 (2006).

Jančová, P., Anzenbacher, P., & Anzenbacherova, E. Phase II drug metabolizing enzymes. *Biomed. J.* **154**, 103-116 (2010).

Jančová, P., & Šiller, M. Phase II drug metabolism. *Intech* (2012).

Jayatilleke, K.M., & Hulett, M.D. Heparanase and the hallmarks of cancer. *J Transl. Med.* **18**, (2020).

Johnson, D.E., Ostrowski, P., Jaumouillé, V., & Grinstein, S. The position of lysosomes within the cell determines their luminal pH. *J Cell Biol.* **212**, 677-692 (2016).

Jones, D.T., Taylor, W.R., & Thornton, J.M. The rapid generation of mutation data matrices from protein sequences. *Bioinformatics* **8**, 275-282 (1992).

Josephy, D.P., Guengerich, F., & Miners, J.O. "Phase I and phase II" drug metabolism: terminonology that we should phase out? *Drug. Metab. Rev.* **37**, 575-580 (2005).

Kantoff, P.W., Higano, C.S., Shore, N.D., Berger, E.R., Small, E.J., Penson, D.F., Redfern, C.H., Ferrari, A.C., Dreicer, R., Sims, R.B., Xu, Y., Frohlich, M.W., & Schellhammer, P.F. Sipuleucel-T immunotherapy for castration-resistant prostate cancer. *N. Engl. J. Med.* **363**, 411-422 (2010).

Keyes, M., Crook, J., Morton, G., Vigneault, E., Usmani, N., Morris, W.J. Treatment options for localized prostate cancer. *Can Fam Physician* **59**(12), 1269-1274 (2013).

Kibel, A.S., Cizeki, J.P., Klein, E.A., Reddy, C.A., Lubahn, J.D., Haslag-Minoff, J., Deasy, J.O., Michalski, J.M., Kallogjeri, D., Piccirillo, J.F., Rabah, D.M., Yu, C., Kattan, M.W., & Stephenson, A.J. Survival among men with clinically localized prostate cancer treated with radical prostatectomy or radiation therapy in the prostate specific antigen era. *J. Urol.* **187**(4),1259-1265 (2012).

Kpoghomou, M.A., Soatiana, J.E., Kalembo, F.W., Bishwajit, G., & Sheng, W. UGT2B17 polymorphism and risk of prostate cancer: A meta-analysis. *ISRN oncol.* **2013**, 1-7 (2013).

Koh, C.M., Bieberich, C.J., Dang, C.V., Nelson, W.G., Yegnasubramanian, S., & De Marzo, A.M. MYC and prostate cancer. *Genes Cancer*. **1**(6), 617-628 (2010).

Kosir, M.A, Quinn, C.C., Zukowski, K.L., Grignon, D.J., & Ledbetter, S. Human prostate carcinoma cells produce extracellular heparinase. *J Surg Res.* **67**(1), 98-105 (1997).

Koziolek, M., Grimm, M., Becker, D., Iordanov, V., Zou, H., Shimizu, J., Wanke, C., Garbacz, G., & Weitschies, W. Investigation of pH and temperature profiles in the GI tract of fasted human subjects using the Intellicap® system. *Journal of Pharmaceutical Sciences* **104**(9), 2855-2863 (2015).

Kreamer, B.L, Siegel, F.L., & Gourley, G.R. A novel inhibitor of β-glucuronidase: L-aspartic acid. *Pediatric Research* **50**, 460-466 (2001).

Kumar, A., *et al*. Substantial interindividual and limited intraindividual genomic diversity among tumors from men with metastatic prostate cancer. *Nat Med.* **22**(4), 369-378 (2016).

Kumar, S., Stecher, G., & Tamura, K. MEGA7: Molecular evolutionary genetics analysis version 7.0 for bigger datasets. *Mol. Biol. Evol.* **33**, 1870-1874 (2016).

Lalley, P.A., Brown, J.A., Eddy, R.L., Haley, L.L., Byers, M.G., Goggin, A.P., Shows, T.B. Human beta-glucuronidase: assignment of the structural gene to chromosome 7 using somatic cell hybrids. *Biochem. Genet.* **15**, 367-382 (1977).

Lévesque, E., Labriet, A., Hovington, H., Allain, É.P., Melo-Garcia, L., Rouleau, M., Brisson, H., Turcotte, V., Caron, P., Villeneuve, L., Leclercq M., Droit, A., Audet-Walsh, E., Simonyan, D., Fradet, Y., Lacombe, L., & Guillemette, C. Alternative promotes control UGT2B17-dependent androgen catabolism in prostate cancer and its influence on progression. *Br. J. Cancer* **122**, 1068-1076 (2020).

Levvy, G. The preparation and properties of beta-glucuronidase. IV. Inhibition by sugar acids and their lactones. *Biochem J.* **52**(3), 464-472 (1952).

Liangzhu, F., Ziliang, D., Danlei, T., Yicheng, Z., & Zhuang, L. The acidic tumor microenvironment: a target for smart cancer nano-theranostics. *National Science Review* **5**(2), 269-286 (2018).

Lin, H.Y., Chen, C.Y., Lin, T.C., Yeh, L.F., Hsieh, W.C., Gao, S., Burnouf, P.A., Chen, B.M., Hsieh, T.J., Dashnyam, P., Kuo, Y.H., Tu, Z., Roffler, S.R., & Lin, C.H. Entropy-driven binding of gut bacterial β-glucuronidase inhibitors ameliorates irinotecan-induced toxicity. *Commun. Biol.* **4**(1), 280 (2021).

Little, M.S., Pellock, S.J., Walton, W.G., Tripathy, A., & Redinbo, M.R. Structural basis for the regulation of β-glucuronidase expression by human gut Enterobacteriaceae. *PNAS*, 152-161 (2018).

Liu, J., *et al*. An integrated TCGA pan-cancer clinical data resource to drive high-quality survival outcome analytics. *Cell* **173**(2), 400-416 (2018).

Liu, Y., Badée, J., Takahasi, R.H., Schmidt, S., Parrot, N., Fowler, S., Mackenzie, P.I., Coughtrie, M.W.H., & Collier, A.C. Coexpression of human hepatic uridine diphosphate glucuronosyltransferase proteins: Implications for ontogenetic mechanisms and isoform coregulation. *J. Clin. Pharmacol.* **60**, 722-733 (2020).

Louis, P., Scott, K.P., Duncan, S.H., & Flint, H.J. Understanding the effects of diet on bacterial metabolism in the large intestine. *J. Appl. Microbiol.* **102**, 1197-1208 (2007).

Mackenzie, P.I., Bock, K.W., Burchell, B., Guillemette, C., Ikushiro, S.I., Iyanagi, T., Miners, J.O., Owens, I.S., & Nebert, D.W. Nomenclature update for the mammalian UDP glycosyltransferase (UGT) gene superfamily. *Pharmacogenet. Genomics* **15**(10), 677-685 (2005).

Malik, M.Y., Jaiswal, S., Sharma, A., Shukla, M., & Lal, J. Role of enterohepatic recirculation in drug disposition: cooperation and complications. *Drug Metab Rev.* **48**(2), 281-327 (2016).

Mao, X., Gauche, C., Coughtrie, M.W.H., Bui, C., Gulberti, S., Merhi-Soussi, F., Ramalanjaona, N., Bertin-Jung, I., Diot, A., Dumas, D., De Freitas Caires, N., Thompson, A.M., Bourdon, J.C., Ouzzine, M., & Fournel-Gigleux, S. The heparan sulfate sulfotransferase 3-OST3A (HS3ST3A) is a novel tumor regulator and a prognostic marker in breast cancer. *Oncogene* **35**, 5043-5055 (2016).

Matsumoto, T., Sakari, M., Okada, M., Yokoyama, A., Takahasi, S., Kouzmenko, A., & Kato, S. The androgen receptor in health and disease. *Annu. Rev. Physiol.* **75**, 201-224 (2013).

McCarter, J.D., & Withers, S.G. Mechanisms of enzymatic glycoside hydrolysis. *Curr. Opin. Struct. Biol.* **4**, 885-892 (1994).

McDonald, S., Brive, L., Agus, D.B., Scher, H.I., & Ely, K.R. Ligand responsiveness in human prostate cancer: structural analysis of mutant androgen receptors from LNCaP and CWR22 tumors. *Cancer Res.* **60**(9), 2317-2322 (2000).

McNamara, K.M., Nakamura, Y., Miki, Y., & Sasano, H. Phase two metabolism and its roles in breast and prostate cancer patients. *Front. Endocrinol.* **4**(116), (2013).

Meech, R., & Mackenzie, P.I. UDP-glucuronosyltransferase, the role of the amino terminus in dimerization. *J. Biol. Chem.* **272**(43), 26913-26917 (1997).

Meech, R., & Mackenzie, P.I. Determinants of UDP glucuronosyltransferase membrane association and residency in the endoplasmic reticulum. *Arch. Biochem. Biophys.* **356**, 77-85 (1998).

Meech, R., Mubarokah, N., Shivasami, A., Rogers, A., Nair, P.C., Hu, D.G., McKinnon, R.A., & Mackenzie, P.I. A novel function for UDP glycosyltransferase 8: galactosidation of bile acids. *Mol Pharmacol.* **87**(3), 442-450 (2015).

Meech, R., Hu, D.G., McKinnon, R.A., Mubarokah, S.N., Haines, A.Z., Nair, P.C., Rowland, A. & Mackenzie, P.I. The UDP-glycosyltransferase (UGT) superfamily: New members, new functions, and novel paradigms. *Physiological Reviews* **99**, 1153-1222 (2019).

Mellman, I., Fuchs, R., & Helenius, A. Acidification of the endocytic and exocytic pathways. *Ann. Rev. Biochem.* **55**, 663-700 (1986).

Michikawa, M., Ichinose, H., Momma, M., Biely, P., Jongkees, S., Yoshida, M., Kotake, T., Tsumuraya, Y., Withers, S.G., Fujimoto, Z., & Kaneko, S. Structural and biochemical characterization of glycoside hydrolase family 79 β-glucuronidase from *Acidobacterium capsulatum*. *J. Biol. Chem.* **287**, 14069-14077 (2012).

Miley, M.J., Zielinska, A.K., Keenan, J.E., Bratton, S.M., Radominska-Pandya, A., & Redinbo, M.R. Crystal structure of the cofactor-binding domain of the human phase II drug-metabolism enzyme UDP-glucuronosyltransferase 2B7. *J. Mol. Biol.* **369**, 498-511 (2007).

Miller, R.D., Hoffmann, J.W., Powell, P.P., Kyle, J.W., Shipley, J.M., Bachinsky, D.R., & Sly, W.S. Cloning and characterization of the human beta-glucuronidase gene. *Genomics* **7**(2), 280-283 (1990).

Miller, W.L., & Auchus, R.J. The molecular biology, biochemistry, and physiology of human steroidogenesis and its disorders. *Endocr. Rev.* **32**, 81-151 (2011).

Miners, J.O., Knights, K.M., Houston, J.B., Mackenzie, P.I. In vitro-in vivo correlations for drugs and other compounds eliminated by glucuronidation in humans: pitfalls and promises. *Biochem. Pharmacol.* **71**, 1531-1539 (2006).

Miyagi, S.J., & Collier, A.C. Pediatric development of glucuronidation: The ontogeny of hepatic UGT1A4. *Drug Metab. Dispos.* **35**, 1587-1592 (2007).

Miyagi, S.J., & Collier, A.C. The development of UDP-glucuronosyltransferases 1A1 and 1A6 in the pediatric liver. *Drug Metab. Dispos.* **39**, 912-919 (2011).

Miyagi, S.J., Milne, A.M., Coughtrie, M.W.H., & Collier, A.C. Neonatal development of hepatic UGT1A9: Implications of pediatric pharmacokinetics. *Drug Metab. Dispos.* **40**, 1321-1327 (2012).

Memon, N., Weinberger, B.I., Hegyi, T., & Aleksunes, L.M. Inherited disorders of bilirubin clearance. *Pediatr. Res.* **79**, 378-386 (2016).

Montaño, A.M., Lock-Hock, N., Steiner, R.D., Graham, B.H., Szlago, M., Greenstein, R., Pineda, M., Gonzalez-Meneses, A., Çoker, M., Bartholomew, D., Sands, M.S., Wang, R.,

Giugliani, R., Macaya, A., Pastores, G., Ketko, A.K., Ezgü, F., Tanaka, A., Arash, L., Beck, M., Falk, R.E., Bhattacharya, K., Franco, J., White, K.K., Mitchell, G.A., Cimbalistiene, L., Holtz, M., & Sly, W.S. Clinical course of sly syndrome (mucopolysaccharidosis type VII). *J. Med. Genet.* **53**, 403-418 (2016).

Montgomery, R.B., Mostaghel, E.A., Vessella, R., Hess, D.L., Kalhorn, T.F., Higano, C.S., True, L.D., & Nelson, P.S. Maintenance of intratumoral androgens in metastatic prostate cancer: A mechanism for castration-resistant tumor growth. *Cancer Res.* **68**, 4447-4454 (2008).

Mürdter, T.E., Sperker, B., Kivistö, K.T., McClellan, M., Fritz, P., Friedel, G., Linder, A., Bosslet, K., Toomes, H., Dierkesmann, R., & Kroemer, H.K. Enhanced uptake of doxorubicin into bronchial carcinoma: beta-glucuronidase meditates release of doxorubicin from a glucuronide prodrug (HMR 1826) at the tumor site. *Cancer Res*. **57**(12), 2440-2445 (1997).

Nader, R., Amm, J.E., & Aragon-Ching, J.B. Role of chemotherapy in prostate cancer. *Asian J. Androl.* **20**(3), 221-229 (2018).

Nadeau, G., Bellemare, J., Audet-Walsh, É., Flageole, C., Huang, S.P., Bao, B.Y., Douville, P., Caron, P., Fradet, Y., Lacombe, L., Guillemette, C., & Lévesque, E. Deletions of the androgen-metabolizing UGT2B genes have an effect on circulating steroid levels and biochemical recurrence after radical prostatectomy in localized prostate cancer. *J. Clin. Endocrinol. Metab.* **96**, 1550-1557 (2011).

Nakamura, T., Takagaki, K., Majima, M., Kimura, S., Kubo, K., & Endoss, M. A new type of exo-beta-glucuronidase acting only on non-sulfated glycosaminoglycans. *J. Biol. Chem.* **265**, 5390-5397 (1990).

Naz, H., Islam, A., Waheed, A., Sly, W.S., Ahmad, F., & Hassan, M.I. Human β-glucuronidase: structure, function, and application in enzyme replacement therapy. *Rejuvenation Res.* **16**(5), 352-363 (2013).

Norris, G.E., Stillman, T.J., Anderson, B.F., & Baker, E.N. The three-dimensional structure of PNGase F, a glycosyl asparagine from Flavobacterium meningosepticum. *Structure* **2**, 1049-1059 (1994).

Oeser, S., Bingham, J.P., & Collier, A. Regulation of hepatic UGT2B15 by methylation in adults of Asian descent. *Pharmaceutics* **10**(1), 6 (2018).

O'Hara, A.M., & Shanahan, F. The gut flora as a forgotten organ. *EMBO reports* **7**, 688-693 (2006).

Oleson, L. & Court, M.H. Effect of the β-glucuronidase inhbitor saccharolactone on glucuronidation by human tissue microsomes and recombinant UDP-glucuronosyltransferases. *J Pharm Pharmacol.* **60**, 1175-1182 (2008).

Olsson, M., Ekström, L., Guillemette, C., Belanger, A., Rane, A., & Gustafsson, O. Correlation between circulatory, local prostatic, and intra-prostatic androgen levels. *Prostate* **71**(9), 909-914 (2011).

Ouzzine, M., Magdalou, J., Burchell, B., Fournel-Gigleux, S. An internal signal sequence mediates the targeting and retention of the human UDP-glucuronosyltransferase 1A6 to the endoplasmic reticulum. *J. Biol. Chem.* **274**(44), 31401-31409 (1999).

Paigen, K. Mammalian β-glucuronidase: genetics, molecular biology, and cell biology. *Prog. Nucleic Acid Res. Mol. Biol.* **37**, 155-205 (1989).

Parimi, V., Goyal, R., Poropatich, K., & Yang, X.J. Neuroendocrine differentiation of prostate cancer: a review. *Am J Clin Exp Urol.* **2**(4), 273-285 (2014).

Park, J., Chen, L., Ratnashinge, L., Sellers, T.A., Tanner, J.P., Lee, J.H., Dossett, N., Lang, N., Kadlubar, F.F., Ambrosone, C.B., Zachariah, B., Heysek, R.V., Patterson, S., & Pow-Sang, J. Deletion polymorphism of UDP-glucuronosyltransferase 2B17 and risk of prostate cancer in African American and Caucasian men. *Cancer Epidemiol. Biomarkers Prev.* **15**, 1473-1478 (2006).

Parker, C., Nilsson, S., Heinrich, D., Helle, S.I., O'Sullivan, J.M., Fosså, S.D., Chodacki, A., Wiechno, P., Logue, J., Seke, M., Widmark, A., Johannessen, D.C., Hoskin, P., Bottomley, D., James, N.D., Solberg, A., Syndikus, I., Kliment, J., Wedel, S., Boehmer, S., Dall'Oglio, M., Franzén, L., Coleman, R., Vogelzang, N.J., O'Bryan-Tear, C.G., Staudacher, K., Garcia-Vargas, J., Shan, M., Bruland, Ø.S., & Sartor, O. Alpha emitter radium-223 and survival in metastatic protate cancer. *N. Engl. J. Med.* **369**, 213-223 (2013).

Parker, R.J., Hirom, P.C., & Millburn, P. Enterohepatic recycling of phenolphthalein, morphine, lysergic acid diethylamide (LSD) and diphenylacetic acid in the rat. Hydrolysis of glucuronic acid conjugates in the gut lumen. *Xenobiotica* **10**(9), 689-7093 (1980).

Payne, A.H., & Hales, D.B. Overview of steroidogenic enzymes in the pathway from cholesterol to active steroid hormones. *Endocr. Rev.* **25**, 947-970 (2004).

Pearson, J.P., Pretlow, T.P., Bradley, E.L., Mcginnis, M.C., & Pretlow, T.G. Beta-glucuronidase activity in prostatic carcinoma and benign prostatic hyperplasia. *Cancer* **64**, 911-915 (1989).

Pellock, S.J., & Redinbo, M.R. Glucuronides in the gut: Sugar-driven symbioses between microbe and host. *J. Biol. Chem* **292**, 8569-8576 (2017).

Pellock, S.J., Creekmore, B.C., Walton, W.G., Mehta, N., Biernat, K.A., Cesmat, A.P., Ariyarathna, Y., Dunn, Z.D., Li, B., Jin, J., James, L.I., & Redinbo, M.R. Gut microbial β-glucuronidase inhibition via catalytic cycle interception. *ACS Cent. Sci.* **4**, 868-879 (2018).

Perdana, N.R., Mochtar, C.A., Umbas, R., & Hamid, A.R. The risk factors of prostate cancer and its prevention: A literature review. *Acta. Med. Indones.* **48**(3), 228-238 (2016).

Petrylak, D.P., Tangen, C.M., Hussain, M.H., Lara, P.N., Jones, J.A., Taplin, M.E., Burch, P.A., Berry, D., Moinpour, C., Kohli, M., Benson, M.C., Small, E.J., Raghavan, D., & Crawford, E.D. Docetaxel and estramustine compared with mitoxantrone and prednisone for advanced refractory prostate cancer. *N. Engl. J. Med.* **351**(15), 1513-1520 (2004).

Pollet, R.M., D'Agostino, E.H., Walton, W.G., Xu, Y., Little, M.S., Biernat, K.A., Pellock, S.J., Patterson, L.M., Creekmore, B.C., Isenberg, H.N., Bahethi, R.R., Bhatt, A.P., Liu, J., Gharaibeh, R.Z., & Redinbo, M.R. An atlas of β-glucuronidases in the human intestinal microbiome. *Structure* **25**(7), 967-977 (2017).

Peters, W.H., Jansen, P.L., & Nauta, H. The molecular weights of UDP-glucuronosyltransferase determined with radiation-inactivation analysis. A molecular model of bilirubin UDP-glucuronosyltransferase. *J. Biol. Chem.* **259**, 11701-11705 (1984).

Pienta, K.J., & Bradley, D. Mechanism underlying the development of androgen-independent prostate cancer. *Clin Cancer Res.* **12**, 1665-1671 (2006).

Pollet, R.M., D'Agostino, E.H., Walton, W.G., Xu, Y., Little, M.S., Biernat, K.A., Pellock, S.J., Patterson, L.M., Creekmore, B.C., Isenberg, H.N., Bahethi, R.R., Bhatt, A.P., Liu, J., Gharaibeh, R.Z., & Redinbo, M.R. An atlas of β-glucuronidases in the human intestinal microbiome. *Structure* **25**(7), 967-977 (2017).

Porter, M.L., & Dennis, B.L. Hyperbilirubinemia in the term newborn. *Am. Fam. Physician* **65**(4), 599-606 (2002).

Pritchard, C.C., Mateo, J., Walsh, M.F., De Sarkar, N., Abida, W., Beltran, H., Garofalo, A., Gulati, R., Carreira, S., Eeles, R., Elemento, O., Rubin, M.A., Robinson, D., Lonigro, R., Hussain, M., Chinnaiyan, A., Vinson, J., Filipenko, J., Garraway, L., Taplin, M.E., Aldubayan, S., Han, G.C., Beightol, M., Morrissey, C., Nghiem, B., Cheng, H.H., Montgomery, B., Walsh, T., Casadei, S., Berger, M., Zhang, L., Zehir, A., Vijai, J., Scher, H.I., Sawyers, C., Schultz, N., Kantoff, P.W. Solit, D., Robson, M., Van Allen, E.M., Offit, K., De Bono, J., & Nelson, P.S. Inherited DNA-repair gene mutations in men with metastaticp prostate cancer. *N. Engl. J. Med.* **375**, 443-453 (2016).

Quinn, D.I., Sandler, H.M., Horvath, L.G., Goldkorn, A., Eastham, J.A. The evolution of chemotherapy for the treatment of prostate cancer. *Ann. Oncol.* **28**(11), 2658-2669 (2017).

Radominska-Pandya, A., Pokrovskaya, I.D., Xu, J., Little, J.M., Jude, A.R., Kurten, R.C., & Czernik, P.J. Nuclear UDP-glucuronosyltransferases: Identification of UGT2B7 and UGT1A6 in human liver nuclear membranes. *Arch. Biochem. Biophys.* **399**, 37-48 (2002).

Rawla, P. Epidemiology of prostate cancer. *World J. Oncol.* **10**(2), 63-89 (2019).

Reuter, B.K., Davies, N.M., & Wallace, J.L. Nonsteroidal anti-inflammatory drug enteropathy in rats: role of permeability, bacteria, and enterohepatic circulation. *Gastroenterology* **112**, 109-117 (1997).

Rice, M.A., Malhotra, S.V., & Stoyanova, T. Second-generation antiandrogens: from discovery to standard of care in castration resistant prostate cancer. *Front. Oncol.* **9**, 801 (2019).

Roberts, M.S., Magnusson, B.M., Burczynski, F.J., & Weiss, M. Enterohepatic circulation: physiological, pharmacokientic and clinical implications. *Clin Pharmacokinet.* **41**(10) 751-790 (2002).

Rosner, W., Hryb, D.J., Nakhla, A.M., & Romas, N.A. Sex hormone-binding globulin: anatomy and physiology of a new regulatory system. *J. Steroid Biochem. Mol. Biol.* **40**(4-6), 813-820 (1991).

Ross, R.K., Bernstein, L., Lobo, R.A., Shimizu, H., Stanczyk, F.Z., Pike, M.C., & Henderson, B.E. 5-alpha-reductase activity and risk of prostate cancer among Japanese and US white and black males. *Lancet* **339**(8798), 887-889 (1992).

Saha, A.K., Glew, R.H., Kotler, D.P. & Omene, J.A. Elevated serum β-glucuronidase activity in acquired immunodeficiency syndrome. *Clin. Chim. Acta* **199**, 311-316 (1991).

Saitta, K.S., Zhang, C., Lee, K.K., Fujimoto, K., Redinbo, M.R., & Boelsterli, U.A. Bacterial β-glucuronidase inhibition protects mice against enteropathy induced by indomethacin, ketoprofen or diclofenac: mode of action and pharmacokinetics. *Xenobiotica* **44**(1), 28-35 (2014).

Salar, U., Taha, M., Ismail, N.H., Khan K.M., Imran, S., Perveen S., Wadood, A., & Riaz, M. Thiadiazole derivatives as new class of β-glucuronidase inhibitors. *Bioorg Med Chem.* **24**(8), 1909-1918 (2016).

SEER Cancer Statistics Review, 1975-2013. National Cancer Institute, Bethesda, MD. 2016. Available from: https://seer.cancer.gov/csr/1975_2015/. Accessed 01 August 2021. SEER, 2018. Available from: https://seer.cancer.gov/explorer/application.php.

Sekirov, I., Russell, S.L., Antunes, L.C., & Finlay B.B. Gut microbiota in health and disease. *Physiol Rev.* **90**(3), 859-904 (2010).

Sender, R., Fuchs, S., & Milo, R. Revised estimates for the number of human and bacterial cells in the body. *PLOS Biology* **14**, doi:10.1371/journal.pbio.1002533 (2016).

Setlur, S.R., Mertz, K.D., Hoshida, Y., Demichelis, F., Lupien, M., Perner, S., Sboner, A., Pawitan, Y., Andrén, O., Johnson, L.A., Tang, J., Adami, H.O., Calza, S., Chinnaiyan, A.M., Rhodes, D., Tomlins, S., Fall, K., Mucci, L.A., Kantoff, P.W., Stampfer, M.J., Andersson, S.O., Varenhorst, E., Johansson, J.E., Brown, M., Golub, T.R., & Rubin, M.A. Estrogen-dependent signaling in a molecularly distinct subclass of aggressive prostate cancer. *J. Natl. Cancer Inst.* **100**, 815-825 (2008).

Sgouros, G., Bodei, L., McDevitt, M.R., & Nedrow, J.R. Radiopharmaceutical therapy in cancer: clinical advances and challenges. *Nat. Rev. Drug Discov.* **19**, 589-608 (2020).

Shafi, A.A., Yen, A.E., Weigel, N.L. Androgen receptors in hormone-dependent and castration-resistant prostate cancer. *Pharmacol. Ther.* **140**, 223-238 (2013).

Shafiee-Kermani, F., Carney, S.T., Jima, D., Utin, U.C., Farrar, L.B., Oputa, M.O., Hines, M.R., Kinyamu, H.K., Trotter, K.W., Archer, T.K., Hoyo, C., Koller, B.H., Freedland, S.J., & Grant, D.J. Expression of UDP glucuronosyltransferases 2B15 and 2B17 is associated with methylation status in prostate cancer cells. *Epigenetics* **16**, 289-299 (2021).

Sharifi, N., Gulley, J.L., & Dahut, W.L. Androgen deprivation therapy for prostate cancer. *JAMA* **294**, 238 (2005).

Sharma, A., Yeow, W.S., Ertel, A., Coleman, I., Clegg, N., Thangavel, C., Morrissey, C., Zhang, X., Comstock, C.E., Witkiewicz, A.K., Gomella, L., Knudsen, E.S., Nelson, P.S., & Knudsen, K.E. The retinoblastoma tumor suppressor controls androgen signaling and human prostate cancer progression. *J. Clin. Invest.* **120**(12), 4478-4492 (2010).

Sharp, P.M., & Hahn, B.H. Origins of HIV and the AIDS pandemic. *Cold Spring Harb. Perspect. Med.* **1**(1), (2011).

Shipley, J.M., Grubb, J.H., & Sly, W.S. The role of glycosylation and phosphorylation in the expression of active human beta-glucuronidase. *J. Biol. Chem.* **268**, 12193-12198 (1993).

Shreiner, A.B., Kao, J.Y., & Young, V.B. The gut microbiome in health and in disease. *Curr. Opin. Gastroenterol.* **31**, 69-75 (2015).

Sirota, L. Ferrera, M., & Dulitzky, F. Beta glucuronidase and hyperbilirubinemia in breast fed infants of diabetic mothers. *Arch. Dis. Child.* **67**, 120-121 (1992).

Sizemore, G.M. Pitarresi, J.R., Balakrishnan, S., & Ostrowski, M.C. The ETS family of oncogenic transcription factors in solid tumours. *Nat. Rev. Cancer* **17**, 337-351 (2017).

Sly, W.S., Quinton, B.A., McAlister, W.H., and Rimoin, D.L. Beta glucuronidase deficiency: report of clinical, radiologic, and biochemical features of a new mucopolysaccharidosis. *J. Pediatr.* **82**(2), 249-257 (1973).

Small, E.J., Schellhammer, P.F., Higano, C.S., Redfern, C.H., Nemunaitis, J.J., Valone, F.H., Verjee, S.S., Jones, L.A., & Hershberg, R.M. Placebo-controlled phase III trial of immunologic therapy with Sipuleucel-T (APC8015) in patients with metastatic asymptomatic hormone refractory prostate cancer. *J. Clin. Oncol.* **24**, 3089-3094 (2006).

Sperker, B., Backman, J.T., & Kroemer, H.K. The role of β-glucuronidase in drug disposition and drug targeting in humans. *Clin. Pharmacokinet.* **33**, 18-31 (1997).

Sperker, B., Mürdter, T.E., Schick, M., Eckhardt, K., Bosslet, K., & Kroemer, H.K. Interindividual variability in expression and activity of human beta-glucuronidase in liver and kidney: consequences for drug metabolism. *J Pharmacol Exp Ther.* **281**(2), 914-920 (1997).

Sperker, B., Werner, U., Mürdter, T.E., Tekkaya, C., Fritz, P., Wacke, R., Adam, U., Gerken, M., Drewelow, B., & Kroemer, H.K. Expression and function of beta-glucuronidase in pancreatic cancer: a potential role in drug targeting. *Naunyn Schmiedebergs Arch Pharmacol*. **362**(2), 110-115 (2000).

Sramkoski, R.M., Pretlow, T.G., Giaconia, J.M., Pretlow, T.P, Schwartz, S., Sy, M.S., Marengo, S.R., Rhim, J.S., Zhang, D., & Jacobberger, J.W. A new human prostate carcinoma cell line, 22Rv1. *In Vitro Cellular & Developmental Biology* **35**, 403-409 (1999).

Suzuki, K., Nishiyama, T., Hara, N., Yamana, K., Takahasi, K., & Labrie, F. Importance of the intracrine metabolism of adrenal androgens in androgen-dependent prostate cancer. *Prostate Cancer and Prostatic Diseases* **10**, 301-306 (2007).

Taha, M., Imran, S., Alomari, M., Rahim, F., Wadood, A., Mosaddik, A., Uddin, N., Gollapalli, M., Alqahtani, M.A., & Bamarouf, Y.A. Synthesis of oxadiazole-coupled-thiadiazole derivatives as a potent β-glucuronidase inhibitors and their molecular docking study. *Bioorg. Med. Chem.* **27**(14), 3145-3155 (2019).

Tai, S., Sun, Y., Squires, J.M., Zhang, H., Oh, W.K., Liang, C.Z., & Huang, J. PC3 is a cell line characteristic of prostatic small cell carcinoma. *The Prostate* **71**, 1668-1679 (2011).

Tan, M.E., Li, J., Xu, H.E., Melcher, K., Yong, E.L. Androgen receptor: structure, role in prostate cancer and drug discovery. *Acta Pharmacol. Sin.* **36**, 3-23 (2015).

Tannock, I., Gospodarowicz, M., Meakin, W., Panzarella, T., Stewart, L., & Rider, W. Treatment of metastatic prostatic cancer with low-dose prednisone: evaluation of pain and quality of life as pragmatic indices of response. *J. Clin. Oncol.* **7**(5), 590-597 (1989).

Taplin, M.E. Drug insight: role of the androgen receptor in the development and progression of prostate cancer. *Nat. Clin. Pract. Oncol.* **4**, 236-244 (2007).

Teo, M.Y., Rathkopf, D.E., & Kantoff, P. Treatment of advanced prostate cancer. *Annu. Rev. Med.* **70**, 479-499 (2019).

Tomatsu, S., Montaño, A.M., Dung, V.C., Grubb, J.H., & Sly, W.S. Mutations and polymorphisms in GUSB gene in mucopolysaccharidosis VII (Sly syndrome). *Hum Mutat.* **30**(4), 511-519 (2009).

Trubetskoy, O. and Shaw, P. A fluorescent assay amenable to measuring production of beta-D-glucuronides produced from recombinant UDP-glycosyl transferase enzyme. *Drug Metab. Dispos.* **27**, 555-557 (1999).

Tukey, R.H., & Strassburg, C.P. Human UDP-glucuronosyltransferases: metabolism, expression, and disease. *Annu. Rev. Pharmacol. Toxicol.* **40**, 581-616 (2000).

Turgeon, D., Carrier, J.S., Lévesque, E., Hum, D.W., & Bélanger, A. Relative enzymatic activity, protein stability, and tissue distribution of human steroid-metabolizing UGT2B subfamily members. *Endocrinology* **142**, 778-787 (2001).

Uchaipichat, V., Mackenzie, P.I., Guo, X.H., Gardner-Stephen, D., Galetin, A., Houston, J.B., & Miners, J.O. Human UDP-glucuronosyltransferases: Isoform selectivity and kinetics of 4-methylumbelliferone and 1-napthol glucuronidation, effects of organic solvents, and inhibition by diclofenac and probenecid. *Drug Metab. Dispos.* **32**(4), 413-423 (2004).

Ueda, T., Bruchovsky, N., & Sadar, M.D. Activation of the androgen receptor N-terminal domain by interleukin-6 via MAPK and STAT3 signal transduction pathways. *J. Biol. Chem.* **277**(9), 7076-7085 (2002).

Valdes, A.M., Walter, J., Segal, E., Spector, T.D. Role of the gut microbiota in nutrition and health. *BMJ* (2018).

Vlodavsky, I., Elkin, M., Ilan, N. Impact of heparinase and the tumor microenvironment on cancer metastasis and angiogenesis: basic aspects and clinical applications. *Rambam Maimonides Med. J.* **2**(1), (2011).

Wallace, B.D., Wang, H., Lane, K.T., Scott, J.E., Orans, J., Koo, J.S., Venkatesh, M. Jobin, C., Yeh, L.A., Mani, S., & Redinbo, M.R. Alleviating cancer drug toxicity by inhibiting a bacterial enzyme. *Science* **330**(6005), 831-835 (2010).

Wang, C.C., & Touster, O. Studies of catalysis of β-glucuronidase. *J. Biol. Chem.* **247**(9), 2650-2656 (1972).

Wang, G., Zhao, D., Spring, D.J., Depinho, R.A. Genetics and biology of prostate cancer. *Genes Dev.* **32**, 1105-1140 (2018).

Waszkiewicz, N., Szajda, S.D, Konarzewska-Duchnowska, E., Zalewska-Szajda, B., Galazkowski, R., Sawko, A., Nammous, H., Buko, V., Szulc, A., Zwierz, K., & Ładny, J.R. Serum β-glucuronidase as a potential colon cancer marker: a preliminary study. *Advances in Hygiene and Experimental Medicine* **69**, 436-439 (2015).

Watchko, J.F., & Tiribelli, C. Bilirubin-induced neurological damage--mechanisms and management approaches. *N. Engl. J. Med.* **369**(21), 2021-2030 (2013).

Watson, P.A., Chen, Y.F., Balbas, M.D., Wongvipat, J., Socci, N.D., Viale, A., Kim, K., & Sawyers, C.L. Constitutively active androgen receptor splice variants expressed in castration-resistant prostate cancer require full-length androgen receptor. *PNAS* **107**(39), 16759-16765 (2010).

Weyel. D., Sedlacek, H.H., Müller, R., *et al*. Secreted human β-glucuronidase: a novel tool for gene-directed enzyme prodrug therapy. *Gene Ther.* **7**, 224-231 (2000).

Whiting, J.F., Narciso, J.P., Chapman, V., Ransil, B.J., Swank, R.T., & Gollan, J.L. Deconjugation of bilirubin-IX alpha glucuronides: a physiologic role of hepatic microsomal beta-glucuronidase. *J. Biol. Chem.* **268**(31), 23197-23201 (1993).

Whittemore, A.S., Wu, A.H., Kolonel, L.N., John, E.M., Gallagher, R.P., Howe, G.R., West, D.W., The, C.Z., & Stamey, T. Family history and prostate cancer risk in black, white, and Asian men in the United States and Canada. *Am. J. Epidemiol.* **141**(8), 732-740 (1995).

Wong, A.W., He, S., Grubb, J.H., Sly, W.S., & Withers, S.G. Identification of Glu-540 as the catalytic nucleophile of human beta-glucuronidase using electrospray mass spectrometry. *J. Biol. Chem.* **273**(51), 34057-34062 (1998).

Wright, A.S., Thomas, L.N., Douglas, R.C., Lazier, C.B., & Rittmaster, R.S. Relative potency of testosterone and dihydrotestosterone in preventing atrophy and apoptosis in the prostate of the castrated rat. *J. Clin. Invest.* **98**(11), 2558-2563 (1996).

Wu, H.C., Hsieh, J.T., Gleave, M.E., Brown, N.M., Pathak, S., & Chung, L.W. Derivation of androgen-independent human LNCaP prostatic cancer cell sublines: role of bone stromal cells. *Int J Cancer.* **57**(3), 406-412 (1994).

Xu, C., Li, C.Y.T., & Kong, A.N.T. Induction of phase I, II, and III drug metabolism/transport by xenobiotics. *Arch. Pharm. Res.* **28**, 249-268 (2005).

Zhang, D., Zhao, S., Li, X., Kirk, J.S., & Tang, D.G. Prostate luminal progenitor cells in development and cancer. *Trends Cancer* **4**(11), 769-783 (2018).

Zhang, L., Zhu, L., Qu, W., Wu, F., Hu, M., Xie, W., Liu, Z., & Wang, C. Insight into tartrate inhibition patterns in vitro and in vivo based on cocrystal structure with UDP-glucuronosyltransferase 2B15. *Biochem. Pharmacol.* **172**, 113753 (2020).

Zhau, H.Y.E., Chang, S.M., Chen, B.Q., Wang, Y., Zhang, H., Kao, C., Sang, Q.A., Pathak, S.J., & Chung, L.W.K. Androgen-repressed phenotype in human prostate cancer. *PNAS* **93**, 15152-15157 (1996).

Zhi, H., Wang, J., Wang, S., & Wei, Y. Fluorescent properties of hymecromone and fluorimetric analysis of hymecromone in compound dantong capsule. *Journal of Spectroscopy* **2013**, 1-9 (2013).

Zhou, T.S., Wei, B., He, M., Li, Y.S., Wang, Y.K., Wang, S.J., Chen, J.W., Zhang, H.W., Cui, Z.N., & Wang, H. Thiazolidin-2-cyanamides derivatives as novel potent Escherichia coli β-glucuronidase inhibitors and their structure-inhibitory activity relationships. *J Enzyme Inhib Med Chem* **35**, 1736-1742 (2020).

Zhunussova, A., Sen, B., Friedman, L., Tuleukhanov, S., Brooks, A., Sensenig, R., & Orynbayeva, Z. Tumor microenvironment promotes dicarboxylic acid carrier-mediated transport of succinate to fuel prostate cancer mitochondria. *Am J Cancer Res.* **5**(5), 1665-1679 (2015).